Probe Characterisation, Design and Evaluation for the Real-time Quality Indication of Milk

by

Petrus Johannes van der Westhuyzen

Thesis presented in partial fulfilment of the requirements for the degree of Master of Science (Engineering) at the University of Stellenbosch

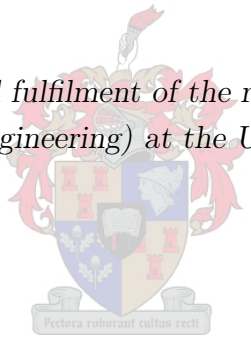

Department of Electrical and Electronic Engineering
University of Stellenbosch
Private Bag X1, 7602 Matieland, South Africa

Supervisor: Dr. C.J. Fourie

December 2006

Declaration

I, the undersigned, hereby declare that the work contained in this thesis is my own original work and that I have not previously in its entirety or in part submitted it at any university for a degree.

Signature: .....

Petrus Johannes van der Westhuyzen

Date: .....

Abstract

In order to rapidly detect, monitor and predict changes in milk as it ferments, sensors would need to be designed specifically for milk. To this end, invasive surgical stainless steel probes were investigated and the probe impedances were characterised according to measurements made in various saline concentrations. Based on these findings, specific probes were designed that were robust and easy to use in milk.

To measure multiple probe sensors continuously and accurately, an automatic measurement device was designed and manufactured. The device was self-sustaining, portable and calculated and stored all probe impedance data internally, allowing experimental runs to take place in controlled laboratory environments.

The probes designed in this thesis were consequently tested in various milk fermentation experiments and it was found that surgical stainless steel probes were effective at detecting and monitoring fermentation changes. The probe impedance changes also lead the pH changes in milk, giving it a predictive element.

The probe sensor studies provided enough data so that studies could be done into potential non-invasive sensors. Therefore, capacitive sensors were investigated and a fringe field capacitor was presented as a potential non-invasive milk fermentation sensor.

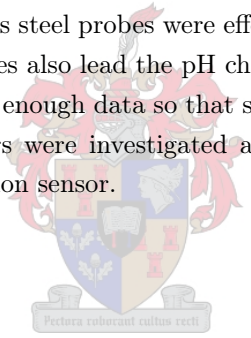

Opsomming

Om melk se suurwordproses vinnig te meet, te monitor en te voorspel, moet spesifieke melksensors ontwerp word. Indringende probes, gemaak van chirurgiese vlekvrye staal, is ondersoek en die probes se impedansies is gekarakteriseer namate metings in verskeie soutoplossings geneem is. Die bevindinge is gebruik om spesifieke melkprobes te ontwerp, sodat metings in melk vergemaklik is.

Verder is 'n outomatiese meetinstrument ontwerp sodat 'n aantal probes konstant en akkuraat gemeet kon word. Die instrument is selfstandig en draagbaar en het al die probes se impedansies bereken en gestoor. Die instrument se ontwerp het toegelaat dat eksperimente in laboratoria met beheerde omstandighede gedoen kon word.

Die probes wat in hierdie tesis ontwerp is, is getoets in verskeie melkeksperimente. Die resultate het getoon dat chirurgiese vlekvrye staal goed geskik is vir die meet en monitor van melk se suurwordproses. Die probes se impedansieveranderinge het ook die pH-veranderinge gelei, wat die probes 'n element van voorspelbaarheid gegee het.

Die data verkryg van die probe-studies het 'n goeie grondslag van kennis gegee sodat moontlike nie-indringende sensors ondersoek kon word. Kapasatiewe sensors is dus ondersoek en 'n nie-indringende sensor, in die vorm van 'n spreiveld-kapasitor, is beskryf as 'n moontlike melksensor.

Acknowledgements

Thank you to:

- My parents for their endless love and support throughout this thesis.
- The University of Stellenbosch, specifically the Department of Electrical and Electronic Engineering and the Department of Microbiology, for the use of the resources and equipment required to complete this thesis.
- The National Research Fund (NRF) for their financial contributions to this thesis.
- Dr. C. J. Fourie for his seemingly endless ideas, support and enthusiasm throughout the progress of this thesis.
- Dr. S. Todorov for preparing the different bacterial samples, helping with the experimental preparations, general laboratory guides and biological information.
- CES (Central Electronic Services), specifically Mr. U. Buttner and Mr. W. Croukamp for their ideas and help in finding practical probe manufacturing methods.
- Mr. N. van Graan for his support during times when electronic components were required from storage (and for putting up with the endless probe experiments in his labs).
- Mr. A. Cupido for the creation of the different (sometimes "creative") PCB's used in this thesis.
- The SSL labs, specifically Mr. E. Laubscher, Mr. W. A. Burger and Mr. P. C. van Niekerk for their respective inputs and contributions during the various stages of this thesis.
- The DSP labs, specifically Mr. R. Brand for his help with Matlab code and general mathematical insights.
- Mr. P. Lötter for providing Lyx, the program used to type this thesis, and the different programs and templates required to create the complete package.
- Miss A. H. Rothmann for her help in finding appropriate reference materials.

Dedications

To my Heavenly Father,
my Saviour Jesus Christ and

my Helper, the Holy Spirit.

Contents

List of Figures

List of Tables

List of Abbreviations

DNA	Deoxyribonucleic acid
LTH	Low temperature holding
HTST	High temperature short time
UHT	Ultra high temperature
DC	Direct current
AC	Alternating current
IDT	Impedance detection time
QCM	Quartz crystal microbalance
GND	Signal ground, or 0 Volts.
ISR	Interrupt service routine
ADC	Analog to digital conversion
PET	Polyethylene terephthalate (plastic)
CMOS	Complementary metal-oxide-semiconductor
ISP	In-system programming
SPI	Serial peripheral interface
DIP	Dual in-line package
PWM	Pulse-width modulation
A/D	Analog to digital
D/A	Digital to analog
MSB	Most significant bit
bps	bits per second
LED	Light emitting diode

PCB	Printed circuit board
opamp	Operational Amplifier
EEPROM	Electronically erasable programmable read-only memory
DB9	D-subminiature connecter (Also called the DE9)
MOSFET	Metal-oxide-semiconductor field-effect transistor
PC	Personal computer
AMD	Automatic measurement device (local shorthand in this thesis)

List of Symbols

Constants:

$\pi =$	pi, 3.141 592 654
$\epsilon_0 =$	permittivity of free space, 8, 854.10^{-12}
$\mu_0 =$	permeability of free space, 4π.10^{-7}
j =	$\sqrt{-1}$
c =	centi, scale constant, 1.10^{-2}
m =	milli, scale constant, 1.10^{-3}
$\mu =$	micro, scale constant, 1.10^{-6}
n =	nano, scale constant, 1.10^{-9}
p =	pico, scale constant, 1.10^{-12}
k =	kilo, scale constant, 1.10^{3}
M =	Mega, scale constant, 1.10^{6}
G =	Giga, scale constant, 1.10^{9}

Units of measurement

pH	Acidity level
pK_a	Buffering capacity
°C	Degrees Celsius
K	Kelvin
V	Volt
A	Ampère
Ω	Ohm
F	Farad
Hz	Hertz
s	Seconds
min	Minutes
h	Hours
l	Litres
g	gram

Variables

ϵ_r	Relative permittivity
ϵ	Total permittivity, $(\epsilon_0\epsilon_r)$
μ_r	Relative permeability
I	Current, Ampère
R	Resistance, Ohm
G	Conductance, Siemens
X	Reactance, Ohm
Z	Impedance, Ohm
L	Inductance, Henry
C	Capacitance, Farad
J	Current density, taken as mA/cm^2 in this thesis
f	Frequency, Hertz
w	Frequency, $2\pi f$, radians
V_b	Voltage measured across probes
V_r	Voltage measured across resistance
V_t	Voltage measured across total probe sensor system
min	Minutes, time

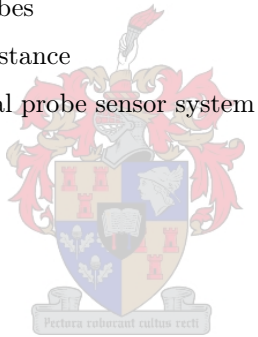

Chapter 1

Introduction

Milk. A substance well known to man, yet a natural wonder. Milk is a creamy white substance that is secreted by a mother after giving birth and it acts as a source of nourishment for the new born mammals. However, mankind has found milk to have more than just an infantile use, since it provides us with a range of food products that few other substances can give.

The control and production of milk products is something that the dairy industry has prided itself upon. The dairy industry has set extremely high standards when it comes to sanitary practices, product evaluation and product improvement. Most countries have local dairy regulations and a few international regulatory bodies exist as well. However, disease outbreaks has caused the public to become aware of the dangers that lurk in dairy products. In addition, people are becoming more critical about what they buy in the stores. These facts have forced the dairy industry to exert even greater control on the production, evaluation, storing and transporting facets of dairy products.

In an effort to aid the dairy industry in its task, a variety of electronic monitoring aids have come to the scene. The instruments have allowed the industry to monitor the production of the different dairy products much more closely than it would have been possible before. More recent developments even allowed the monitoring of the bacterial activity within the different dairy products, something previously left to educated guesswork. However, the greatest problem still facing most of the instruments is the problem of contamination.

Any instrument that would require direct contact with the substance to be tested would effectively cause a potential contamination scenario. The dairy industry controls bacterial contamination very closely, so such a scenario is unacceptable. Therefore, any instrument that tests milk is either already part of the equipment, or requires that dairy samples be taken from the product - something that cannot always be done. This means that the real time monitoring of dairy products, without using invasive systems, remain largely unrealised.

It was the eventual goal of this thesis to do studies into the possible application of a non-invasive measurement system that would measure the fermentation process of milk. However, knowledge about different milk measuring methods were either complicated, limited to a certain area, or not specifically meant for milk products. Therefore, the study would include an investigation into a system that would be designed specifically for milk, albeit an invasive one.

The fundamental core of this thesis was to test and develop a variety of electrical sensors, or to make it possible for the continuation of the development procedure once the sensor design criteria were well known.

A minimal understanding of the work required to create such sensors existed, so a thorough literature study had to be done, followed by a prototype sensor design. Once the prototype sensor was built, tests and measurements had to confirm its functionality. This meant that a bottleneck existed at the design of the first prototype sensor, since all other consequent sensor design data would be compared to the data of the first sensor.

This meant that the first prototype had to be based on a sensor that was either well known, or well investigated and that was easy enough to construct. The knowledge that would be gained through designing the prototype sensor should aid any other sensor designs that would follow. Ultimately, the goal of a non-invasive design could only be reached once previous sensor systems were understood, since results obtained with a non-invasive system studied by this thesis would need to be compared to existing results.

Since a lot of data existed for impedance probes, it was decided that this sensor type would be the first one to be designed. A commercial system, the Bactomer, already existed and most of the literature used it in their studies [10, 12, 27, 22, 21]. This, in turn, meant that a lot of data existed for impedance measurements in milk and the data would aid in the comparing the prototype probe's data to the commercial system's data. In addition, the procedures required to build a probe system could be adapted more easily than the procedure required to build, for example, the resonant LC chip [51].

The final component of the research tree was the measurement system. In order to measure the changes in milk over a 24 hour period, an automatic measurement device would be needed . The device would be able to regulate the measuring procedure and gather data at accurate time intervals. In addition, the device parameters could be changed to fit other sensor types, since the core functionality would essentially remain the same, decreasing development time.

Figure 1.1 illustrates the design procedure followed by this thesis.

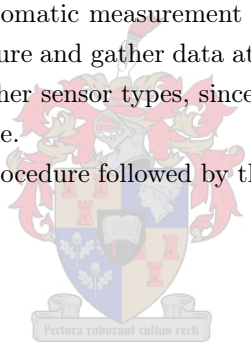

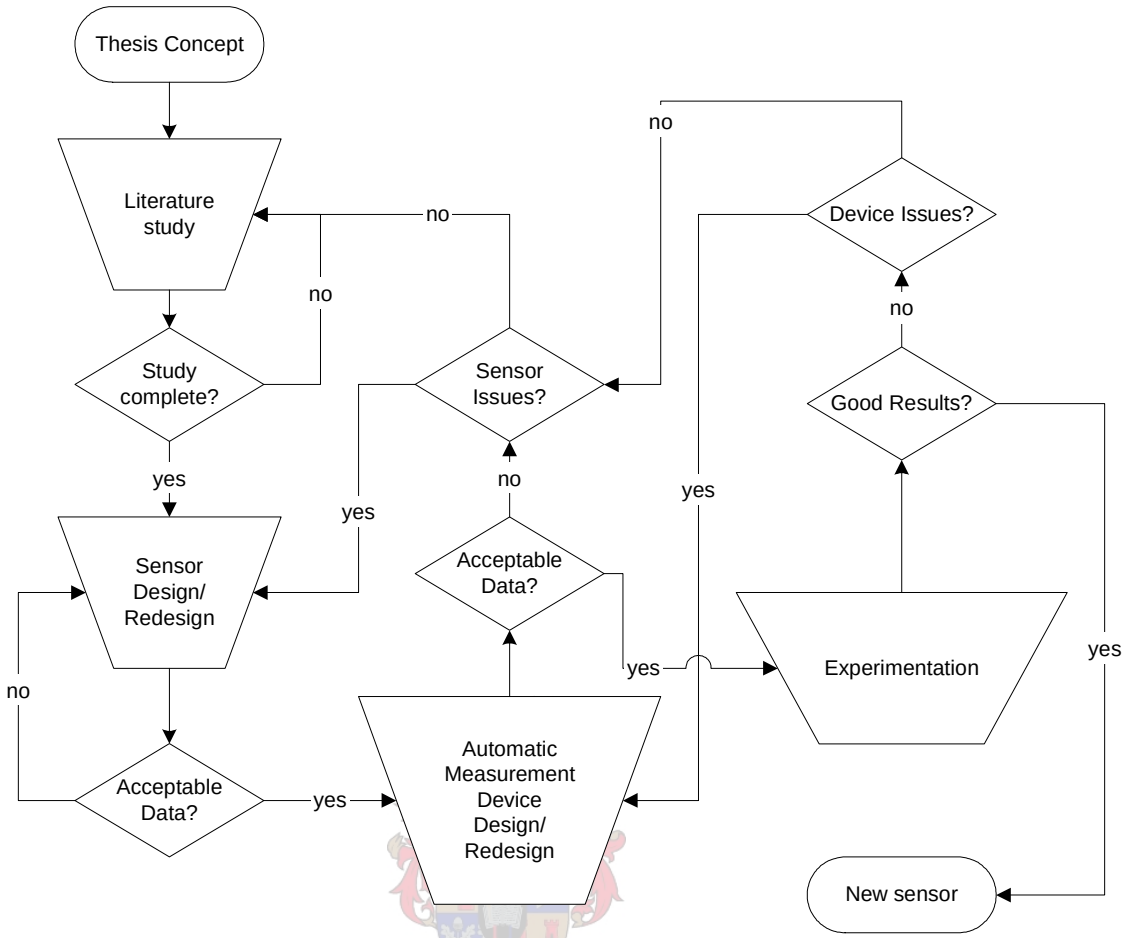

Figure 1.1: Basic research methodology.

The research tree provides the ideal setup, but sometimes a combined look into all facets of the tree had to be done in order to design the sensors correctly.

The next chapter will give a brief overview of the substance of milk, the electronics systems used to monitor milk or milk by-products in the literature as well as the theory that the working of these systems were based on. Chapters 3 and 4 will give details about the theory and design behind every sensor type designed in this thesis. Chapter 5 will discuss the automatic measurement device designed to measured the sensors. Finally, Chapters 6 and 7 will give results of the sensor's measurements, discussions around the results and conclusions made from the work in this thesis.

Chapter 2

Literature Study

Milk is a fundamental part of the human lifestyle. The dairy industry has put a lot of work into understanding what it consists of, how it is produced, how to improve on its quality and how to determine if it is conforming to consumer needs. Only recently has technology and more specifically electronics become part of the diary industry's need to control and monitor its milk produce. This literature study will investigate the knowledge that exists on milk as well as the technological advancements made in characterising milk as an electrical material.

2.1 Milk

The substance of milk is a complex one at best. Not only does it consist out of a myriad of different molecules, but it potentially contains different forms of bacteria, each with its own lifecycle and optimum living conditions. In addition, milk's composition is dependant on a variety of factors - factors that the dairy industry tries to control very closely. These days, even the standard composition of milk might change because of genetic engineering [39]. Therefore, from an electronic point of view, milk is a difficult substance to measure in, since its inherent complexities forces a very specific measurement methodology.

2.1.1 Composition

Milk can be considered to be one of natures great wonders. It is a white to creamy white, watery substance that is secreted by mammals to nourish their young. However, each mammalian species produces its own unique milk composition so that no exact chemical formula can be derived for any specific milk type, especially when one considers that milk contains over 100 000 different molecular components [37, 44, 63]. Even the general milk composition from a specific mammalian species depend on a variety of factors, for which the major influences are environmental, physiological and genetic [55].

Milk's composition also varies throughout the lactation period of any mammal. For example, cow's milk starts off as colostrum - a high fat and high protein, low lactose substance. This substance quickly changes and only after about 8 to 10 weeks the typical cows milk we buy in the stores are milked from the cow's udder. After this initial period, the composition of milk does not change much for the rest of the lactation period [55], which can last up to 305 days for a typical cow [28].

A lot of research has allowed for a generalized chemical classification of milk. In general, the average

gross composition of milk is as follows: 4.1% fat, 3.6% protein, 4.9% lactose and 0.7% ash. The remainder is made up of water (in this case 86.7%). Table 2.1 will give a brief detail of milk's main molecular families and the greatest contributing chemicals in each of those families.

Table 2.1: Milk constituents' largest chemical contributors.

Constituent	Molecular family name	Largest Contributor
Lipids	Neutral Glycerides	Triglycerides
	Phospholipids	Lecithin Ph. ethanolamine
Proteins	Caseins	α_{s1}-Casein β-Casein
	Whey protiens	β-Lactoglobulins α-Lactalbumins Immunoglobulins
	MFGM	-
	Minor proteins	-
	Enzymes	-
Carbohydrates	Disaccharide	Lactose
Minor Components	Minerals	Sodium Potassium Chloride Calcium Magnesium Phosphorus
	Selected Miscellaneous Compounds	Citric Acid
	Vitamins	C
	NPN Compounds	Urea-N Choline N-Acetylneuraminic acid

For more detailed information, refer to [37] and [55].

2.1.2 Microbial organisms in milk

Microbial organisms are living entities that generally cannot be seen by the naked eye, but that are all around us. They perform a myriad of functions in nature, whether for good or for bad [38].

Microbes can be divided into six groups: Archaea, Bacteria, Fungi, Protista, Viruses and Microbial mergers. The groups which could potentially be found in milk are the Bacteria, Fungi (yeasts and molds) and Viruses [38]. However, when compared to the other groups, the bacteria is the group that plays the greatest role in milk, and is therefore of great importance to the dairy industry.

The bacteria themselves form two distinct groups: Harmless bacteria and pathogens. The harmless bacteria group contains useful bacteria that the dairy industry uses to change milk into the different dairy products consumed by humans. These bacterial entities are referred to as starter cultures. Pathogens are the bacteria that cause disease or other harmful effects in humans and animals. Obviously, the presence of these bacteria has to be avoided in milk. [44]

Finally, an extensive classification system exists in order to place any bacterial organism into a family [9]. This system keeps changing as more criteria are being found (such as DNA patterns). For the purposes of this study, only a few basic criteria will be mentioned. These are gram stains reactions, preferred temperatures, oxygen requirements and physical shapes. Table 2.2 will elaborate on the basic classifications [28, 1].

Table 2.2: Basic classification criteria of bacteria.

Classification criteria	Basic groupings
Gram stain reactions	Gram-Positive Gram-Negative
Ideal temperature	Thermophyllic Psychrotrophic Mesophillic
Oxygen requirements	Obligate Aerobes Facultative Microaerophilic Aerotolerant Anaerobes Obligate Anaerobes
Shape of single cell	Cocci Baccili Spirilla

The classifications only serve to indicate to humans how to handle a specific bacterial entity. Based on the classifications, certain probabilities exist over bacterial survivability. As an example, the pathogen Escherichia coli O157:H7 (E. Coli for short) is a Gram-Negative, Facultative Anaerobic Rod, preferring mesophillic temperatures. This means that the process of pasteurization (see subsection 2.1.3) will kill E. Coli, since its Gram-Negative and mesophillic attributes make it vulnerable to high temperatures.

In general, bacteria need moisture, food and a favourable environment. Milk provides them with all of these, since it has an abundance of sugars (lactose), proteins and fat. In addition, it is mostly water and the general temperatures and pH of milk are ideal for most bacterial organisms. The conclusion is that no matter what one does, milk will eventually contain bacteria that will in turn cause the composition of milk to change.

Bacteria multiply through cell division. Through metabolic processes bacteria “eat” the various compounds around them until a sufficient size is reached for cell multiplication to occur. The bacterial cell then divides into two separate cells and the process starts over. If conditions are tough, certain bacteria can reproduce by forming spores. Spores are more resilient to heat and represents a problem for lower temperature pasteurization procedures.

Left to their own devices, bacteria living in ideal condition will continue to multiply until the habitat can no longer support growth. At that point bacteria will continue to reproduce, but others will die. Eventually the environment will be so toxic that the bacteria will die altogether. Under ideal conditions, bacteria can multiply every 30 minutes and since growth is an exponential function, the number of bacteria can reach into the millions in a very short time. For this reason, bacterial control and early detection is a vital component in the dairy industry.

2.1.3 Milk properties and processing

Properties

The different molecular compounds found in milk give it certain properties. In addition, these properties are exploited or suppressed depending on the requirements of the dairy industry. Bacteria change these properties by changing the chemical compounds present in milk and as they grow, the process of change is faster.

In general, the molecular compounds that have the greatest effect on milk's properties are the caseins. The caseins are found in the form of casein micelles, a complex colloidal particle. It is fairly stable and has an average diameter (in milk) of about 25 nm. The clotting of milk is directly caused by these casein micelle aggregations [37, 55].

Another big player in milk's properties are the lipids. It affects the milk's stability, since milk is an emulsion of fat droplets and no emulsion is ever thermodynamically stable. Heating or rapid kinetic movement within milk will alter the "thickness" of milk, better known as creaming [37]. Once again, the dairy industry exploits these properties of milk, depending on their needs.

Lactose and minerals are the final compounds. Lactose gives milk a blood plasma like quality, at least as far as milk's reaction to heat and pressure goes, and the minerals within milk either aid or suppress the casein micelle formations [55].

The properties that specifically interest the field of electronics are the density, freezing point, electrochemistry, acid-base equilibriums, heat capacity, thermal conductivity and optical properties. Each of these have an effect on electronic measurements in some way or another. For example, heat capacity and thermal conductivity will indicate how much stability can be expected in milk when subject to varying temperatures, which in turn will affect the ease of electronic conductivity. Another example is the acid-base equilibriums. Knowledge of the buffering capacity of milk will indicate how much change in acidity is required before a change in pH is measured, in turn indicating how great an effect chemicals, or bacterial by-products, have had on milk. This change in pH could be measured electronically. As a final example, density indicates how tightly packed molecules are and in turn, how big a surface area measurement is required to pick up a reasonable change in milk's molecular constituents.

Processing

Since milk is such a good environment for bacteria, the milk industry has a variety of methods to ensure that bacteria are either eliminated, or that certain bacteria thrive. The products formed by the thriving bacteria are usually the sort of products like yoghurts or cheeses. However, this thesis only measured milk's changes, so only the procedures involved in conditioning drinkable milk will be discussed.

The bacteria that are the greatest problem in milk are the psychrotrophs, since these organisms are capable of growing and reproducing at temperatures as low as $7°C$, the typical storage temperature of milk. Furthermore, organisms classified as thermoduric are organisms that are able to survive pasteurization [38]. Therefore, eliminating thermoduric psychrotrophs (or at least, inactivating them) is paramount of milk keeping quality is to be extended.

In order to ensure public safety and the keeping quality of milk, the industry uses the process of pasteurization to render the bacterial flora inert. Pasteurization is the heat treatment of milk. The process was named after Louis Pasteur, who first used a moderate heating step to control unwanted bacteria in wine [36]. The basic ranges of pasteurisation are the following: Batch pasteurization, sometimes called low

temperature holding (LTH), high temperature short time pasteurization (HTST) and ultra high temperature pasteurization (UHT). LTH requires that milk be held at $63°C$ for 30 minutes, HTST requires that the milk be held at $72°C$ for 15 seconds and UHT requires that milk be held at $138°C$ for 2 seconds. The general tendency is that the higher the temperature is, the more milk's shelf life can be extended, but at the cost of giving it a "cooked" taste. In addition to pasteurization, good sanitation practices ensure that bacterial infection of milk is kept to an absolute minimum. Therefore, milk's shelf life is predicted according to the conditions it was packaged in and the type of pasteurization it has undergone. This has allowed for the development of "long life" milk which can last for months inside an unopened container.

In addition to pasteurization, the milk industry also employs a process called homogenization. Homogenization is the process where the fat emulsion in milk is stabilised by forcing the fat globules into smaller globules. This process happens at a high temperature and pressure, to ensure that the fat is in a liquid state when forced into the homogenization machines [37, 36]. Homogenization is done in order to prevent milk from forming the cream layer on top, since the fat globules' rise rate has been lowered because of its smaller size.

The industry also provides the consumer with different varieties of milk. These milk varieties mostly reflect the fat content of the milk. The basic varieties are full cream, 2% (low fat milk) and skim milk (fat free milk). Generally, full cream milk contains all of the fat in milk. In the case of cows milk, the average fat content would be 3.5% of the total milk content. Low fat or 2% milk has 1.5% to 2% fat content and skim milk or fat free milk has a fat content of less than 0.5% of the milk's content [38].

All of the abovementioned factors contribute to the unique chemical makeup of milk. Therefore, from an electronic measurement point of view, milk provides many different initial conditions for which one must cater. With the conditions in mind, any results can be interpreted with a bias. The bias would incorporate values for milk's fat content, pasteurization method undergone, temperature of storage and finally, expected bacterial content upon opening of containers. The process of souring, or spoiling, is greatly affected by the starting point of any milk product.

2.1.4 Souring process and evaluation

The fermenting of milk is directly caused by bacteria. Different types of bacteria cause different metabolic products within milk and the exact process by which these metabolic products are formed is quite complex. However, the basic fermentation process involves bacteria that change the lactose within the milk into lactic acid [50, 44]. The production of lactic acid has the effect of lowering the pH of milk and it is the presence of this acidity that gives milk a "sour" characteristic.

Milk contains a natural pH buffer, an inherent chemical system that resists the sudden change of pH. A buffer is usually measured by the amount of strong acid or base in moles per litre required per unit change in pH. Buffers usually consist out of weak acids and basis and their respective salts [37]. In addition, buffers have ranges in which they work best. For instance, phosphate causes a buffer at 5.8 pK_a and lactic acid a buffer at around 4 pK_a [37]. Buffers are important in biological systems, since sudden changes in any pH level within living organisms could cause serious damage. Therefore, in order for milk to become acidic, quite a number of microbial organisms have to be present (and in turn, quite a number of the metabolic products). Finally, milk will not easily go below a pH of 4, since lactic acid's concentration in milk is so large at this point that the buffer capacity it creates is quite substantial [37].

The souring process can be summarised as follows:

- Fresh milk is contaminated with bacteria, whether the bacteria's presence is inherent, accidental or purposefully added (such as starter cultures). At this point, the pH in milk is between 6.5 and 6.8.
- Bacteria begin to metabolise lactose into lactic acid (or other by-products).
- Bacteria grow and multiply with time, increasing the rate at which the metabolites are formed.
- The increase in acidic products causes a drop in milk pH.
- The decrease of pH (or rather, increase in acidity) eventually causes the milk (more specifically the casein micelles) to coagulate, giving milk the classic curdled look. At this point, the milk has a pH of around 5.2.
- As the environment becomes more toxic to bacteria, bacteria begin to die off and the metabolic rate begins to reach a steady state. At this point the milk is considered well and truly sour and the pH is around 4.4.

The point at which it is decided that milk has become "unpleasantly" sour depends mostly on sensory perceptions such as taste and smell, since milk is perceived as a nutritional element and not a chemical element. However, pH measurement is a much more accurate way to determine milk's acidity level.

In addition to acidity, a number of off-flavours are associated with milk [37]. However, most of the evaluations and tests done within the dairy industry is done around the acidity level of milk. These tests are all based on human perceptions and therefore any tests done electronically will have to give results similar to the human sensory perceptions.

2.2 Electrical data and measurement applications

The accurate use of electronic measurements in the dairy industry (or for that matter, any industry involving bacterial or other biological entities) has only recently experienced an increase in interest. This interest has lead to further research in order to characterise different biological sensor systems. In addition, the properties of the substances being measured has also been investigated in order to gain greater understanding of the electromagnetic and electronic properties it may possess. Finally, the knowledge and understanding of the electronic properties of microbial entities has sparked new and exciting technologies that are specifically applied to detect and even manipulate these entities.

2.2.1 Sources of electrical data

The changes that occur in milk can be directly ascribed to bacteria. Therefore, when one considers the possible methods to measure these changes, two main measurement disciplines come to mind: Measure the physical properties of milk as it changes, or measure the microbes causing the changes.

In order to use electrical measurements, a measurement system must be able to measure changes in the electrical properties of any material. The law governing all electrical activity would be Ohms law, stating that voltage is equal to current times resistance, or $V = IR$. Another way to understand resistance is in terms of conductance. Conductance is the inverse of resistance, or $G = \frac{1}{R}$. Therefore, one can rewrite Ohms law, for conductivity, as $I = GV$, or in words, current is equal to conductance times voltage. In the case of

electrical materials, it is usually the value of resistance that is determined by the material's properties and therefore it is the change in resistance that is measured by measuring changes of current or voltage.

The law of $V = IR$ governs the DC properties of electricity. However, when one moves into the AC domain of electricity, Ohms law needs to be modified in order to fully describe the nature of the AC voltage and current. In addition, the law requires the use of complex mathematics in order to describe the situation fully. In electrical engineering, the phasor fully describes voltage, current and resistance (called impedance in AC terms). Ohms law now reads $V = IZ$, where impedance is further described as: $Z = R + jX$. Impedance, therefore, exists out of a real and an imaginary part. The real part works in the same way as for the DC characteristics in Ohms law. However, the imaginary part adds extra functionality to this equation. The imaginary part is determined by the dielectric, or magnetic, properties of the material as well as the frequency at which the voltage is applied. The resulting impedances are often referred to as capacitances or inductances. Therefore, any application that applies a voltage at a certain frequency will undoubtedly be looking at impedance changes, or more specifically, capacitive or inductive changes.

Dictating these impedances changes are the changes in a dielectric material's relative permittivity (ϵ_r) or a material's relative permeability (μ_r). The relative permeability is usually associated with inductors and the relative permittivity with capacitors [11]. However, each property is involved with a different set of circumstances and a material rarely possesses both a high permittivity and high permeability value.

Permeability is the degree to which a material can be magnetised in response to a magnetic field. The typical inductor is formed by a solenoid and the inductance of that solenoid can be equated as follows:

$$L = \frac{\mu_0 \mu_r N^2 A}{l} = \frac{\Phi}{i}$$

where L is the inductance, i the current flowing through the wires forming the inductor (or coils), Φ is the magnetic flux, l the length of the wire forming the solenoid, N the number of turns in the solenoid, A the cross sectional area of the solenoid, μ_0 the permeability of free space and μ_r the relative permeability of the material. However, biological materials are usually non-magnetic and therefore the relative permeability of any biological material will not contain any data about biological changes in a specific biological environment. Therefore, the rest of this theoretical analysis will ignore magnetic flux and permeability.

Permittivity is an indication of the ease by which localised electric charge inside a material can be polarized with the application of an electric field. As stated, a measure of a material's permittivity can be described by the relative permittivity, or ϵ_r. The capacitance of a material between two simple parallel plates of a certain area and a certain distance apart can now be described as:

$$C = \frac{\epsilon_0 \epsilon_r A}{d}$$

where ϵ_r is the relative permittivity, ϵ_0 the permittivity of free space, A the area of the plates forming the capacitor and d the distance between the plates.

To conclude the above discussion, one must understand that any sensor will have, at its core, some property that will change based on the permittivity and conductivity (permeability is being ignored, for reasons stated above) of the material causing the change, whether the material is inherent to the sensor or inherent to the material being measured (bulk media) and that certain properties of the dielectric material can be exploited in order to narrow down the type of measurement required for any specific application. For instance, a capacitive sensor will exploit the permittivity of milk and at a certain frequency, whilst a

conductivity sensor will ideally measure only changes in conductance within milk.

Lately, more in depth studies into the dielectric properties of cells have sparked even more options when one considers a sensor application. Cells are usually found in a liquid medium so that the dielectric of the material it is suspended in is affected by the cells own dielectric properties. However, the dielectric properties of cells are complex, since no two cells are exactly the same. In addition, cells grow with time and eventually multiply to form two cells, dynamically affecting the dielectric properties of any medium containing them.

Studies have been done to determine the dielectric properties of cells in the different stages of their lives [2, 3, 4]. These studies indicate that as cells grow, the relative permittivity increases with time and after cell multiplication, it drops of to a value lower than for one longitudinal cell, but slightly higher because there are now two spherical cells present. The general increase in relative permittivity would suggest that bacteria (in general, longitudinal shaped cells) could be detected if capacitive or inductive sensors are tuned into these changes.

Another phenomenon inherent to cells is its unique dielectric dispersions. In order to describe these dispersions, the permittivity of any material can be extended to describe dielectric loss. This permittivity is called the complex permittivity and can be written as $\epsilon_r^* = \epsilon_r^{'} - j\epsilon_r^{''}$, where $\epsilon_r^{'}$ is the permittivity as discussed, and $\epsilon_r^{''}$ is the dielectric loss [62]. In biological situations, the dielectric permittivity and dielectric loss is often displayed as a Cole-Cole plot. The Cole-Cole plot is based on the Debye equation which describes the passive electrical property of a parallel RC circuit. Depending on the frequency applied to a cellular suspension, certain dielectric dispersion areas are prevalent [30]. At these dielectric dispersion, there are jumps in the permittivity and conductivity of a biological system, as the permittivity drops and the conductivity rises. In general, the jumps are situated at around 3.2 kHz, 3.2 Mhz and around 1 Ghz [43]. These corresponds to the so called alpha, beta and delta dispersions and each dispersion is caused by a different electromagnetic effect on biological cells. The degree of dispersion is also dependant on the cell geometries [26].

Therefore, the combined dielectric properties of milk and its bacterial flora, together with the interaction and changes that occur between the bacteria and their environment, requires a sensor that can measure the specific changes without being overwhelmed by too much sensor information. To this end, a variety of sensor applications have been developed, albeit not for milk specifically.

Finally, a number of measurement techniques exist that do not use the electrical properties of a material directly. These techniques would include chemical and optical analysis of a material. Eventually, these changes are transformed into electric signals, thereby measuring a change of the material. It is a more indirect technique and falls outside the scope of this study.

2.2.2 Sensor and measurements to date

As far as the author could establish, the different techniques used to measure changes in biological systems, or in this case milk, have only recently been diversified (compared to the application of the knowledge of electricity). With “diversified” it is meant that the basic electronic sensor types have always been those which were easily constructed and based on basic knowledge of material properties, such as conductivity. Technology has made it possible to construct more sensitive measuring systems that in turn allowed a deeper investigation into different material parameters.

The measurement systems that have been researched, or are currently being researched, or have been commercially employed, can be summarised as follows:

- Conductivity measurements - measuring the change in the bulk media’s conductivity, or resistivity,

with time. Ideally the sensor has no effect on the measurement.

- Impedance measurements - measuring the change of electrodes within a material at a certain frequency (over time). Here the entire system is looked at, both probes and bulk media, although one could dominate.
- Capacitive measurements - measuring the change in capacitance of a section of material between two plates. Ideally, the sensor has no effect on the medium, only the change of the medium's permittivity.
- Inductive measurements - measuring the change in inductance of a section of material between toroidal cores. Once again, the sensor would ideally have no effect on the measurement, only the permittivity has an effect.
- Resonance measurements - measuring the change in resonant frequency of a resonant circuit, either remotely or locally, determined by the material to be measured. These resonant circuits use the permittivity of a material as a basis for its resonant frequency, but the measurement method is applied differently. Once again the sensor should have no effect.

The list is definitely not exhaustive, since new technologies are bound to appear with time. In addition, certain technologies have not been exploited to its full potential (such as capacitive systems). However, the broad idea of the work done in each of these areas will be discussed below.

Conductivity measurements

Conductivity and its application in milk have been studied in a number of experiments, but the most frequent application of conductivity tests have been to detect mastitis in milk [47, 40]. Mastitis infection within a cows udder increases the salt content in milk (or more specifically, the sodium and chloride ions) which in turn increases the conductivity in milk. Mucchetti et al. [45] studied the determining factors for conductivity changes in milk as it fermented. The bacterial metabolites (lactic acid) formed in the milk increased the ion concentration which increased the conductivity. Their conclusion was that conductivity was an acceptable means by which milk fermentation could be detected. Conductivity measurements have also been applied in the monitoring of cheese processes [52], a direct by-product of milk fermentation. Final year pregraduate studies within the University of Stellenbosch also carried out conductivity experiments in milk [6, 16]. The conclusions from these studies confirmed the different conductive parameters for different milk types and different bacterial activities, but also showed that conductivity may be erroneous.

Impedance measurements

Impedance measurements usually involve an electrode of some sort operating at a certain frequency within a medium. Many studies have gone into the characterisation of the electrode-electrolyte interface and how to portray it as an electric circuit [23]. In addition, two mainstream methods exist in which probes are used to measure a materials properties. The methods involve either measuring a two-electrode probe and the changes that occur to it as well as the material in conjunction, or measuring a four-electrode probe, eliminating electrode surface effects, and allowing for a direct measurement of the material [58].

The nature of the interface, as well as the way in which biological materials influence it have been studied by a number of people, such as Felice et al. [20, 19] and Ebina et al. [17]. However, it has been shown that the capacitive component of the electrode-electrolyte interface held much more data when one considered

a biological environment, since this component of the probe impedance tended to exhibit the same type of curve shape as the bacterial growth curve [18, 49]. The ability of impedance to detect bacterial growth in a relative short time meant that a new bacterial testing method was available to microbiologists - the IDT (or impedance detection time) [27, 22, 21]. Subsequently, a number of experiments have been done in order to measure the change in impedance of a number of probes in a number of situations, and of more interest to this thesis, milk [32, 61, 5, 10, 12].

Capacitive measurements

Although a great number of documents speak of capacitance monitoring in biological growth curves, it usually refers to the capacitance element of the impedance technique as discussed above. However, an example of a purely capacitive sensor, that only focuses on the permittivity of the bulk media being measured, has been designed by Grillo et al.[29]. Once again it was applied to detect the presence of mastitis within a cows udder by measuring the somatic cells present in the milk produced by that cow. Another paper compared the different methods used to detect mastitis and declared the capacitive method to be the best [7]. More detailed study into capacitive sensors have allowed the development of interdigital capacitors. These capacitors are small enough to fit on a chip and make use of very specific and very detailed construction techniques in order to build a capacitor that literally traps bacteria on its surface. In so doing the bacteria changes the capacitance measured between the interdigital plates. Radke and Alocilja [53] used such an interdigital design in order to detect the growth of E.Coli, a pathogen that can be present in milk.

Inductive measurements

Inductive sensors (like capacitive sensors) measure permittivity. Instead of two conducting plates that are insulated from the material being measured, two toroidal cores are used, also insulated from the material being measured. The principle of electromagnetic induction is used to measure a change of permittivity within the toroidal cores. It was found that the sensor was successful in detecting biomass changes [60] and basic tests have been done on mastitis detection [40]. This technology seems to be quite new when compared to the other sensor types.

Resonance circuit measurements

Resonance circuits usually encompass an electronic measurement circuit that functions in conjunction with an oscillation section. In turn, the oscillation section contains the sensors in contact with the medium. As the medium changes, it affects a specific property of the sensor that in turn changes the oscillation frequency, or resonance frequency, of the resonant section of the measurement system.

A technique called quartz crystal microbalance (QCM) uses a piezoelectric-type material that changes a change in mass into a change of frequency. The crystal is manufactured in such a way that bacterial mass collects on the quartz crystal, changing the sensor's mass, and the resulting change in oscillation frequency is measured by electronics. This specific sensor does not employ the permittivity of the material. However, an adaptation to this technique involves the impedances of probes. Instead of measuring the change in impedance with a change in material properties, the probes form part of the resonance circuit. The resonant frequency is therefore determined by the combined electrical properties of the quartz crystal and probes [15].

A more direct application of a resonant circuit involves the work done by Ong et al. [51]. The technology was reviewed by Dickert et al. [15]. Here, a resonant LC sensor chip was built to resonate at a specific

frequency when queried by an electromagnetic field, provided in their case by a loop antenna. The resulting radiated frequency was then measured by an impedance analyser connected to either another antenna or the same antenna. Once again, as the material under investigation changed with time, the resonant frequency shifted accordingly. Although this system is a direct application of a capacitive measurement, the added component of an antenna query system puts it in a league of its own.

2.3 Literature conclusion

Milk is a complex liquid medium that presents a challenging measurement environment for any measurement system. However, the different facets of milk's constituencies suggest that sensors could be designed with certain areas of focus, such as density, heat, conductivity, etc. However, the literature study has revealed that most electronic sensors, to date, measure either the conductivity or the permittivity of milk.

The reason these are important is that both the permittivity and the conductivity have measurable changes during the fermentation of milk, albeit small ones. However, these changes are directly caused by bacterial activity in the milk. Bacteria will always be present in milk used by the populace and since milk is such a brilliant environment for bacterial growth, they will multiply. Bacterial by-products are the direct cause of conductivity changes in milk, whilst the bacteria themselves, with their unique dielectric contributions to the total permittivity of milk, are the reasons for a permittivity change in milk.

Most of the sensor data, therefore, are directly interpreted with bacterial growth and the dielectric contribution of bacterial cells in mind. This thesis will base all of the potential sensor results on this fact: Bacterial growth is the single most important change in milk and if one can follow this change, one can begin to predict potential changes. The IDT method used by microbiologists have made use of this fact and have aided the diary industry in better use-by-date predictions.

Chapter 3

Device 1: Probe sensor

The probe sensor had the potential to be a simple device since the application of the electromagnetic theory describing its working was relatively simple. However, the development of the probe sensor required an in depth knowledge of the interaction between the probe and the material being measured. Knowledge about the probe's material properties and the influence it had on the measurements were also required. Different probe geometrical configurations were also investigated since the probes themselves presented interesting practical issues during their use in the experiments. Finally, a solid manufacturing and application procedure had to be found in order to ensure that any sensor would be easy to use, since the people who will eventually use the probes will want to do so at a minimum cost to time.

The next few sections will describe the processes and measurements that were required to design and manufacture a probe sensor. The manufactured probes will also be evaluated.

3.1 Probe Theory

When one thinks of probes, a rod-like metallic object springs to mind. This is, in general, the basic idea behind probes. Probes consist out of two conductors that are shaped and separated in some way and that are inserted into the media of choice so that a certain exposed area of both conductors is in contact with the medium.

Probes and their interaction with a liquid medium have been the focal point of a great many studies over the past 100 years. However, an exact theory describing this interaction, and therefore the probes characteristics, has not yet been given. This has lead to a variety of theoretical models describing the probe's characteristics in different situations. A paper by L. A. Geddes [23] summarizes the evolution of the electrode-electrolyte circuit model quite well and most of the facts mentioned here can be found there.

The first steps taken to model the electrode-electrolyte interface was done by Helmholtz. He proposed that a double layer of charge existed at the interface, giving the model a capacitive element, and since current had to pass through the interface, the model would also required a resistance component. Warburg took the next steps by analysing the nature of the interface as based on frequency. He proposed that the capacitance varied inversely with the square root of frequency and that a constant phase angle of 45 degrees existed between the capacitance and resitance components of the probes. Therefore, the model proposed that the reactance was equal to the resistance. This model was based on an infinitely low current density and did not provide for the possibility of direct current passing through the interface. Figure 3.1 illustrates the Warburg

model.

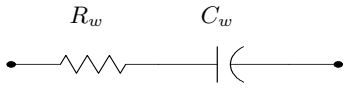

Figure 3.1: The Warburg model for the probe interface.

In addition, the following conditions are given for the Warburg model:

$$\phi = \frac{\pi}{4} \tag{3.1}$$

$$tan\phi = 1 = \frac{X_w}{R_w} \tag{3.2}$$

$$C_w = \frac{k}{f^{0.5}} \tag{3.3}$$

Fricke modified the model to account for different material properties, since measurements showed that the resistance was not always equal to the reactance. Randles and Sluyters-Rehbach modified the model even more, but still did not account for the direct current properties of the interface. Further studies into numerous impedance-frequency curves led Geddes and Baker to propose two detailed models in order to allow for the direct current properties of the interface.

The studies by Onaral and Schwan found that between the frequency ranges of 0.001 to 1000 Hz, the Warburg model was a fair approximation. However, experimentally obtained data could rarely be fit to the Warburg model, which led Ragheb and Geddes to fit the data to

$$R_w = \frac{A}{f^{\alpha}} \tag{3.4}$$

and

$$X_w = \frac{B}{f^{\beta}} \tag{3.5}$$

With most biological probes, the circuit model used is the Warburg model and if the sensor data is not approximated to the Warburg impedances, the data is fit to equations 3.4 and 3.5 [24, 32]. A brief explanation of the variables used will be given: The the variables A, B, k, α and β are metal-specific constant that were found by means of data fitting and its typical use can be seen from the applications in the same literature [24, 32]. R_w, X_w and C_w refer to the Warburg resistance, reactance and capacitance in all cases and f is the frequency at which the sine wave is applied. ϕ is the angle between resistance and reactance, which is always 45 degrees for the Warburg model.

A further characteristic of probes (or wire electrodes) is the unique relationships that exists between probe impedance and probe current density as well as probe impedance and probe frequency. Studies done by Geddes et al. [24] for stainless steel electrodes determined that the resistance and capacitance component remained the same for an increase in current density in the low current density regions. However, at a certain point, a further increase in current density caused the resistance to drop sharply and the capacitance to rise sharply. Therefore, the linearity of the impedance graph was lost above a certain point in current density. A further study (by Ragheb and Geddes [54]) involving current density was carried out for other electrode

types, such as aluminium, copper and platinum. It was found that the same relationship was true for all the material types. In addition to the current density effect, the frequency of measurement also determined the extent of the impedance change. At lower frequencies and low current densities, the value of resistance and capacitance was larger than it would be for the same current density but at higher frequencies. Figures 3.2 and 3.3 are approximate representations of the findings of Geddes et al. for stainless steel probes. The figures only give two frequency examples.

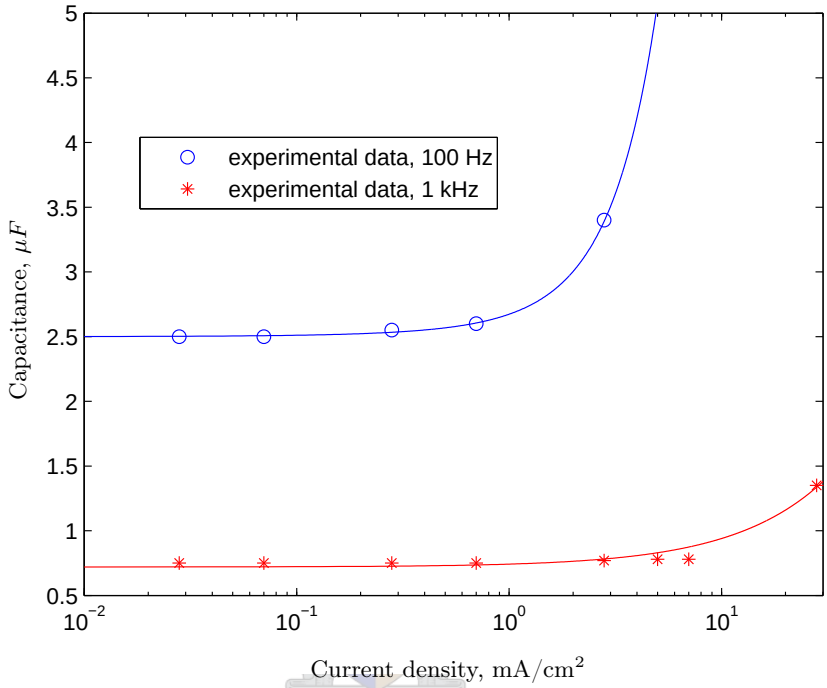

Figure 3.2: Stainless steel electrode capacitance vs current density in 0.9% saline solution. Lines represent average path of change.

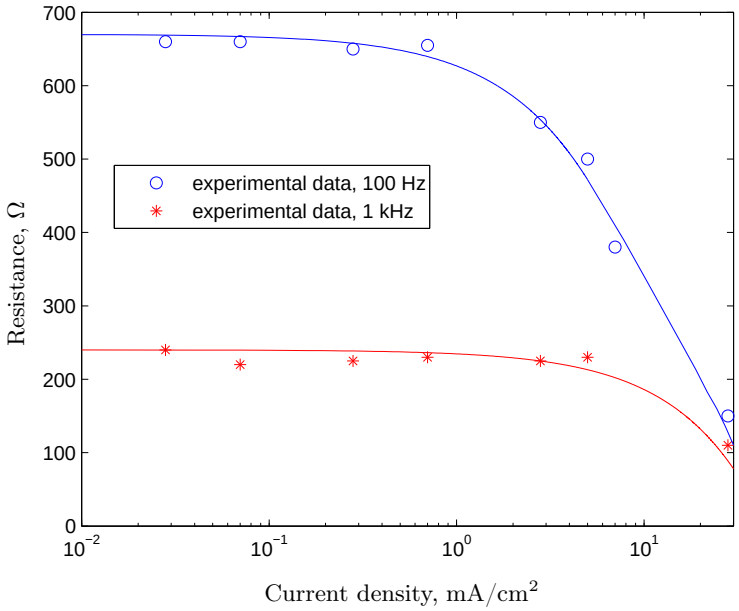

Figure 3.3: Stainless steel electrode resistance vs current density in 0.9% saline solution. Lines represent average path of change.

Figure 3.4 will illustrate the application of equations 3.4 and 3.5 on measured data. The data in the figure is approximated from Geddes et al.

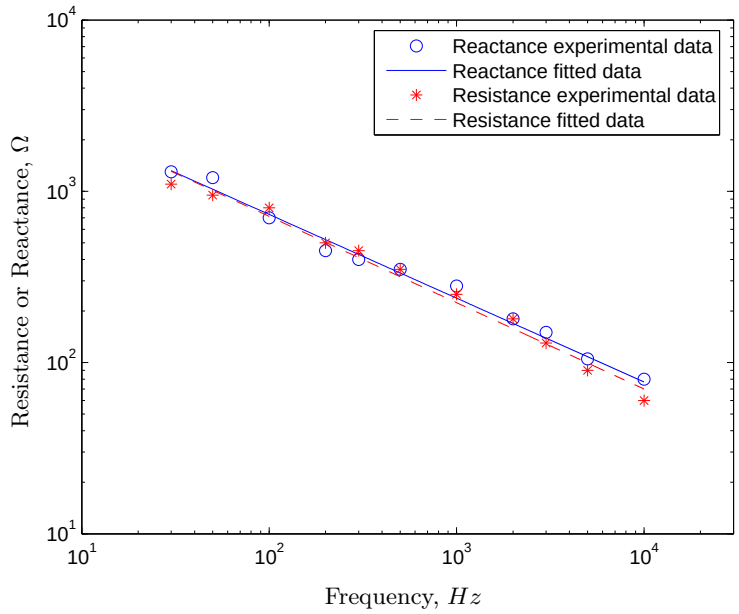

Figure 3.4: Combined plot of reactance and resistance vs frequency of stainless steel electrodes at a current density of 0.025mA/cm^2.

From Figure 3.4 one can see that the plots for both reactance ($X_w = 6963f^{-0.489}$, obtained from [24])

and resistance ($R_w = 7269f^{-0.504}$, obtained from [24]) lie very close together and with more or less the same values. One can therefore conclude that the Warburg model is sufficient to predict the impedance components of stainless steel electrodes at low current densities, since both equations are more or less equal to $7000f^{-0.5}$, confirming equations 3.2 and 3.1.

In addition to the basic electrode-electrolyte theory, electrode polarisation and electrode rectification must also be mentioned. Electrode polarisation was investigated by De Rosa and Beard [14] for smooth noble metal surfaces. They found that the electrical models that described the electrode-electrolyte interface were not sufficient to predict electrode polarisation. Their measurement data suggests that lower frequencies have higher polarisation impedances and that adsorption on the interface decreases the polarisation impedance with time up to a certain point, depending on the electrolyte solution as well as the type of electrode material. Therefore, their findings add another reason for allowing the electrode-electrolyte interface to stabilise before measurements are taken. Hause et al. [32] also found that measurements below 100 Hz suffered from nonlinear effects which they also ascribed to electrode polarisation. A study done by H. P. Schwan [56] found that electrode polarization impedances caused the electrode impedance to have a larger capacitance in biological materials than would normally be expected. In addition, the error increased with a decrease in frequency. These findings support the findings of Hause et al.

Finally, rectification for stainless steel electrodes was studied by Geddes et al. [25]. Rectification occurred when a high current density was applied to an electrode. However, they found that as the frequency was increased, the current density also had to be increased in order for the rectification effect to return. The historical study by Geddes [23] also mentions that electrode rectifiers were of the first uses for electrodes. A small area electrode paired with a large area electrode caused rectification at the electrode with the smaller area. The conclusion is that an electrode pair has to be comparable in surface area if electrode rectification is to be prevented, bearing in mind that the current density falls within acceptable parameters for one of them.

The development of the electrodes used in this thesis was mostly based on the work done by Hause et al. [32]. Their work provided a good starting point for the development of new probes, since they found that an electrode-electrolyte interface would detect the increase in bacterial growth. In addition, they provided an electromagnetic quantification of current density vs. probe area, an important facet for probe design.

The abovementioned theory, together with the paper by Hause et al., provides a set of constraints for any electrode designs. The constraints can be summarised as follows:

- Choice of frequency: Lower frequencies give larger impedance values for a specific current density, but also give larger impedance changes with a change in current density. If the frequency is too low, however, the electrodes could suffer from serious polarisation effects.

- Choice of current density: In order to preserve a linear relationship between frequency increases and impedance decreases, the current density must be low. High current densities cause the relationship to become non-linear and can even cause rectification to occur.

- Choice of measurement system: Although not specifically mentioned, the measurement electronics may require that certain electrode characters must dominate, or at least be measurable. This means that electrodes may be subject to further constraints, such as minimum (or maximum) electrode surface area, which translates into current density constraints.

With the knowledge of basic electrode theory and functionality, the theory of the measurement system

employed by this thesis to measure the electrode-electrolyte system can be explained. The core idea of the measurement system was taken from Hause et al.[32] and the electrode circuit model from Geddes et al. [24].

Firstly, the complete electric circuit for an electrode-electrolyte interface (at low frequencies) will be given by Figure 3.5.

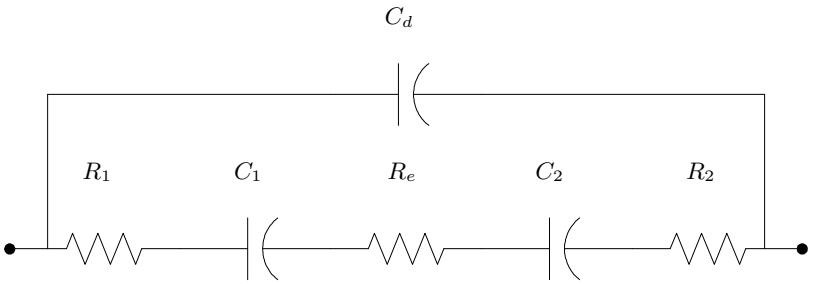

Figure 3.5: Complete electrode-electrolyte model.

C_d is the cell capacitance, assuming the electrodes are seen as parallel plates and the electrolyte as a dielectric, R_e is the resistive component of the electrolyte impedance which, at low frequencies, can be seen to represent the complete electrolyte model, R_1 and C_1 represents the resistive and capacitive components of the electrode-electrolyte interface of one of the probe conductors and R_2 and C_2 represents the other conductor.

Geddes et al. suggests that at low frequencies and with the geometric setup used in their paper, the cell capacitance C_d could be neglected. Therefore, the electrode-electrolyte model can be simplified to consists out of the two electrode-electrolyte impedances and the medium resistance. Indeed, if one assumes that the electrode geometry is of such a nature that the two electrodes are comparable, then the total impedance seen at the probe connectors can be described as a resistance with twice the value of a single electrode's resistance and a capacitance with half the value of a single electrode's capacitance , in series with the medium resistance. Experimental proof of the validity of these assumptions for the probes designed in this thesis can be found in subsection 3.3.2.

In order to use the probes as sensors, a measurement circuit must be designed to interpret the changes. The measurement circuitry itself was a basic setup - a simple resistor of predetermined value in series with the probes over which a sinusoidal voltage is applied. See Figure 3.6.

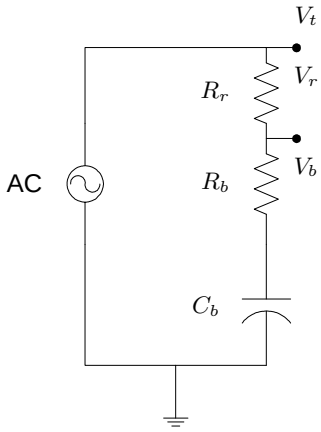

Figure 3.6: Probe measurement setup.

The measurement circuitry will require measurements to be taken at certain points: The voltage (V_t) applied across the total circuit impedances, the voltage (V_r) measured across the series resistor (R_r) and the voltage (V_b) measured across the probe (R_b and C_b).

The nature of the probe model requires that a sinusoidal voltage be applied over the probes. The sinusoidal nature of the voltage waveforms measured across the different components allows the use of phasors to calculate the different impedances' values. A phasor is a mathematical representation of a sinusoidal voltage (or current) and phase, defined as $V = A\angle\Theta$ (or $I = A\angle\Theta$ for current, where the amplitude (A) and phase angle (Θ) represents the time at which the waveform was viewed [48]. A graphical representation of a few phasors is given in Figure 3.7.

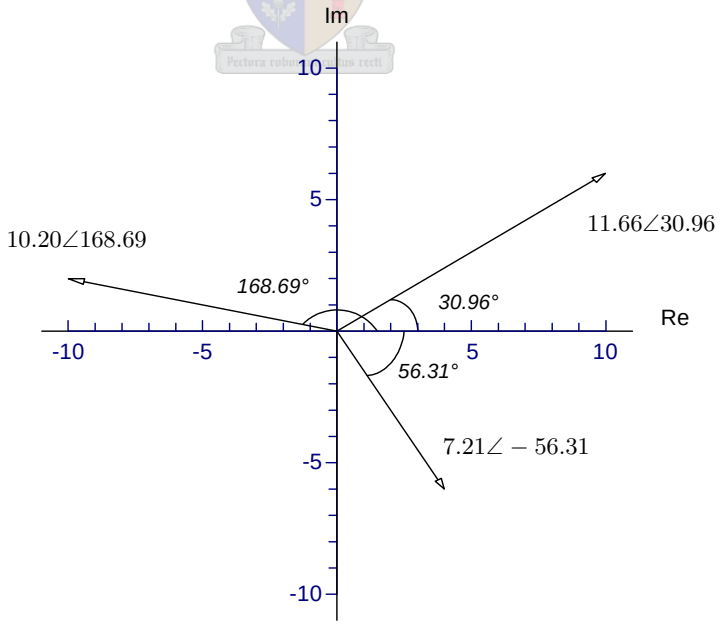

Figure 3.7: Phasor representations.

The nature of the measurement setup allows a few assumptions. Firstly, the sinusoidal voltage applied across the entire circuit is assumed to have zero phase shift. Secondly, the electrode-electrolyte model is assumed to be capacitive in nature, allowing the expectation that the phasor representing the probe voltages will always have a negative angle, or in other words, lagging phase. Lastly, the series resistor is purely resistive and adds or subtracts no phase shifts whatsoever, allowing the exact current to be extracted from this phasor.

Figure 3.8 will illustrate the expected phasor diagram for the measurement setup as described in Figure 3.6.

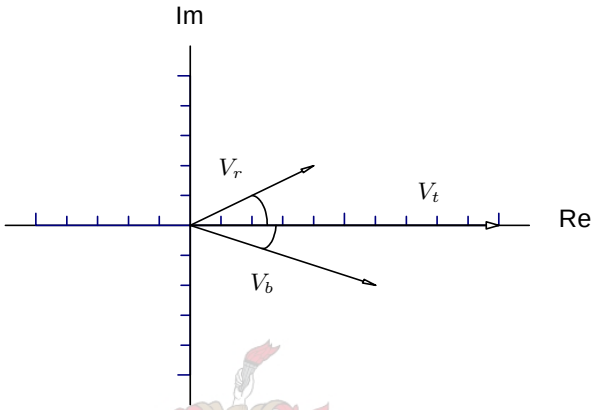

Figure 3.8: Phasor diagram of expected probe measurements.

The phasor diagram will in essence form a parallelogram, since the voltages represented by phasors V_r and V_b must add up to give the value of the total applied voltage, or phasor V_t. In other words, the phasors can be drawn differently in order to form a triangle. This will aid the understanding of the next step in the measurement system theory. Figure 3.9 will illustrate the changes.

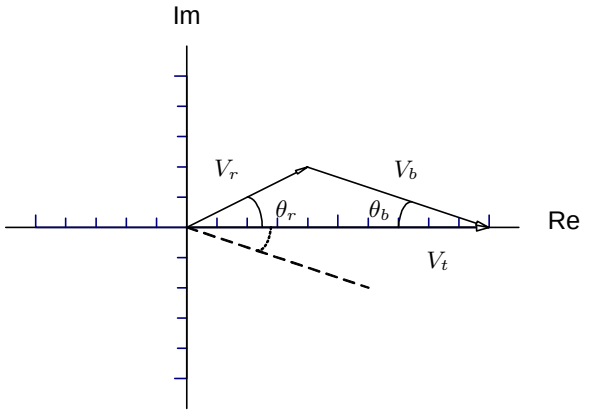

Figure 3.9: Triangular phasor representation.

The measurement system was set up so that the only measurements taken were that of the peak voltage values across the different components. The peak values represent the length of the different phasors, but

no phase information can be gained from this information. However, the fact that the different phasors form a triangle allows the use of the cosine law (or sine law) to determine the values of the angles subtending each phasor. Assume that the triangle formed by the different phasors of the probe system is represented by Figure 3.10

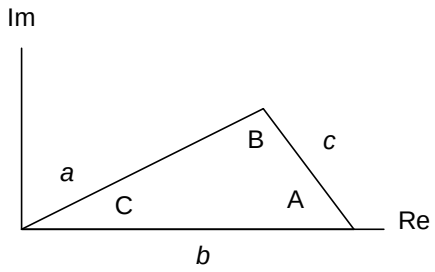

Figure 3.10: Cosine (or sine) law illustration.

The capital letters represent angles, the normal letters the amplitudes. Then, the cosine law can be written as follows:

$$a^2 = b^2 + c^2 - 2bc\cos A \tag{3.6}$$

The cosine law was taken from reference [42] but based on figure 3.10. Now, equation 3.6 can be rewritten to isolate the angle. This gives

$$A = \arccos\left(\frac{a^2 - b^2 - c^2}{-2bc}\right) \tag{3.7}$$

The same steps can be taken to find the other angle values.

If the variables a, b and c represent the phasors V_r, V_t and V_b then the angles A and C represent the phases θ_b and θ_b of phasors V_b and V_r respectively. Compare figures 3.10 and 3.9 to understand the connection between angles and the amplitudes. It should also be remembered that the angle of the phasor representing the voltage measured across the probes is negative, although the angle found from the cosine law will be positive.

The current flowing through the entire load can now be found by using the following equation (see Figure 3.6 for impedance variable names):

$$I = \frac{V_r \angle \theta_r}{R_r} \tag{3.8}$$

In addition, the probe impedance can be found by using the following equation:

$$Z_b = \frac{V_b \angle -\theta_b}{I \angle \theta_r} \tag{3.9}$$

Equation 3.9 can be rewritten to the following:

$$Z_b = \frac{V_b}{I} \angle (-\theta_b - \theta_r) \tag{3.10}$$

Equation 3.10 will give a result that contains an amplitude and negative angle (because both angles are negative, adding them together will always give a negative result). Therefore, the impedance will have the following form:

$$Z_b = R_b - jX_b \tag{3.11}$$

$$R_b = \frac{V_b}{I}\cos(-\theta_b - \theta_r) \tag{3.12}$$

$$X_b = \frac{-V_b}{I}\sin(-\theta_b - \theta_r) \tag{3.13}$$

Finally, the capacitance can be found from the reactance by using the following equation:

$$C_b = \frac{1}{2\pi f X_b} \tag{3.14}$$

The values of R_b and C_b represent the values of the entire probe system. Therefore, the true values of the probe resistance cannot be extracted from the resistance R_b, since it contains the medium resistance, but the true capacitance can be extracted. We know that there are two capacitors in series and if the probes are equal in impedance, the capacitance for one electrode is twice the measured capacitance. From here, the approximate probe resistance can be found by using Warburg's model, or equations 3.3 and 3.2.

A very important control point is the probe current density. The peak value of the current flowing through the loads can be found by getting the absolute value of equation 3.8. By assuming that the current density is uniform over the electrode surface area in contact with the electrolyte (based on the fact that the wavelength of the current waveform is much larger than the surface area in contact with the electrolyte), the average probe current density can be found by simply dividing the peak value of the current by the total surface area of one of the probe electrodes. The following equation will illustrate:

$$J = \frac{I}{A} \tag{3.15}$$

Where A is the surface area in cm^2 and I is the current amplitude, as calculated from 3.8, in mA. The choice of dimensions were determined by the literature and it allows for a direct comparison with their results.

3.2 Preliminary probe measurements

Criteria

Based on the theory, basic experimental setups can be devised in order to test the basic electrode parameters, as it was discussed in section 3.1. The experimental setups devised in this thesis would investigate the following variables:

- Probe material type
- Probe surface area tests
- Probe current density tests
- Probe sensitivity to electrolytic concentration changes
- Probe geometry - distance between electrodes and electrode shapes

- Probes in milk - the detection of the milk fermentation process

All of the tests would be guided by two factors: a minimum and maximum voltage application limit and a minimum and maximum detectable probe impedance change. The probes were tested and designed with the understanding that it would interface with a 5 V digital measurement system. The measurement system design is discussed in Chapter 5. Therefore, the tests will show what probe types work best within the 5 V system.

The reasons for the different investigation choices were based on their effects on measured impedances. Firstly, most of the data found in the different references used stainless steel probes. However, it was decided that different probe materials should be investigated in order to determine if an alternative existed that would function similar to the stainless steel probe type. Secondly, since probe surface areas affect the impedance of the probe directly, it was decided that knowledge of the linearity of the surface area changes vs. measured impedances were of great importance. This will allow for an ideal probe design, based on a minimal (or maximal) electrode surface area in contact with the electrolyte. Probe current density requirements were also of great importance. If a specific probe type had a large impedance value, the voltage levels (and therefore current levels) required to give the probe a certain current density might be too large or too small. The resulting voltage peaks measured across the probes might not be large enough for a 5 V system to pick it up effectively.

As far as sensitivity goes, if a certain type of probe's impedance changes more with a change in electrolyte concentration than another type of probe's impedance, then the first one would be the obvious choice for a sensor, since a large change is easier to detect than a small one.

Probe geometry should also be studied since a specific geometry might make measurements more (or less) accurate than another geometrical setup. Geometry has an practical implication as well, since it will allow one to determine the best probe manufacturing process. The geometry will finally indicate how an experimental setup should be performed.

Finally, the milk test. If the probes manage to perform well in all the criteria, they must perform well in this last test. If the probes do not detect a fermentation change, or somehow change either the milk, or change themselves within the milk, then their potential application falls away.

3.2.1 Initial probe investigations

The measurement setup was a basic one at best. The idea was not to characterise the exact values of every probe, but to test the approximate probe characteristics, as well as its potential application as a sensor within a milk environment. Figure 3.11 will illustrate the setup.

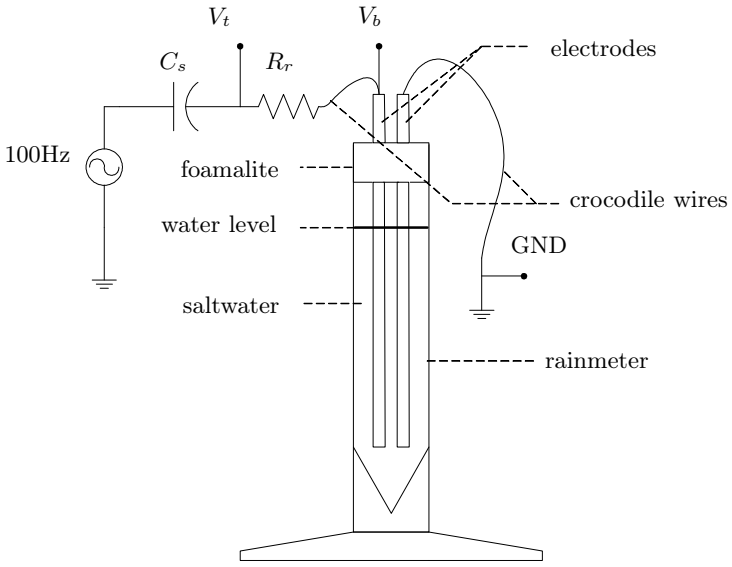

Figure 3.11: Initial experimental setup for probe evaluation

The measurement setup had the following elements:

- A 100 Hz sine wave generator. The make was a Goldstar FG-8002 and it was set to zero voltage offset. The voltage amplitude could be varied as needed.
- A 1μF capacitor (C_s) connected in series with the entire circuit. The capacitor acts as an extra precaution to any accidental voltage offsets, ensuring a centred AC wave. The reason that the AC wave must have zero offset voltage is that any DC current will cause electrolysis, effectively changing the entire measurement setup and causing different chemicals to form within the electrolyte. In addition, the DC current is not catered for by the Warburg model. The capacitor value is chosen large enough so that its effect on the circuit impedance is negligible.
- A series resistor (R_r). This resistor will have a known value and can be changed in order to obtain a certain current density through the probes, since different probe material types may have different impedance values which in turn affects the total load impedance and therefore the total current flowing through the system.
- A rain meter with a 127 mm diameter. The rain meter had a long and narrow chamber and was marked with 10 mm increments. The main reason for choosing a rain meter as a container was the fact that the container was narrow. This allowed testing of probes submerged into a liquid up to 50 mm deep, with room to spare. A bonus was the millimetre markings on the side, since it could be used as a gauge for liquid volumes. This allowed repeatability accuracy when the measurement setup had to be repeated.
- Saltwater. The saltwater would be made more salty as the experiments continued in order to test the probes' sensitivity to electrolyte concentration changes.
- Foamalite. The foamalite's purpose was to hold the probes in position as well as prevent the probes from falling deeper into the liquid once the required depth was obtained. Probes were immersed into

the liquid of choice in certain increments and the foamalite allowed the easy repetition of the different level setups.

- Crocodile wire extensions. The probes were not changed in any way from their basic rod-like nature. Therefore, in order to connect them to the rest of the electronic circuitry, crocodile wire extensions were used. It was assumed that the frequency at which was measured would not cause any stray capacitance values to be added because of the crocodile clamps and that the wires were short enough so that there would be no coupling because of 50 Hz devices. The clamps also allowed a certain measure of flexibility during the depth changes, since connections could be broken and remade easily.
- Probes. The different probes to be tested.
- Measuring points V_t, V_b and GND. These point would be measured by a Goldstar OS-9040D oscilloscope. The scope has an internal invert and add function that would allow the last required voltage wave V_r to be found, since it can not be measured directly from the setup.

The different experimental test parameters were mostly obtained from literature. However, certain decisions were based on the availability of the desired materials or the impact that a certain test might have on future designs. A discussion of the different parameters follow:

Materials: Types tested were copper, brass and stainless steel. The quality of the different probes could be described as average, since no extra polishing was done and no finish added onto the electrode surfaces. The copper material was obtained from a copper spool originally intended for a high voltage transformer coil. The copper could be bent to a straight rod and could keep its form, but lost its straight shaped quite easily of slight force was applied. The plastic around the copper wire was removed with a sharp knife before the probes were tested. The brass was obtained from brass rods that was available in the engineering faculty. The origin or purpose of the brass rods were not known. The brass rods were robust and did not lose their straight shapes easily. The stainless steel rods were also obtained from the engineering faculty. The rods were not of a high grade and were intended as welding rods. The stainless steel rods were also robust and kept their shapes throughout handling.

Concentrations: The different salt solution strengths were chosen in order to compare measured results to literature, as well as gauge the potential use of the probes in a higher (or lower) electrolytic concentration environment. Most of the literature used saline solutions to measure the impedance of probes in order to compare their possible use in a medical field. This meant that knowledge of different electrode-electrolyte impedances in milk was not available, which necessitated the different salinity concentration tests. The reason for this is that the saline tests could double as a calibration test, since milk might "look" like a certain concentration of salinity when certain probes are used as sensors. The different saline concentrations were chosen as: tap water, 0.5%, 1%, 2% and 5%. The concentrations were made by taking tap water (from the Stellenbosch water system) as base and adding a percentage of salt to the solution, based on volume. The volume of tap water used in the experiments was 150 ml, since this volume provided an ideal height in the rain meter. Therefore, a 1% salt solution meant that a mass of 1.5 g salt was added to the water and the solution stirred until the salt was dissolved. The salt was bought from the store and was iodated salt, or iodated sodium chloride, and contained free flowing agents.

Current: Current density values were chosen as 0.5, 0.75, 1, 1.25, 1.5, 1.75 and 2 mA/cm^2. The choices were based on the findings of Hause et al. [32] who found that the ideal current density range for their stainless steel probes was between 0.5 and 2 mA/cm^2. This would be the range used for all the probe types, since the desire was to find a probe that could be compared to, or do better than the stainless steel probes and in order to compare the different results, the same current density ranges need to be used.

Geometry: The probe geometry was a simple one during the experimental tests. All probes were space 10 mm apart, as measured from the centre of one electrode diameter to the centre of the other electrode diameter. As for the electrodes themselves, the simple geometrical shape of a thin rod was used for all the probes. The diameters differed slightly, though. The copper probe had a 1.7 mm electrode diameter, the brass probe had a 2 mm electrode diameter and the stainless steel probe had a 1.6 mm electrode diameter. The tips had no special shapes, but was a straight cut with the diameter of the rods.

Depth: The depth that the probes were below the water level would in effect test probe surface area effects, such as a potential increase in sensitivity with an increase in area, as well as determine at what depth the current densities that would be required by the probe would be beyond reach. The different depth parameters were chosen as 5 mm, 20 mm and 50 mm. The values were chosen arbitrarily, but was centred around the literature's typical experimental depth parameters, as well as electrode surface areas that were in contact with the electrolyte. Therefore, the surface areas tested per probe varied, since compensation was not made for the slight variation of each type of electrode's diameter. Table 3.1 will give the different surface areas tested per electrode:

Table 3.1: Surface areas tested per depth setting per probe type

Depth (cm)	Copper (cm^2)	Brass (cm^2)	Stainless Steel (cm^2)
0.5	26.7	31.4	25.1
2	106.8	125.7	100.5
5	267.0	314.2	251.3

Table 3.1 shows that the surface areas of brass vary up to 25% from stainless steel and that the size difference between the surface areas became larger with increased probe depth. Therefore, when a final judgement was made into the suitability of brass, this had to be taken into account.

Measuring: In order to measure the peak values of the different voltages as it existed over the different components, the oscilloscope had to be connected to the points marked V_t and V_b in Figure 3.11. Therefore, the crocodile clamps were connected so that the two negatives were connected to GND and the two positives to the two measuring points respectively. The voltage V_t was connected to channel one and the voltage V_r to channel two. Channel two could be inverted by hardware situated within the oscilloscope, allowing the third voltage to be found (and displayed) by adding the voltage V_t and the inverted voltage V_r through the oscilloscope's add function. The peak value of every voltage waveform was read off on the smallest voltage division possible, in order to prevent unwanted roundoff errors from entering into the experimental results. Equations 3.6 to 3.15 can then be used to find the current density and probe impedances.

The experimental procedure involved a lot of repetition. To begin with, the required salt solution would be poured into the container. The probe type of choice would then be inserted at the deepest depth, and the electronics connected. The generator and oscilloscope would be switched on but not connected, to allow the machines to warm up and stabilise. The warm-up procedure would be done only if the systems were previously switched off, not before every measurement. The systems would then be connected but measurements would only be taken and hour after probe insertion in order to allow the electrode interface to reach equilibrium. The measurements involved starting at the lowest current density of choice and increasing the current density in increments up to the maximum current density of choice. The probes would then be raised higher and the process would be repeated. It was assumed that the equilibrium would remain stable for the probe surfaces still in contact with the electrolyte and therefore no extra stabilisation time was added after the electrodes were lifted. Once one set of probes were completed, another probe type would be inserted into the same solution and the entire measurement process repeated. If all the probe types were tested, the salt solution would be replaced with a stronger concentration of salt solution and the entire process repeated for every probe.

The measurement results can be found in Appendix A. The basic comparisons between the different probes will be given here. However, comparisons will only be made on the 2 cm depth and the 1% saline solution since this specific measurement was the best one to compare to the experimental results from the paper by Hause et al. Comparisons between probe impedance values for a specific depth but different salinity concentrations will also be given.

Firstly, Figures 3.12 and 3.13 will give the different impedance components.

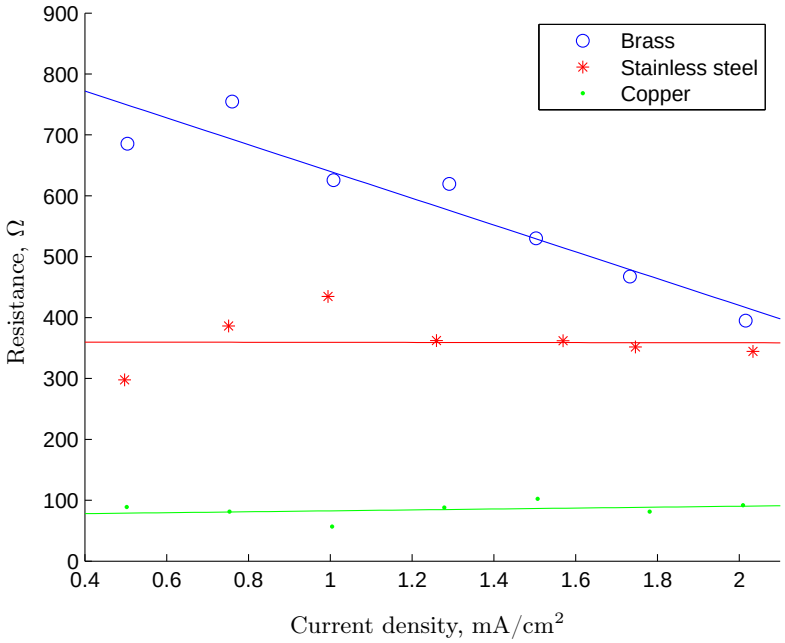

Figure 3.12: Total probe resistance for different probe material types. The lines represent a simple linear fit (done by Matlab) for the impedance's path of change.

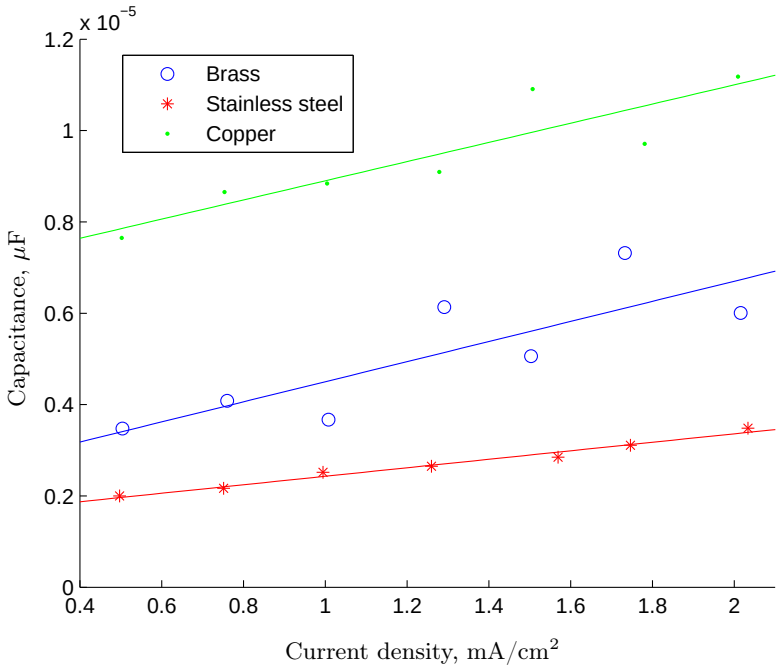

Figure 3.13: Total probe capacitance for different probe material types.The lines represent a simple linear fit (done by Matlab) for the impedance's path of change.

Secondly, figure 3.14 will give the comparative impedance measurements per electrolytic solution strength.

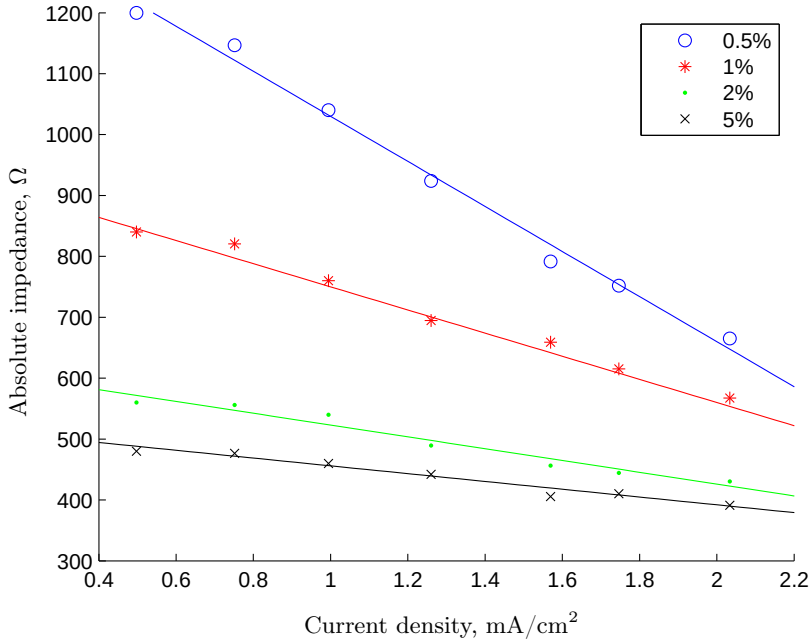

Figure 3.14: Comparison between different impedance curves for different saline concentration strengths as seen by stainless steel electrodes.The lines represent a simple linear fit (done by Matlab) for the impedance's path of change.

Figures 3.12 and 3.13 have a few interesting features, but the most important piece of information that can be gathered from the graphs is the flatness of the impedance values. The measured points are represented by circles, dots and asterixes respectively. The range of current density points should allow for this approximation, since the stainless steel probes should not change abruptly in this range. Based on the fitted line, it can be seen that stainless steel electrodes have more or less the same resistance over the current density range, but that the capacitance has a slight increase with current density. Copper electrodes also keep the same values across the current density range, but the capacitance increases at a greater angle. Brass electrodes, however, do not share the same flatness. The resistance drops with current density and the capacitance increases at more or less the same angle as the copper. One reason for this could simply be that the linearity range for brass falls far below our working current density test range.

The resistance and capacitance values also indicate that a brass electrode in contact with saline will have a higher impedance value when compared to the other probes. This is especially true if one remembers that the brass probe had a larger surface area in contact with the salt solution but that probe impedance decreases with an increase in surface area (Appendix A). The higher impedance could be an advantage if a low current system is sought after.

Copper presents an interesting scenario. Its resistance resembles a similar flat line to stainless steel, but its capacitance does not. In addition, the impedance of copper electrodes seem to be very low. If the probe impedances are too low, then it would mean the voltages required to obtain the necessary current densities might be too low to detect. However, a factor called probe roughness will have a profound effect on impedance measurements [24] and since no probe was polished, the copper probes are not disqualified yet. Probe roughness will be elaborated on in section 3.3.

Figure 3.14 shows the plots of absolute impedance. Absolute impedance is simply the absolute value of impedance as found through equation 3.11. To put it in equation form, the absolute impedance can be written as:

$$|Z_b| = \sqrt{R_b^2 + X_b^2} \tag{3.16}$$

Another name for the absolute probe impedance is the magnitude of the probe impedance. The reason that the magnitude plot is considered important is because the Warburg model shows the real and imaginary part of the probe impedance to be more or less equal to each other. This means that the absolute value of impedance will be influenced equally by the real and imaginary components. Therefore, the probe's magnitude plot can be seen as a good representation of the typical curves that either the resistance or reactance of a probe will follow.

Figure 3.14 clearly indicates that an increase in the salinity concentration causes a measurable decrease in the probe impedance. This is good news for a potential fermentation detection, since theory has indicated that an increase in milk sourness is cause by lactic acid and other bacterial metabolites. This increase in metabolites can be represented by the increase in salinity concentration. The absolute impedance does not follow a flat figure, though. The decreasing nature in the absolute impedance graphs can be explained if the paper by Geddes et al. [24] is investigated. In their paper, the electrode impedance linearity already showed an increase in capacitance or decrease in resistance past the 0.5 mA/cm^2 point. In addition, the 20% increase locus lies just before the 2 mA/cm^2 point. If this data is taken into account, then the absolute impedance graph, as illustrated by these findings, will have a decreasing nature. These values translate into big impedance components that in turn cause a larger gradient in the graphs. Based on figure 3.14, it can be said that the current density choices will cause an inherent non-linear nature, but it is assumed to be

within an acceptable parameter decrease, or 20% from the linear region's impedance.

Figure 3.14 only shows the values for stainless steel, but the other probes showed the same effects. Again, refer to Appendix A. As a final graph, the total gathered information will be displayed in figure 3.15. The figure will only display measurements made by stainless steel electrodes.

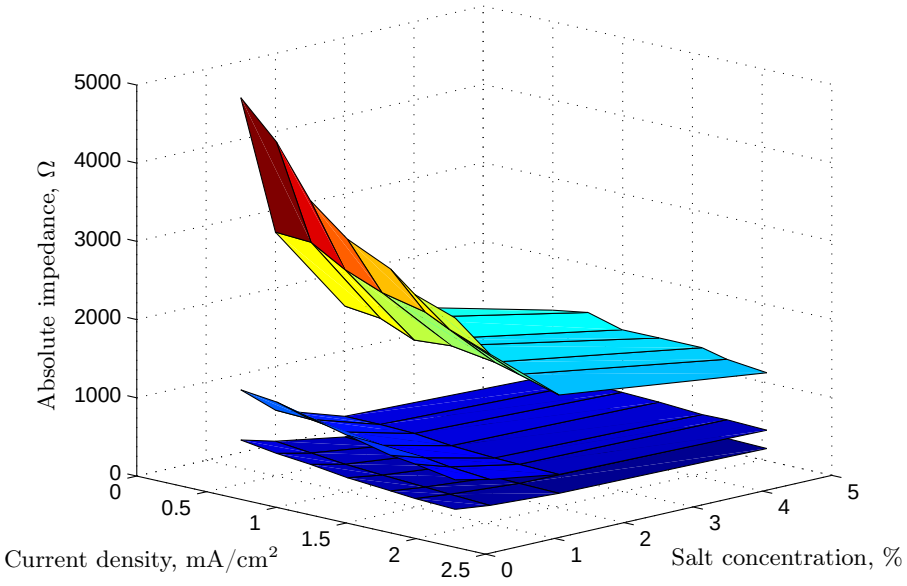

Figure 3.15: Stainless steel impedance values based on current density, salinity concentration and surface area (probe depth).

Figure 3.15 displays the entire spectrum of data within one volumetric space. The three separate areas resemble the three different surface areas, or depths of measurement. In this case, the top contour resembles measurements taken at the depth of 0.5 cm, the middle one measurements taken at 2 cm and the bottom one measurements taken at 5 cm. The axis has all three zeros on the bottom left point of the graph so that the dimensions of height, depth and width resemble increases in impedance, salt concentration and current density respectively.

The 2000 Ω drop that seems to exist between the 0.5% and 1% salinity concentrations for the 1 cm depth requires some explanation. It can directly be ascribed to measurement errors, since at this depth, the probes have a large impedance which translates to a large voltage drop. In turn, the voltage that is measured over the series resistor becomes small, so that it is difficult to measure through the simple measurements setup used in this experiment. In addition, a 0.5% salinity also causes the probes to have a large impedance. The result is that the voltage drop over the probes are comparable to the applied voltage and the oscilloscope's internal inverter ends up showing a such a small voltage waveform that the measurement certainty drops severely. Therefore, the values at low salinity and low surface area contact should be considered estimates, at best.

3.2.2 Initial measurement in milk

The final test was to investigate the probe's performance in milk. The milk used was fresh milk bought from the store. It was still well before its use by date, so it was assumed that the milk would have minimal bacterial activity. It was produced by Fair Cape and was full cream milk. The milk was poured into the rain meter and the millimetre markings on the side was used to check if the volume of milk was the same amount as the volume of salt water used. After it was poured in, the milk was spiked with a small amount of bacteria obtained from already sour milk. The probes were inserted afterwards and left for an hour in order to allow the equilibrium to stabilise. The average measurement time was at intervals of about 10 hours. The temperature was not controlled, as the entire experiment was set up in an open lab room in the fourth floor of the electronic engineering faculty. This meant that temperatures hotter than ambient could be expected, which at the time of the experiment was between 24 and 30 degrees Celsius. These conditions should be more than acceptable for bacterial growth.

The measurement setup was exactly the same as for the saline solutions (refer to Figure 3.11. However, it was decided to test only one depth (5 cm) and at one current density value (1 mA/cm^2). The reason is a practical one - redundancy. The knowledge gained with the previous salinity measurements have shown that the probes tend to have similarly shaped impedance curves vs. current density for different surface areas in contact with the electrolyte. Therefore, one surface area will suffice to show the general tendency of the probe as a whole. The 5 cm depth was chosen since it was found that it was the depth at which the probe's voltage drops could be measured more accurately when compared to the other measurements. In addition, the current density choice was based on the fact that it was more or less the centre point for the current density range and the choice would make the data comparable to the work done by Hause et al.

During the milk fermentation process, it was ensured that the current density remained constant throughout the entire measurement cycle. To do so, a few measurements were taken, the current density calculated and if it was too low or too high, the voltage adapted, based on previous calculations. Once the current density was in an acceptable range, the measurements were finalised. Every probe was also given its own test run, since probe removal was not an option once the experiments began. The reason the probes had to stay inside the container was so that it could be ensured that there could be no potential probe contamination. There had to be certainty that the change in data was because of the milk fermentation process and not an accidental probe interface change.

The initial measurement results put the data gathered by the probes at the start of the experiment at more or less the same values as data gathered by the probes in a 1.6% saline solution. However, too little information existed around the potential comparisons between probes in milk and probes in a solution with a certain percentage of salt. It did, however, indicate that any future milk probe designs could be roughly based on the probe's characteristics in a salt solution.

At around three days after the experiment started, the milk started to curdle and the experiment was stopped. The data for the brass and copper probes indicated that these two probe types were of no use in milk. Neither of the probes' impedance changed during the three days. This meant that the probes could not detect the fermentation process. The stainless steel probes did detect a change, though. At around day two the impedance components started to drop.

Here is a graph of the basic data points as it was found for stainless steel.

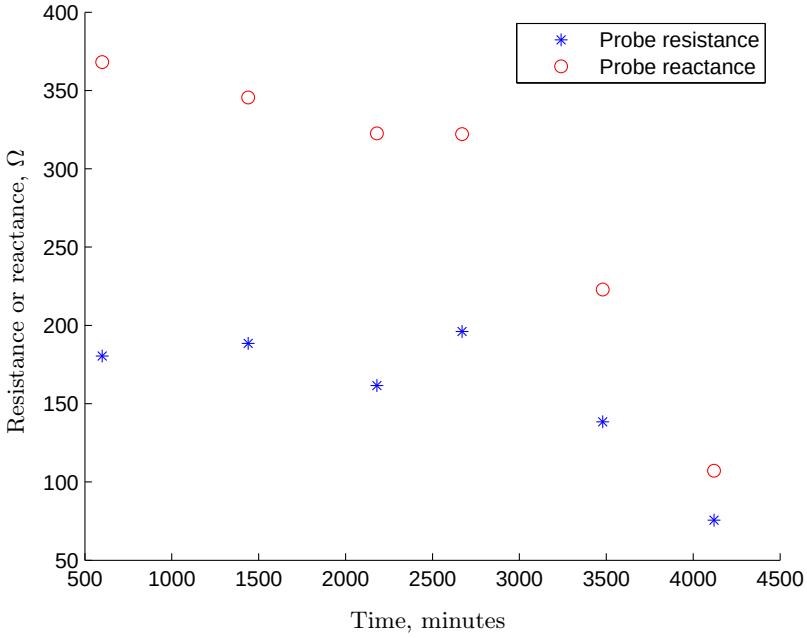

Figure 3.16: Stainless steel probe measurements in milk.

Based on the preliminary data obtained from this test run, it was decided that all future probes would be made from stainless steel. In addition, the data shows that the probe resistance and reactance values drop to about 40% of its original values, a drop that should be readily detectable.

3.2.3 Measurement conclusions

The different probe characteristics gave a broad idea of what to expect when a certain probe material type was used to measure a solution with a certain electron mobility (or in other words, salinity concentration). The different measurements showed that all metal types exhibited a sensitivity to electrolytic changes. This meant that all the probe types could effectively be used to measure changes in milk, if the changes were comparable. However, the tests done in milk revealed that only certain materials were effective at detection milk fermentation. More studies need to be done in order to determine what these materials are, but this study ruled out brass and copper as candidates. It is not certain why brass and copper displayed an insensitivity to milk fermentation, but one theory suggests that the brass and copper formed an oxidisation layer on the surface which overwhelmed the interface capacitance and resistance. The result was that the fermentation process had a minimal effect on the total capacitive and resistive components of the electrode-electrolyte interface, causing it to remain constant with change. Studies of the brass and copper probes after the milk experiment did reveal a discoloration of the metal surface. Cleaning of the probe surface had a minimal effect of removing the discoloration, suggesting a change on the molecular level.

The different probe materials also had more or less the same impedance curves, based on current density and electrode surface area. In each case, the impedance decreased with an increase in current density and also decreased with an increase in electrode surface area. Comparisons between the different materials put brass as the material that develops the highest interface impedance, followed by stainless steel and copper.

However, these comparisons may not be valid since no attempt was made to make the probe surfaces as smooth as possible. Most of the literature did so with their probes. Once again, the reader must remember that the different impedance curves obtained by the initial experiments was only required to show how different metals reacted to the electrolytes surrounding them, not give an exact characterisation of the materials themselves. However, the reason the results can be used even with unpolished probes was that the impedance curves obtained from them would follow the same general lines as the impedance curves obtained from literature, albeit at a value different from theirs. The fact that the stainless steel did follow more or less the same impedance curve as existing literature confirms this statement.

The different impedance characteristics also allowed an assessment to be made about the different probe constructions. The measurements showed that electrode surface area is directly proportional to the probe's capacitance and inversely proportional to the probes resistance. The more electrode surface area is in contact with the electrolyte, the less the resistance, but the higher the capacitance becomes. Therefore, an ideal probe impedance can be designed based on available voltage and current supplies. Probe with low impedances, or rather, large electrode surface areas in contact with the electrolyte, will have low voltage drops over them, but will require a large current to flow in the system in order to reach a high enough current density level. Inversely, a probe with a high impedance, or small electrode surface area, has a large voltage drop but requires little current to obtain a high enough current density level. Therefore, the conclusion that can be drawn from the impedance characteristics is that current density is the greatest deciding factor in electrode design. A measurement system must be able to provide a high enough current density without compromising on the ability to detect small changes.

As an example: The measurement system, using copper probes measured at a depth of 5 cm and at a current density of 0.75 mA/cm^2 with a 1% salt solution, had the following voltages: $V_t = 0.72$ V, $V_r = 0.64$ V and $V_b = 0.22$ V. In a 2% salt solution, the voltages measured as: $V_t = 0.68$ V, $V_r = 0.64$ V and V_b 0.16 V. If we assume that the minimum change that needs to take place before it is detected is 20 mV, or 0,020 V, then the voltages measured over the probes for the 1% and 2% have three detectable jump between them, or 60 mV. If one considers that a single jump error can cause a third of the information to be lost, then the conclusion can be made that the system is too sensitive to noise.

Finally, the measurements in salt water and milk allowed a basic calibration to be developed. Stainless steel probes showed to have the same impedance in fresh milk as they had in a 1% salt solution. Therefore, probe design could be tested and retested in saltwater before any form of milk had to be tested. This allowed for a much cleaner and faster development procedure to be followed, since no biological system would be involved in the initial probe design. However, since the stainless steel grade was unknown, the initial calibration system obtained from these values could not be taken as a universal stainless steel calibration, until more stainless steel grades were tested.

3.3 Other measurements and observations

During the experimental procedure, and following, quite a few observations were made concerning adverse probe effects. An adverse effect was considered to be anything that caused the measurements of the probe impedances to be either different than previous measurements, or cause unfavourable results. In addition, certain modifications were done to the probes and the resulting measurements investigated. The findings will be discussed in this section:

3.3.1 Probe roughness

The greatest factor influencing probe impedances is probe roughness. Probe roughness refers to the surface area quality of the electrodes in contact with the electrolyte. If the surface is polished, it is considered smooth, whilst a surface containing lots of handling damage, such as scratches and knocks, is considered rough.

Geddes et al. [24] mentioned that probe roughness had a marked effect on measured probe impedance, specifically capacitance. Increasing the effective area through probe roughening also increased the probe's capacitive attributes. Local tests showed that a smooth probe surface containing a single deep scratch already lowers the impedance of that probe to a completely different value. Further tests with sandblasted and smooth stainless steel probes were done by connecting a single series resistor to probes with around 1.5 cm surface area in contact with a 1.6% salt solution and applying a 1.8 V 100 Hz sine wave across them. The smooth probe caused a voltage drop of 0.85 V over the series resistor, whilst the sandblasted probe caused a voltage drop of 1.6 V over the series resistor. Depending on the vector of the probe impedance (since it was not explicitly measured), the probe impedance can have a 25% to 50% impedance decrease simply because of probe roughening.

Probe roughening could also explain why the copper probes measured during the initial experimental measurements had such a low impedance when compared to the other probe types. The way the copper probes were cleaned left a lot of scratches on the surface and in light of the measurement made afterwards the lowered impedance values were blamed on probe roughening.

In an attempt to find alternative stainless steel probe sensor options, sandblasted stainless steel electrodes were also tested in milk. The results showed that the roughened probes could not pick up the fermentation change. It is not known why this was the case, since the same sandblasted probes did pick up changes in electrolytic concentration changes when tested with salt water. One theory is that the upper limit of detection was reached when the probes were inserted into fresh milk and therefore any rise in electrolytic concentrations would not be detected.

Needless to say, a lot more studies need to be done in order to find a proper model for probe roughness. Geddes et al. also suggested a probe augmentation factor in order to compensate for the probe surface area effect. This augmentation factor would allow one to compare all probe measurements to the "ideal" smooth probe and allow probes made from the same material but displaying different impedance values in the same electrolyte to be compared regardless of their inherent differences.

3.3.2 Distance tests

Distance tests refer to the geometrical probe configuration parameter of distance between the two probe electrodes and the effect that this distance has on the measured probe impedance. The tests done involved stainless steel electrodes that were placed at certain distances from each other in different saline concentrations. The results showed the following:

- At lower saline concentrations, up to about 1% saline concentrations, the effect of probe distance could be detected. More detail to follow.
- Above 1% saline concentrations, the effect that distance variations had on the measurements seemed to disappear. No difference in voltage amplitude could be detected between electrodes which were 50 mm apart and electrodes which were 1 mm apart.

The lower concentration solutions revealed that the probes had a very high impedance and as the electrodes moved closer together, the impedance would drop down to a minimum value. If we follow the Warburg model, we know that the electrode electrolyte interface has three components: electrode-electrolyte capacitance, probe resistance and electrolyte resistance. Since the interface capacitance and probe resistance is not distance dependant, it would suggest that the medium resistance is so large that distance variations cause medium resistance variations comparable to the interface impedance. Distance variations cause resistance variations since the resistance of a material is determined by the amount, or type, of dielectric an electron has to flow through and so, if the distance is short, the resistance is small.

However, the more the electrolyte becomes ionic, the more the medium resistance becomes smaller and smaller up to a point where a large variation in distance is no longer detected. This would mean that the electrodes would measure the same impedance in a strong ionic solution simply because the electrolyte resistance component differences are no longer detectable. Added onto this is the fact that at 100 Hz, the probe interface components dominate the measured impedances.

Since it was found that milk looked the same as a 1% saline solution to stainless steel probes, and since the distance variation tests showed stainless steel probes to detect the same impedance in a 1% solution whether close or far apart, it was decided that probes made for milk would be designed around practical use, not distance issues. Finally, the lack of measurable change caused by distance variations also confirmed that the inter-probe capacitance element between the two probes could be considered small enough to ignore. The assumptions of section 3.1 are therefore confirmed by these distance tests.

3.3.3 Probe isolation

One of the major modifications considered in the probe design was a surface area isolation layer. This layer would allow the quick and effortless insertion of probes into a medium of choice, without having to check liquid level or probe placement, since the isolation layer would prevent any other part of the electrode to form an electrode-electrolyte interface other than the uncovered surface area. A surface area of depth of 2 cm can therefore be simulated by creating a probe with a 2 cm open area and then just placing the probe as deep as it wants to go, over and above the required surface area contact requirements.

Hause et al. mentioned that their probes did not have an isolation layer in order to maximize the stability of measurements during a four-wire electrode measurement. The four-wire electrode measurement is typically used to negate electrode surface effects. They also mention that the four-wire technique will be predominated by media effects. Therefore, adding an isolation layer to a two-wire probe in a highly conductive solution - a situation that is expected in milk and that has been measured in the 1% saline solution - should not adversely affect measurements. The distance tests have revealed that the probe impedance is dominated by the electrode-electrolyte interface and that the media resistance has a minimal effect.

The isolation layer of choice was heat shrink. Heat shrink is a plastic tube that shrunk to more or less half its diameter when heated and remained in that form after the heat was removed. It is typically used to isolate electric conductors from potential human contact. Heat shrink was applied to a few stainless steel electrodes and a surface area of 2 cm in length was left open. Initial tests involved leaving the probes in a liquid and checking if the heat shrink prevented any capillary action, or experienced gradual moisture absorption. The heat shrink was then removed and the probe surfaces that were underneath the heat shrink as well as the heat shrink itself were studied. The tests proved that heat shrink was a good isolation medium, since no water was absorbed and no water seeped in underneath the heat shrink isolation layer.

Tests were also done to test the effectiveness of the heat shrink isolation. The probes were inserted into a 1% saline solution and slowly pushed deeper whilst the measured voltage waveform over the probe was watched closely. As the probes were pushed deeper, the voltage measured over the probes decreased and at the exact point where the isolation started, the voltage magnitude did not decrease with an increase in electrode depth. Therefore, as far as the minimum probe impedance could be controlled, the isolation proved effective.

Further tests involved closing off the electrode tips. The electrode tip was an area that was hard to control, since manufacturing exact probe tips proved difficult and probe tips tended to concentrate the electric field toward itself. Therefore, it was theorized that isolation of the electrode tips would further stabilise the electrode-electrolyte interface layer and in so doing, raise the probe impedance values. A practical reason for closing off the tips was that during experimentation, it was found that the probes could end up resting on the bottom of the container and part of the electrode tips could be isolated from the electrolyte. A very slight impedance rise was detected when this happened. Therefore, in order to avoid this situation altogether, the tip isolation option was applied.

Measurements were done with probe electrodes having a 2 cm isolated front end, then a 2 cm open area, then again isolated for the rest of the probe length. The probe was then slowly lowered into a 1% saline solution and the voltage waveform studied. The voltage measurements for a probe that had no contact with an electrolyte showed that almost all the applied voltage was lost over the probes and that the series resistor had almost no voltage over it at all. As the probe was lowered deeper into the solution, the probe impedance, which at this point was very high, was observed to decrease very slightly with depth. However, as soon as the open surface area got into contact with the solution, the probe impedance would be dominated by this layer and further increase in depth beyond the open surface area did not cause a further decrease in impedance.

The conclusion is that in a typical measurement environment, the effect that isolation has on probe impedance is minimal, at best. The impedance values will be dominated by the open surface area in contact with an electrolyte. In addition, the isolation proved effective in ensuring that only the surface area of choice was ever involved in forming the electrode-electrolyte interface layer. It was decided that all subsequent probe designs will contain these isolation layers.

3.3.4 Bubbles

One of the more troublesome occurrences was the forming of bubbles at the electrode surface. Bubble forming is known to happen, since some literature pieces specifically mention removing any bubble from the electrode surface. The formation of bubbles cause the impedance of the probes to behave erratically, since the interface layer cannot form normally.

Bubbles formed on probes inserted into the different saline concentrations during different experimental tests. The position and speed at which bubbles formed was random, so no prediction could be done on probe shape or bubble formation probability. Therefore, probes were actively monitored and were shaken around if any bubbles formed on the electrode surfaces.

Bubble formation within milk could not be monitored visually. Therefore, preliminary impedance measurements were checked to see if such formation did occur. Nothing obvious was detected, so it was assumed that if bubbles did form, it did not have a drastic effect on the probe impedance.

3.3.5 Milk effects

During the fermentation of milk, the milk coagulates and separates from the whey proteins. Observations have noted that the separation first causes the milk to form "pockets" of whey areas, but after a while the curd and whey separates completely as the curd rises to the top. The effect that this separation has on probe impedance measurements cannot be said for certain. However, the point at which milk coagulates is considered well beyond the limit at which milk is considered drinkable. Therefore, measuring the probes at this point is considered pointless, since it is already well into the fermentation process and most people will get rid of milk well before it reaches this state.

The effects are mentioned in order to confirm that the state of the milk does not interfere with the initial detection of bacterial growth. Tests were done in these environments, however, and it was found that the probes and the heat shrink survive such environments. In addition, it was found that at the point where milk starts to separate into curd and whey, the probe impedances tend to stabilise at a minimum value. However, repeatability tests were not performed in this area, since the focus of the probe tests were on milk fermentation, not potential cheese forming processes.

3.3.6 Probe cleaning

A factor that had a profound effect on experimental repeatability was probe cleansing. The literature all have different ways in which they cleaned their probes, but in general it involved some form of acid or ethanol cleansing, followed by a rinsing in distilled water. This thesis used the ethanol and water method.

Tests on the effect of probe cleansing was done with a few basic milk fermentation tests. Probes were cleaned as mentioned and place into fresh milk (long life full cream). The milk was spiked with bacteria and allowed to ferment. After the milk coagulated, the probes were removed, only cleaned with water, then reinserted into another experimental setup with a new batch of fresh long life full cream milk. The results showed that the probes showed an impedance value similar to the value it had at the end of the first experiment. This result is clearly false, proving that probe cleansing has a marked effect.

3.3.7 Voltage wave distortions

One of the stranger effects noticed during multiple probe tests was the sine wave distortion of voltages measured across the different circuit elements. The reasons for these distortions could not be determined, but the author feels it necessary to mention the distortions in case other researches come across it. These distortions were measured in saline solutions.

The distortion took on different forms. One of the basic distortions was the flattening of the voltage peak measured across the different components. Another distortion took on the form of a asymmetrical voltage wave, where the positive peaks and negative peaks had completely different shapes and values. The positive peaks had a fattened sine wave look, whilst the negative peaks had a triangular look.

Investigation into the reasons for the voltage distortions showed that the surface area had a slight effect on the amount of distortion. If the surface area decreased, the wave's distortion increased, up to a maximum effect. What that maximum was depended on the probe, it seemed, since it could not be reproduced.

As a final piece of information, the probes used were stainless steel probes, grade 316 (surgical stainless steel) and the probes were constructed so that 20 mm surface area was in contact with the electrolyte. The rest of the electrodes were covered in heat shrink and the probes were close together (1 mm apart). The

distortions were tested in different concentrations of salt solutions and it was found that the distorted waves looked their worst in a 1.2% salt solution.

The reason these waves are considered a problem is that the voltage peaks used in the different equations in order to determine the probe impedances cannot be used unless the voltage waves are sinusoidal in nature. Any other wave type would require a different set of rules to be applied, since the phasor rule only works for sinusoids. It was therefore considered paramount to develop probes that would allow the proper formation of sinusoidal waveforms.

Finally, these distortions were only seen with two sets of probes. No other probes showed any side effect whatsoever, but these observations meant that each probe had to be tested before it could be considered usable. Unfortunately, the waves could not be captured or simulated for this thesis.

3.4 Final Probe construction.

All of the information gathered by the different experiments has allowed a probe manufacturing and testing scheme to be developed. The ideal probe surface area and roughness, the typical probe geometry as well as the different practical issues surrounding the final probe construction will be discussed in this section. In addition, the steps taken to construct the probes will be given here.

3.4.1 Basic construction criteria

The material type used in the final probe constructions was chosen based on the types used in the different literature studies. For the most part, their material of choice was surgical stainless steel, or stainless steel grade 316, and the diameter of the electrodes used by Hause et al. were no more than 0.064 cm. The electrode diameter of the probes used in this thesis was four times that of the literature, at around 0.25 cm.

The multitude of tests and voltage requirements has led to the conclusion that the ideal surface area length that the stainless steel electrodes needs to have in contact with the electrolyte is around 1.5 cm. If a comparison is made between the wire electrodes' surface areas used in Hause et al. and the typical surface areas of the wire electrodes as used in this thesis, then the following can be noticed:

- Hause et al. electrode surface area: $\pi.0,064.2,54 = 0,51$ cm^2.
- Thesis electrode surface area: $\pi.0,25.1,50 = 1,178$ cm^2.

Or in other words, the surface area of the electrodes used in this thesis was chosen to be twice that of the electrode surface area used by Hause et al.

The probes were constructed in such a way that the general distance the electrodes were positioned from each other was 1 cm. However, because of slight lengthwise electrode warping and the fact that the connectors used to keep the electrodes from each other was slightly flexible, this distance varied between each probe. However, the tests and measurements done beforehand determined that this would not be an issue in the environments that these probes would be used in.

Finally, the surface roughness that would be used would be as smooth as possible, since any roughened probes proved difficult to predict and very rough probes did not work at all in the milk environment, as determined by previous tests.

3.4.2 Final manufacturing

The manufacturing method involved a lot of human interaction, but it is something that could not be prevented. The human element caused variations between each probe sensor and it is this variation that will inevitably lead to differences in probe impedance measurements. However, as far as was possible, the following exact manufacturing steps were followed:

1. The stainless steel rods were cut into lengths of around 20 cm using a fine toothed metal saw. Stainless steel is a hard material, so the rods had uncut edges where the rods broke apart from each other once sawed through. Absolute care was taken that no saw marks were left on the metal surface, as this would dramatically increase surface roughness and would not be polished away easily.

2. The rods were taken to a sanding machine where the jagged edges were sanded off. This will prevent the probe tips from damaging any heat shrink isolation as it is applied.

3. The rods were now taken to a turntable. The turntable would then be switched on and used to check the straightness of the rods, since the rods would clearly spin off-axis if any warping existed in its length. The rods were then bent into position until no off-axis elements were present during spinning.

4. The rods would now be sanded with the smoothest sandpaper available, or in this case, emery paper. The rods would be sanded axially and a slow up and down movement utilised in order to sand about a 5 cm section of electrode, as measured from the tip. The up and down procedure would be done around three times in order to give a system of reproducibility.

5. Brasso would be applied after the sanding was complete. The same up and down motion would be used to polish the electrodes until a bright sheen appeared. The up and down motion would once again be repeated three times.

6. After the Brasso was applied, the probes would be further cleaned and polished by applying a cloth and using the same up and down motion until the electrode left no more residue on the cloth. No water was applied in any of the steps.

7. The polished rods would now be cleaned with ethanol and left to dry.

8. After the ethanol, heat shrink with a diameter of 3.6 mm would be slipped over the rods. However, the wire extensions required to connect the probe to the rest of the circuitry would be stripped and wound around the stainless steel before the heat shrink was slipped over. Heat was applied until the heat shrink fit tightly around the stainless steel. Care was taken to ensure that at least 3 cm of open probe length was still present at the probe tip after the heat shrink was applied.

9. Another 3.6 mm sleeve of heat shrink would then be cut and shrunk around the tip of the probe so that an electrode surface length of 1.5 cm was left uncovered. The tip of the heat shrink would then be sealed with wax, since wax does not react to electricity or biological materials (wax is a common cheese covering agent in the dairy industry).

10. The probes would be checked and tested to see if the heat shrink and wire extensions remained in position during handling and if there was ohmic continuity. Once this tests was successful, a “chocolate block” connector would be connected to the probes. This connector would keep the probes apart during insertion and handling.

The probes were also designed with one major practical concern in mind: Ease of cleaning. It was important that the different electrodes could be easily cleaned with ethanol after every experiment. The flexibility of the chocolate block allowed the probes to be pulled far enough apart in order to clean the full surface area of every electrode.

In addition, the wire extensions were soldered onto a pin-header connector. The pin headers proved effective in providing a sturdy contact to the measurement circuitry.

Figure 3.17 will illustrate the final probe geometry and dimensions.

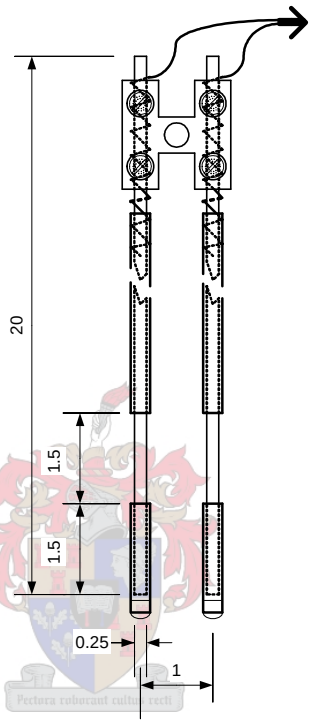

Figure 3.17: Probe geometry and dimensions.

All of the dimensions in Figure 3.17 are in cm. The heat shrink is represented by the thicker outlines and the wire extensions are the zigzag lines that form into the arrow.

The manufactured probes were then screened and tested in a 1.6% salt solution, simulating sour milk, and only used in the milk experiments if they performed adequately in these tests. The experimental results as measured by the probes can be found in Chapter 6.

3.5 Screening results

A total of 16 probes were manufactured and screened. The measurements were done with the automatic measurement device designed in Chapter 5.

The screening tests involved applying a 2 V sine wave across the probes and series resistor and measuring the probe impedances over a period of three days. By allowing three days of measurements, the extended measurements would give an excellent idea of the typical probe performances over time. Finally, in order to

show the effect that temperature variations have on the probes' impedances, the ambient air temperature was also recorded each time the impedance value was measured.

The screening tests were done in the fourth floor labs of the Engineering faculty. The labs' temperature varied with the day-night cycle. Figure 3.18 will show a plot of temperature overlaid the average probe absolute impedance measurements.

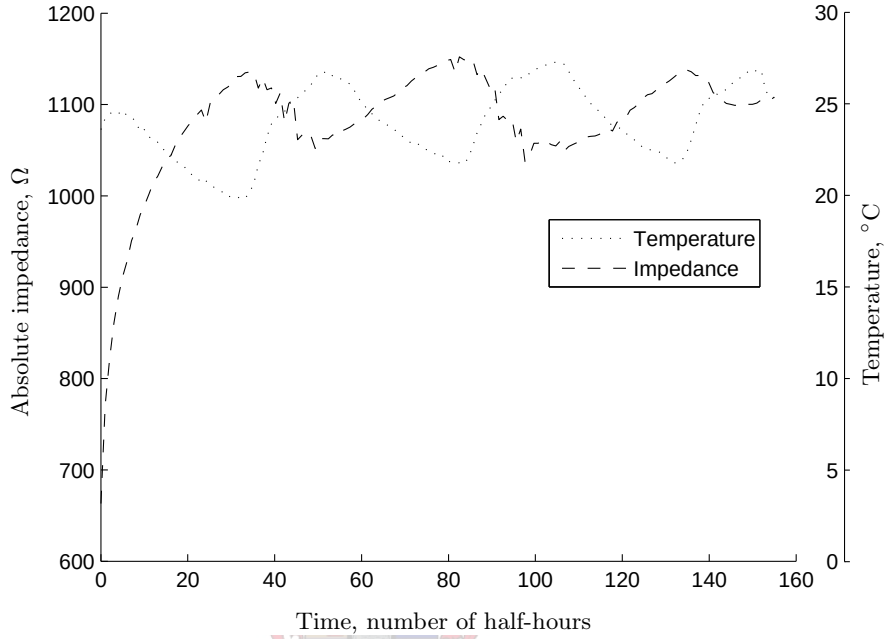

Figure 3.18: Temperature variations overlaid on absolute impedance measurements. Note the different scales.

Figure 3.18 reveals a few interesting phenomenon. Firstly, it can be seen that over the period of three days, the impedance values seem to climb from its initial value until it reaches some form of stability at around 15 hours after the probes were placed into the salt solution. This gradual climb is not the effect of the probe adaptation times that needs to be given to every probe in a new environment, since this adaptation time was seen in the first two hours of measurements. Secondly, the effects of the temperature can be clearly seen on the impedance curve and the overlaid plot shows that the impedance drops with a rise in temperature and vice versa.

As far as the author could determine, no extended time measurements for any probes in a saline solution has been done. Therefore, the gradual impedance climb picked up by the measurement requires more study in order to determine its cause. In addition, the effect that time dependency would have on the measurements in milk could not be determined, since milk changes over time and affects the probe impedances as it changes. Furthermore, the author could not determine if there were existing work regarding temperature calibrations for probe impedance measurements. The effects of temperature variations on impedances were clear, but this thesis made no attempt to cater for the effects. The reason was that the typical milk experiments would take place in a temperature controlled environment. However, if the impedance measurement method was to be applied in a real-world application, the temperature would need to be taken into account in order to prevent false detection data.

The data presented in Figure 3.18 fails to show one very important observation made during the probe screening tests. Although every possible step was taken to make the probes physically similar, the measured impedances had a large variation per probe. In a 1.6% salt solution, the probe with the lowest impedance had a value of 450 Ω and the probe with the highest impedance had a value of 2100 Ω. It was not known how the probes could have such a large impedance variation, but the average probe impedance values agree with the findings of Geddes et al. [24] for their measurements done with probes in a 0.9% saline solution. The average capacitance was measured as 2 μF and the average resistance as 550 Ω. Geddes et al. found the values, at 100 Hz, to be 2.2 μF for the capacitance and 713 Ω for the resistance. However, it must be remembered that the average values cannot be taken as exact, since the probe characterisation done by this thesis have shown that the expected impedance values, for stainless steel probes in a 1.6% saline concentration, should have a higher capacitance and a lower resistance than the ones given by Geddes et al. In this case, both the capacitance and resistance values were lower than the values given by Geddes at el.

The diverse impedances suggests that any newly manufactured probe should be measured against an average impedance value and a calibration system used to augment the measured impedances, if different from the average. This step was not taken by this thesis, since all the probes should show the same percentage in impedance variations within milk, albeit at different levels.

3.6 Conclusion

This various probe studies and experiments have shown that probe impedance measurements are effective at detecting electrical changes within a liquid medium and that relatively simple measurement circuitry can be used to measure the changes in these impedances. However, the studies also revealed that probes are subject to a myriad of physical and electrical phenomena. In addition, some of these effects could not be explained by this author, which suggests that a lot more research can be added to the 100 years of existing research around probes and probe sensors.

The following conclusions can be made from the probe characterisation tests done by this thesis:

- The Warburg electrode-electrolyte model proved effective in predicting probe impedance measurements, since basic probe characterisations followed the same principles as those suggested by the literature.
- Probe current density was the biggest factor in determining the probe impedances. Above a certain current density level, probe impedances started to drop drastically, so that the a linear impedance change with current density was lost. The level seemed to vary between different metal types, since for the same current density range, the brass probes showed a gradual drop in impedance whilst the stainless steel impedances remained more stable.
- A surface area “sweet spot” existed for the probe sensors. Probe surface areas determined the size of the total current required from a measurement system. Probes with large surface areas had low impedance values, which meant that impedance variations could be lost amongst the large applied voltages. Inversely, probes with small surface areas had large impedance values, but the applied voltage levels may be too small to measure.
- Of all the metal types tested, stainless steel was the only metal that could measure the milk fermentation process effectively. In addition, the stainless steel had to be smooth, since stainless steel probes with a roughened surface area did not seem to detect milk fermentation processes. It seemed as if bacteria

did not like the presence of copper or brass and although the milk fermented, the probes did not pick it up.

- The various observations made during probe tests revealed that probe surface roughness had a profound effect on the measured impedance values. A roughened probe's impedance was considerably lower than a polished probe's impedance.
- The various modifications made to the standard metal wire probes were found to be effective. The heat shrink isolation only allowed the uncovered probe surfaces to create a interface layer and the distance tests revealed that probes did not need to have a rigid structure within milk at a 100 Hz.

The following conclusions were drawn from the screening tests done on the probes created in this thesis:

- The probes showed a large variation in their initial measured impedances. These variations were of such a nature that it was far above and far below the stainless steel impedance values mentioned by Geddes et al. [24]. However, the average probe impedances were quite close to the ones found by Geddes et al.
- Based on the impedance variations, two solutions are suggested:
  - Any manufactured probe should be measured against average values taken from a large sample of similarly manufactured probes and a "probe calibration factor" should be used to equalise the probe impedances to the average.
  - Probe materials should have very little variation and manufacturing methods should be automated in order to be able to reproduce the same physical characteristic in all manufactured probes. In theory, such probes should have the same surface areas and therefore, the same impedance values.
- Temperature was not tested during initial probe characterisations, but during the screening tests it was observed that temperature did have a measurable effect on the probe impedances. A real world probe application should therefore cater for temperature variations. Temperature calibrations should also be investigated, since it does not seem as if any exist.
- The probe impedances increased sharply at first, but reached a stable point after about 15 hours. However, the initial measurements in milk showed that impedance values dropped with time. Therefore, it is concluded that the observed increases cannot be mistaken as milk fermentation curves, since the impedance drops with an increase in bacteria and acidity and does not rise as it did in the 1.6% salt solution. Finally, if this phenomenon is shown to be inherent to probes (since it could not be explained by the author), further time dependant impedance calibrations could be used to phase out the initial measurement errors.

A lot more probe-centred research still needs to be done. However, for the purpose of this thesis, the designed probes' screening tests revealed that the probes would be effective at detecting sour milk changes and all subsequent tests were done with the newly manufactured probes.

Chapter 4

Device 2: Capacitive sensor

A non-invasive sensor could be based, theoretically, on a few sensor types. Amongst the different types, the non-invasive capacitive sensor was considered as the best candidate for initial study. Once again, the initial sensor concept was relatively simple, but the detail behind the exact interaction of the materials affecting the capacitor's electric fields required more investigation. The shape of the capacitive plates were also of great importance, since the different shapes could either inhibit or promote the capacitive sensing abilities. The theory behind capacitive sensors and the potential application it has as a non-invasive milk fermentation sensor will be discussed in this chapter.

4.1 Theory

Capacitors are electric components that are defined around electric fields and charge. Capacitance has already been touched on in subsection 2.2.1. However, the permittivity was the focal point during that discussion, not specifically the capacitance. Therefore, this section will be discussing the permittivity and the capacitance and how they are defined.

4.1.1 Capacitance theory

A greatly simplified summary of the capacitor's theoretical description will be presented here, based on the theory found in a book by Haus and Melcher [31]. To begin, electric field theory makes use of Maxwell's equations to describe any electric field between any geometrical form of conductive plates. By assuming that there is no magnetic induction, which is typically for situations involving electric fields, an electroquasistatic analysis of the electric field can be done. The electroquasistatic simplifications allow the electric fields to be described by superposition integrals. These superposition integrals are calculated from a specific reference point. In addition, the results of the integrals describe equipotential surfaces. As a basic rule, electric fields start and terminate perpendicularly on any equipotential surface, including the conductive plates, and tend to follow the shortest route, from high to low potential, possible. If one takes the reference point as ground voltage and the equipotential surfaces as another voltage level, then a complete capacitive system has been described.

Haus and Melcher also describes how the capacitance can be calculated from the knowledge of the electric fields and the geometrical shapes of the charges (read conductive surfaces) that creates them. These initial

equations only describe a capacitance of a geometrical setup around free space, but Haus and Melcher later describe the effect that a dielectric material has on capacitance as a whole. The simplest geometrical form is the classic parallel plate capacitor. This geometrical setup has two plates of equal surface area placed a certain distance apart. Based on this geometry, a capacitor with a dielectric material between the plates will have the following capacitance equation:

$$C = \frac{\epsilon_0 \epsilon_r A}{d}$$

where A is the area of the plates, d the distance between the plates, ϵ_0 the permittivity of free space and ϵ_r the relative permittivity of the dielectric material. The origins of the equations for the dielectric permittivity is also discussed by Haus and Melcher and will not be mentioned here.

The effect that multiple layers of different dielectrics permittivities will have on the total capacitance must be discussed in a little more detail, since non-invasive capacitors will have at least two different dielectrics between the conductive plates. Haus and Melcher investigated this situation and explained that a surface charge existed at the interface between the different dielectric materials. Another way of understanding surface charge is to see the surface charge as an infinitely thin conductive plate [59]. Therefore, a capacitor with three layers of dielectric placed between the two conductive plates can be seen as an electric circuit with three different capacitors in series. Figure 4.1 will give an illustration of the physical and electrical configurations.

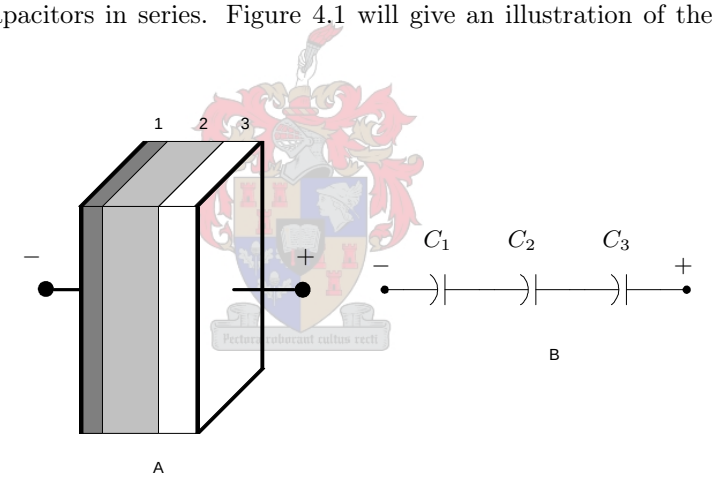

Figure 4.1: Capacitor with different dielectrics between the plates, illustrated by the physical setup (A) and the electric circuit simplification (B).

Now, the total capacitance of the multi-layered capacitor can be computed as the sum of the three different capacitances in series. Capacitances in series are summed in parallel, so the multi layered capacitor can be computed by:

$$C_T = \left(\frac{d_1}{\epsilon_0 \epsilon_{r1} A} + \frac{d_2}{\epsilon_0 \epsilon_{r2} A} + \frac{d_3}{\epsilon_0 \epsilon_{r3} A} \right)^{-1} \tag{4.1}$$

Where C_T is the total capacitance and the subscripts 1, 2 and 3 represent the different dielectrics with their respective permittivity and depth values. Equation 4.1 assumes that the areas of the interfaces and the conductive plates are the same for all the capacitors. If we understand that a general non-invasive capacitor

design will have the two layers of the container and the medium between the container walls as dielectric materials, equation 4.1 can be simplified to:

$$C_T = \left(\frac{d_1}{\epsilon_0 \epsilon_{r1} A} + \frac{2d_2}{\epsilon_0 \epsilon_{r2} A} \right)^{-1} \tag{4.2}$$

where d_2 represents the depth (thickness) of one container wall and d_1 represents the depth (thickness) of the medium between the walls.

It must be remembered that equation 4.2 represents a non-invasive capacitor in a parallel plate design. In practice, such a design may be unrealisable, since the shape and size of the experimental or commercial containers may be totally incompatible with a parallel plate capacitor design. However, the core of the theory is applicable to any shape of capacitor and the capacitor shape will only result in a different capacitance, not a different physical phenomenon.

All of the above equations ignore the effect of fringe capacitance. Fringe capacitance is caused by electric fields that do not remain inside the capacitor's dimensions and that "bend" outwards. Fringe fields cause the capacitance to increase and the size of the increase depends and the geometry of the capacitor. In addition, fringe fields may be useful for a non-invasive capacitor, since fringing fields can be used to penetrate a material without enclosing the material between the capacitor's plates. Therefore, if the capacitor is specifically designed around the fringe field effect, a much smaller capacitor design may result, since fringe fields will be able to measure a much smaller sample of material than the parallel plate capacitor design may be able to measure.

The major conclusions that can be taken from the above summary and discussion is that the required electric field shape determines your capacitive sensor's conductive plate design and that the permittivity between the conductive plates determine the size of the capacitance, if the area and distance parameters remain unchanged.

4.1.2 Capacitive detection theory

Based on the basic understanding of capacitors, an initial capacitive sensor could be conceived. However, the capacitive sensor required two design parts. Firstly, the capacitor itself needed to be designed, followed by a design of a measurement system that could detect the changes in capacitance.

Basic capacitance sensor criteria

In order to design a proper capacitive sensor, the typical permittivity changes of the materials being measured must be investigated. Subsection 2.2.1 mentioned a few papers that studied the permittivity of biological cells at a specific range of frequencies. Those, and others, were: The papers that studied the dielectric permittivity of bacteria at radio frequencies [30, 43], the general studies of the dielectric properties of yeast cells by Asami et al. [3, 2, 4], and the report of experience gained with dielectric data in biological materials [57].

Subsection 2.2.1 already mentions some of the findings of the above papers. However, with the focus on capacitance, the criteria that has the greatest impact on this study, as found from these papers, can be summed up as follows:

- Biological cells show dielectric dispersion phenomenon at certain frequency ranges. The most important dispersions are called the alpha, beta and gamma dispersions.

- For the ideal situation, the alpha dispersions fall between 100 Hz and 100 kHz, the beta dispersion fall between 100 kHz and 100 MHz and the gamma dispersions fall above 1 GHz.
- Dielectric dispersions cause a drop in permittivity as the frequency of measurement is increased. For the general frequency range between 100 kHz and 100 MHz, the beta-dispersion will affect the measured permittivity values. This range represents the typical test range of the different papers. Therefore, the highest permittivity value will be measured at low frequencies.
- An increase in biological material cause an increase in the measured permittivity. In other words, an increase in the capacitance can be measured as the microbial population increases with time.
- Various biological phenomenon, such as cell orientation and cell division, affect the capacitance growth curve. Therefore, the exact capacitance may differ for different bacterial species, since the variety of differences, especially geometrically, that exist for different bacterial species are numerous.
- An external increase in conductance within a cellular suspension may also cause an increase in measured capacitance. As an aside, the studies around this phenomenon were specifically done for yeast cells, so it was not known if the fermentation of milk would also display this characteristic. In addition, there was a point where an increase in conductance did not cause an increase in the capacitance. Milk is already quite conductive, so the increase in conductance, caused by the fermentation process, may not add to the capacitance at all.

Some preliminary detection parameters could be put together based on these dielectric studies as well as the knowledge around the makeup of milk. However, to get an idea of the capacitance values that could be expected with non-invasive designs, the following must be kept in mind:

- Milk is mostly water. The relative permittivity of water at 298 K is given as 78.4 [30].
- The permittivity contributions of the various constituent components in milk could not be determined beforehand. However, a final year study has determined the relative permittivity of milk to be around 80 [16]. Therefore, by using the relative permittivity of water as a representative value of the relative permittivity of milk, a fairly accurate idea of the total capacitance can be computed.
- A non-invasive design will most likely have the layers of the milk's container as part of the capacitance. Laboratory experiments usually have glass containers and commercial containers are usually plastic (PET). The relative permittivity of glass is taken at around 5.6 and of the plastic at around 3.2.
- Depending on the exact frequency of choice, a relative permittivity increase of $\epsilon_r 20$ to 30 units can be expected for biological growth [3]. In other words, the capacitance will increase with an increase in biological materials. However, the previous study was done on yeast cells and it was not known if the same permittivity increases could be expected for bacterial growth. Therefore, these values should be taken as a guide of what to expect with a non-invasive capacitor design.

As a crude example, the typical expected parameters for a parallel plate capacitor surrounding an ideal rectangular container will be computed. (See Figure 4.2 for a graphical representation).

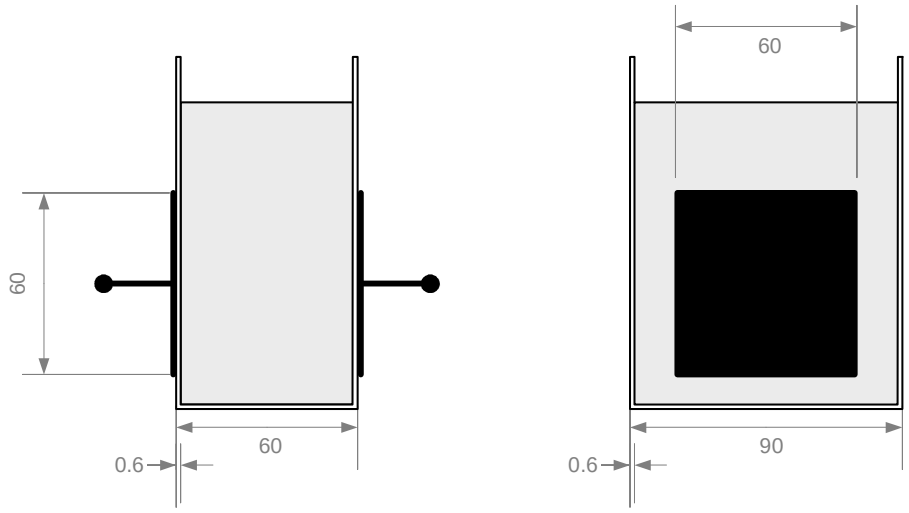

Figure 4.2: Front and side view of example's milk measuring non-invasive capacitor (grey material represents milk). Distances are in millimetres.

The square conductive plates have an area of 0.0036 m^2, the total distance between the plates are 60 mm and the thickness of the plastic container is 0.6 mm. These values were based on actual plastic bottle thickness and actual long life milk box sizes. The plate sizes were chosen based on the box's geometry. Using equation 4.2, the capacitance of "milk" without bacterial growth is computed as:

$$C_T = \left(\frac{0.0588}{8.85 \times 10^{-12} \times 78.4 \times 0.0036} + \frac{0.0012}{8.85 \times 10^{-12} \times 3.2 \times 0.0036} \right)^{-1}$$

Which gives 28.32 pF. If the permittivity increase caused by bacterial growth is added to the permittivity of water, equation 4.2 becomes:

$$C_T = \left(\frac{0.0588}{8.85 \times 10^{-12} \times 108.4 \times 0.0036} + \frac{0.0012}{8.85 \times 10^{-12} \times 3.2 \times 0.0036} \right)^{-1}$$

Which gives 34.73 pF. It is clear that the total value of capacitance and the difference between the total capacitance value for the two bacterial growth states are quite small.

If one looks at equation 4.2, representing the simple and ideal non-invasive parallel capacitor capacitance, a few practical implications spring to mind. First of all, a rule of thumb when adding capacitors in series is that the sum of the components will always be less than the component with the smallest value. This stems from the fact that capacitors in series are summed in parallel. Furthermore, the only variable that can be controlled by the designer is the areas of the conductive plates. The permittivities and thickness of the different dielectrics are predefined by the container. Now, the value of permittivity for the container is a lot less than the typical value for water. This means that the value of capacitance for the container will be less than that of the water and the container will therefore dictate the total value of the capacitance seen between the conductive plates of the non-invasive capacitor. This could be a problem, since it is the permittivity of the water (milk) that increases, not the container's permittivity.

There are a few fairly simple ways to cater for this problem:

- Minimize the thickness of the container so that the capacitance is dictated by the water. This is based on the fact that the smaller the thickness of the container's dielectric is, the larger the container's capacitance will be. Therefore, the size of the container's capacitance can be made very large if the thickness of the container is very thin which will allow the water to be the smaller of the two capacitances.
- Maximize the size of the conductive plates. If the container's capacitance is a lot smaller than the water's capacitance, the difference that there might be between the total capacitance of two different bacterial growth states may not be measurable. By increasing the size of the plates, the area is increased which causes the total capacitance to increase. By increasing the capacitance, the difference between the two states is also increased and the increased difference may be large enough to measure.
- Ensure that the two capacitances are more or less comparable, so that the effect that the smaller capacitance has on the total capacitance is minimized. Practically, this can only be done if the container is made out of a special material that has a permittivity comparable to the water.
- Multiple non-invasive capacitors. By connecting multiple non-invasive capacitors in parallel, the total capacitance measured between the positive and negative side of the combined conductive plates is increased. Once again, if changes in the capacitance was too small to be measured before, this solution might make the capacitive changes large enough to measure.

The basics for a non-invasive sensor can now be used to develop a more refined capacitor geometry.

Capacitance measurement systems

The non-invasive capacitor forms the basis of the capacitive sensor design. However, if the subtle changes in capacitance cannot be measured properly, the sensor becomes useless. In addition, it has been shown that the expected values for a non-invasive sensor is at most in the hundreds of picofarads. Therefore, a measurement system must work with the picofarad range and be able to distinguish between single picofarads to tens of femtofarads.

Although minimal study has been put into this phase of the capacitive sensor design, a few potential capacitive measurement systems have been investigated. These were oscillator circuits, synchronous demodulator circuits and bridge circuits. Brief discussions will be given for all of them.

There are a few oscillator circuits who's oscillating frequencies are controlled by capacitance. The ones considered by this thesis were the classic 555 timer oscillator and the Colpitts oscillator. If the non-invasive capacitor is used as the capacitor that determines the oscillating frequency, then these circuits will change their oscillating frequency as the capacitance changes with bacterial growth. A frequency counting system can then be used to measure the frequency. If the oscillating frequency is too high, the oscillating signal can be mixed down and the beat frequency can be counted. Two main problems with the oscillator circuits could be oscillation stability during a frequency change, or designing a large enough frequency change with a change in capacitance.

The synchronous demodulator and capacitive bridge circuit basics were obtained from a book by L. K. Baxter [8]. The synchronous demodulator circuit is based on a capacitance or impedance measurement and gives a linear voltage output based on the change in capacitance. In order to measure the capacitance, a specific

frequency is applied to the capacitance under test, then amplified and then applied to a demodulating circuit. In turn, the demodulating circuit changes the amplified AC voltages into a DC voltage. Specific circuit details are not given, so the eventual circuit complexity may be considerable. This measurement system is an accurate capacitance measurement circuit and might be the only one capable of measuring the small capacitance differences expected for the non-invasive capacitance measurements.

The bridge circuit, or more specifically the capacitance bridge, uses a balanced capacitance bridge circuit to measure a change in capacitance in one leg of the bridge. During balance, the bridge output is 0 V. Once the bridge becomes unbalanced, the voltage output rises. The greater the change, the higher the voltage output. The greatest problem with the capacitance bridge is stability, since the one side of the bridge requires identical capacitors. Such capacitors may need to be manufactured specifically for a high accuracy capacitance bridge design. The greatest asset of the bridge circuit is its potential sensitivity to capacitance changes of mere femtofarads.

Another option that one has with the capacitive measurement circuits is the wave shape of the oscillating frequency. When one thinks of an oscillating frequency, sine waves usually spring to mind. However, the capacitive circuits will function just as well with square waves. Square waves are preferred for CMOS circuits and since most microcontrollers are of CMOS design, this fact will prove advantageous during the design of an automatic capacitance measurement device. The reason square waves are preferred is because CMOS chips can easily generate a stable square wave with a specific frequency and amplitude.

To conclude, the measurement system design can only be finalised once the non-invasive capacitor design has been completed, since the capacitance range and capacitance size determine the exact component values that will be used in the various stages of the measurement circuits. However, it will be said that the system that will have the quickest development time is the 555 timer oscillator, since the chips are common and the oscillator circuit simple to construct.

4.2 Potential non-invasive capacitor

The theory presented in section 4.1 can be applied to any situation involving capacitors and capacitance. However, the exact capacitance parameters will be limited by the practical capacitor design. In addition, the effect that the biological element will have on the total capacitance of the non-invasive capacitor remains, largely, unknown.

In an effort to design an elegant and practical non-invasive capacitor, the fringe field capacitor design was investigated. To this end, a few papers around the typical shape and expected capacitance for fringe capacitors were studied. The review article by Heerens [34] gave the complete but complex mathematical representations of capacitances for various toroidal capacitors. These equations take into account the distance, conductive plate size and various fringe field parameters. Heerens also discusses the guarding concept (the use of a capacitive "shell" to limit stray capacitances) and illustrates how to properly apply it in capacitor design. Unfortunately, the direct application of the complex mathematical equations presented by Heerens are impractical. The conclusion is that although the absolute capacitance for a circular shaped fringe capacitor is calculable, computer aided design will most likely be required for practical designs analysis.

Finally, two papers mentioned the use of fringe field capacitors to detect moisture. These were the paper by Li et al. [41] and the recent paper by Hazarika et al. [33]. Li et al. never developed the fringe capacitor, but Hazarika et al. developed and reported on the use of a fringe field capacitor for the detection of water in tea leaves. This paper used most of the suggested sensor methods mentioned in section 4.1. To summarise:

- Their final fringe capacitor was a combination of four fringe capacitors in parallel.
- Their measurement circuit is the 555 timer oscillator.
- They used computer design to predict the capacitance of the fringe capacitor.
- The capacitance was small (5.9 pF) and the change in capacitance for their specific detection criteria was even smaller (0.1 pF). However, this change caused a sufficient change in oscillating frequency to make it detectable.

Their capacitance was small because of the fact that it measured air. The presence of tea leaves (and therefore, water in the leaves) raised this capacitance slightly, but the presence of air will limit the capacitance.

Based on these findings, this thesis suggests that a prototype non-invasive capacitor can be based on the exact parameters of the fringe field capacitor designed by Hazarika et al. Figure 4.3 will illustrate their design.

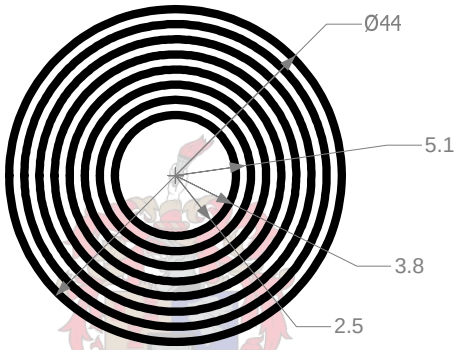

Figure 4.3: Top view of fringe capacitor design. Dimensions are in mm. Taken from [33].

The size of the capacitor is ideal, since it will fit underneath most containers. In addition, the capacitor design should be fairly simple to reproduce with most circuit board manufacturing methods. The copper strips and the distances between the copper strips are all 1.3 mm wide.

Based on the discussion so far, the following could be expected if the fringe field capacitor is used to measure milk through a 2 mm glass container (a typical experimental setup):

- If air can be eliminated, especially between the capacitor and the container, the capacitance values should be larger than those mentioned by Hazarika et al.
- The capacitance will be dominated by the container. Glass has the highest permittivity, at a value of 5.6, but it is still about 13 times less than water's permittivity.
- Lower frequencies are not only better for the biological dispersion effect, but will allow the fringe fields to penetrate the container to a greater depth. Therefore, the best results are expected for capacitive frequencies between 100 kHz and 300 kHz. However, most of the biological dielectric data have been found from 300 kHz and upward, so this may be the better frequency choice if comparisons are to be made.

- The 0.1 pF capacitance difference between the high and low capacitance points of Hazarika et al. was detected and followed with sufficient measurement resolution. Therefore, if a larger capacitance is present (because of the elimination of air), then the capacitance change that may be caused by the increase in bacteria may also be larger and indeed be more than sufficient to be detected by the fringe field capacitor.
- If the circular fringe field capacitor is combined with the guarding principles discussed in the paper by Heerens [34], the penetration depth may be increased

It must be remembered that the ideal capacitor construction for the requirements of a biological fermentation process may take many design iterations and until physical measurements are done with the suggested designs, the suggestions should be seen as guidelines only.

4.3 Conclusion

Although no physical measurement evidence was presented by this chapter, the theory governing the design and expected results for a non-invasive fringe field capacitor have been presented. It was concluded that the size advantages of a fringe field capacitor, together with the practical aspects of the capacitor's measurement application, made it a good candidate for a non-invasive sensor. In addition, the fringe field capacitor should penetrate deep enough into the container to be affected by a permittivity change within the milk. Finally, a circular fringe field capacitor would be able to make use of guarding to focus the fringe fields towards the measured sample.

Other conclusions were:

- Practically, computer aided design will be required to simulate any fringe field capacitor design before it is built.
- The non-invasive capacitors will have small capacitances, typically in the order of picofarads, dictated by the container.
- The potential difference between the capacitance of a "zero-bacteria" state and the capacitance of a "peak-bacteria" state as measured by the fringe capacitor may be only femtofarads in size.
- Biological capacitive measurements should be done at the lowest working frequency possible in order to maximize the measured permittivity and in turn, the size of the capacitance.
- An increase in biological cells within a solution cause an increase in the measured permittivity of the solution.
- 555 timer oscillators will provide the quickest measurement circuitry development time, but may lack sensitivity. Greater measurement sensitivity may be achieved with the synchronised demodulator design, at the cost of measurement system complexity.

The author is confident that the a circular fringe field capacitor can be used to measure the fermentation process of milk and that the measurement circuitry will be fully compatible with simple CMOS-based measurement systems.

Chapter 5

Automatic measurement device

5.1 Measurement device overview

The need to reliably record detailed and accurate measurements in future milk experiments meant that a device had to be designed to remove the human error aspect from any measurement. In addition, the length of time that experiments would take to complete meant that the device had to be automated in order to record sensor data at exact intervals. Therefore, the automatic measurement device (dubbed AMD) was designed and applied to the measurement of the probe sensors discussed in the previous chapters.

This chapter will discuss the measurement device built for the probe sensors. The design methodology, hardware and software designs and the final device performance will be discussed in separate sections.

5.1.1 Basic design criteria

In order to design an effective measurement device, detailed knowledge of the sensor it would be using was required. The investigations in Chapter 3 provided enough of such knowledge for the confident design of the AMD.

The basic requirements the AMD had to meet were the needs of the sensor, measurement and storage of probe impedances, time interval management and system-wide monitoring abilities. This meant that the device required digital and analog circuitry, since the analog circuitry would provide the proper measurement conditions and the digital circuitry would control and store impedance data. A human interface would also be required, since the device had to be able to relay any information it acquired to the researcher.

Other requirements would be centred around the typical measurement environment that the device would be working in. The device will most likely be measuring in small laboratories, be measuring for long periods of time and be used by people who have no engineering backgrounds. Therefore, the device had to be small, easy to use and reliable. In addition, no computers were present in the direct vicinity of the measurement device which meant that the device had to be moved after every experiment. In order to make this process as painless as possible, the device had to be portable and self-sustaining.

5.1.2 Detailed design criteria

Based on the research done around probe sensors, the basic criteria mentioned above and the expected experimental requirements, the following detailed design criteria was formed:

- The probes designed in this thesis required a minimum current density of 0.5 mA/cm^2 but no more than 2 mA/cm^2. The device would therefore have to provide a nominal current density value of 1 mA/cm^2.
- Voltage levels measured across the different circuit components had to be comparable in order to ensure measurement accuracy. This meant that the design had to provide the correct series resistor value in order to ensure unbiased voltage levels.
- The probes must receive zero DC offset, pure sinusoidal AC waves.
- Measurement circuitry must be able to provide undistorted voltage measurements for the applied voltage (V_t), series resistor voltage (V_r) and probe voltage (V_b) respectively.
- A diverse supply range has to be available for analog and digital circuitry. The digital logic would most likely require a constant 5 V supply and the analog measurement circuitry would most likely require a dual supply range for which the values will depend on the components used in the design.
- Digital logic must control the time at which a measurement is made. This will allow the measurement intervals to be changed based on the experiment's needs.
- The device must be able to measure multiple probes in order to test parallel bacterial growth times. Therefore, logic will be required in order to choose which probes to measure and which probes to ignore. Multiplexers will most likely be used to choose between the probes and programming will control the order of measurement. A minimum of three probes must be catered for.
- The digital logic must calculate the probe impedances internally, in order to save time during data analysis. The mathematics involved is complex in nature, so the internal calculations must be able to make accurate calculations and not be troubled by imaginary numbers.
- Resulting probe impedances must be stored in a non-volatile medium in order to allow the retrieval of the data at a later stage. In addition, the stored values must retain a certain degree of accuracy.
- The measurement device must be able to measure temperature, since temperature affects the growth curves of bacteria and must be taken into account during data analysis. It will also aid in revealing to what extent temperature affects the probe impedances.
- The device must be equipped with human interaction (or communication). This will allow the researcher to monitor the device's functions and retrieve the stored impedance data. A serial communications port should be sufficient for this purpose.
- The programming must be changeable. To this end, a reprogrammable microcontroller chip and ISP must be implemented, since the chip may not be removed from the circuit board once it is soldered onto it.
- The device must be battery powered. This will ensure self-sustainability and portability. In addition, it must be able to work for longer than the longest experimental cycle from one set of batteries.
- In order to maximise battery life, the device must be able to power down between measurement cycles. In addition, the total power consumption during measurement times must be kept to a minimum and the measurement length time as short as possible.

- The device must be as small as possible. The use of surface mount chips will aid in this endeavour.
- The device must be able to perform in a temperature range of between 8 degrees Celsius and 35 degrees Celsius. This meant that component tolerances and chip functions must not change between these temperatures.
- Cost must be kept to a minimum, where possible. No measurement device will have any form of real world susceptibility if the cost of production is too high.

It was decided that a specific design process would be followed in order to create and test the AMD. This design process involved two stages: First, a prototype device would be designed. This device would be made out of large components that would be soldered onto a generic circuit board, allowing for easy access to measuring points as well as the ability to be easily modified. Secondly, a final and specific circuit board would be designed that and only this design would be used to measure the probes in the final milk fermentation experiments. This design would be drawn directly from the prototype, but all the components would be as small as possible and the board will be as compact as possible. It is this final design that will be discussed in the following sections.

5.2 Hardware design

The hardware and software designs were developed in unison, since the software controlled the hardware and the hardware, in turn, provided the correct voltage levels to the analog and digital interfaces. However, the designs will be discussed separately.

The core of the entire AMD was the sensor. If the sensor did not function correctly, or the sensor circuitry was unreliable, the rest of the device's functions were useless. However, if the chip's functions were unreliable, the sensor's measurement capabilities would not matter. Therefore, a solid hardware design was called for.

The hardware discussions will begin at the power circuitry, then the sensor, then move on to the measurement circuitry, then the core processor, followed by data, communication and overhead circuitry. Any of the core chip data can be found in the datasheets in Appendix E. A complete schematic of the hardware can be found in Appendix B.

5.2.1 Power circuit

The power circuit is the life-line of the entire AMD. If the life-line is not designed properly, the device may shut down prematurely, or drain a lot of power, all of which must be prevented. Figure 5.1 will illustrate the circuit as used in the AMD.

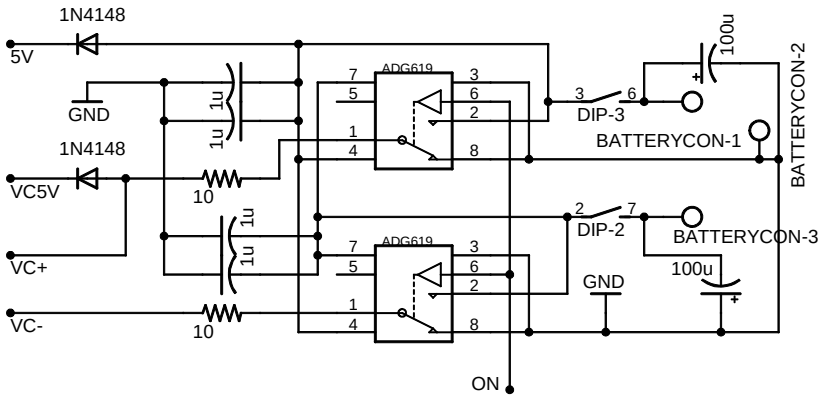

Figure 5.1: Power circuitry.

Figure 5.1 has the following distinct areas: The outputs, defined as $5V$, $VC5V$, $VC+$ and $VC-$, the two ADG619 circuit-wide power switching chips and their activation pins, called ON, the dip-switches (DIP 2 and 3) and the battery connectors, defined as $BATTERYCON$ 1, 2 and 3.

The different power requirements and the low power constraint meant that different power outputs had to be provided by the power circuitry. A 5 V constant power supply was required by the microprocessor, since it had to stay active throughout all the measurement cycles. A separate 5 V supply was required for the different chips communicating with the microprocessor, since these chips would most likely need to power down after every measurement. Finally, a separate positive and negative supply rail (6 V) was required for the analog sensor and measurement circuits, but these supply rails would also need to shut down after measurements. The microchip's dedicated constant 5 V supply is indicated as $5V$, the switching 5 V supply as $VC5V$ and the positive and negative switching 6 V supplies as $VC+$ and $VC-$ respectively.

The battery supply was made up by connecting eight 1.5 V AA batteries in series. The positive and negative voltages were taken at the begin and endpoints of the series battery connections, whilst the signal ground was taken halfway between the series battery connection. This effectively created a ± 6 V supply, from which all the chips were powered.

It was well known that batteries' nominal voltage levels dropped as they delivered their current over time. Therefore, 6 V was chosen as the minimum required voltage that a new battery pack had to provide, since the drop in nominal voltage had to be catered for.

The purpose of the diodes was to cause a sufficient voltage drop and bring the battery's voltage supply levels to an acceptable level for the digital logic chips. The 1N4148 diodes had an average voltage drop of 0.6 to 0.8 V and therefore a voltage level of 5.4 to 5.2 V was provided at the $5V$ and $VC5V$ points.

The ADG619 switches were used to switch on the $VC5V$, $VC+$, and $VC-$ supplies if the required pin was made high by the microprocessor, in this case pin 6. The ADG619 switches required very little power (smaller than 1 μW) to operate at any switch position, which made it an ideal standby switch for power regulation purposes. The four 1 μF capacitors shown in Figure 5.1 were added as decoupling capacitors for the two ADG619 chips.

An interesting component is the 10 Ω resistor present between the outputs of the ADG619 chips and the different supply outputs. The reason for these resistors was to limit transient switching effects by limiting inrush current during switching. It was found that the microprocessor restarted from its reset vector if the chip was commanded to switch on the power circuits. The reason was that during the switch, the inrush

current flowing towards the different chips would cause power to drain away from the microprocessor, causing the chip to experience a brownout and reset. When the 10 Ω resistor was inserted, this effect stopped. In addition, the supply voltage did not have a noticeable drop because of the 10 Ω resistor's presence, making at an elegant solution to the problem.

The DIP switches ($DIP2$ and $DIP3$) were added so that the positive and negative 6 V supplies could be shut off from the circuit during the times the device would not be used. However, both switches had to be on during normal device use, whether for measurements or to program the microprocessor, since the entire circuit needed stable supplies during any one of these events.

Finally, the battery connectors were added so that either different battery packs, or a separate power supply could be connected to the device. Regardless of the supply source, the positive rail voltage must always be connected to $BATTERYCON1$, the ground to $BATTERYCON2$ and the negative supply rail to $BATTERYCON3$. The two 100 μF capacitors were added as the supply rail stabilisers.

5.2.2 Sensor circuit

The circuit diagram of the core sensor layout has been given in figure 3.6. Through intensive testing, it was determined that the series resistor had to be 1 kΩ to facilitate comparable voltage levels across the series resistor and probe sensor. However, the probes would not be connected directly to the series resistor, but would be connected to an analog multiplexing circuit that will switch in the probe of choice during the measurement cycles. The chip used as the probe analog multiplexer was the ADG706. This chip will be discussed later.

5.2.3 Pre-sensor circuitry

Figure 5.2 illustrates the pre-sensor circuitry.

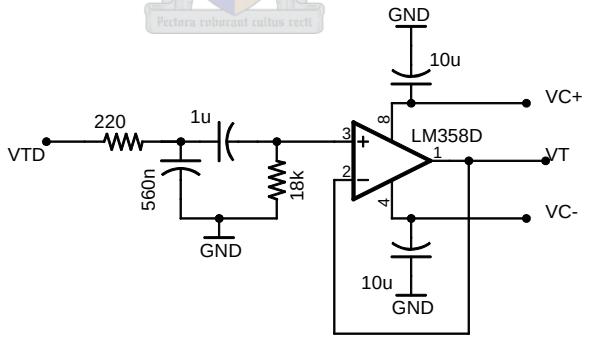

Figure 5.2: Pre-sensor circuitry.

The pre-sensor circuitry contains two major elements: A simple filter design and a buffer. This circuit was required to provide the probes with the correct sinusoidal voltage waveforms at the correct frequency. The principle was to create a 100 Hz PWM wave (VTD) with the microprocessor and to filter this PWM wave around the 100 Hz frequency in order to obtain a sinusoidal wave at 100 Hz (VT). In addition, the filter design was necessary since the source of the sinusoidal voltage wave would contain a DC offset voltage. The buffer was required since it would prevent any potential loading effects that might be caused by the

probe and series resistor on the filter circuit. More exact detail on the PWM created wave can be found in the programming section (section 5.3).

The filter was purposefully designed to have a separate low pass and high pass section following each other. In addition, the different filter stages were designed with passive components, negating any potential oscillation instabilities or operational amplifier (opamp) distortions that is sometimes observed with active filters.

The different filter stages can be seen from Figure 5.2 as follows: Moving from left to right in the figure, the low pass filter contains a series 220 Ω resistor and 560 nF capacitor to ground and the high pass filter contains a series 1 μF capacitor and an 18 kΩ resistor to ground.

The frequency cut-off points were chosen to be 10Hz for the high pass filter and 1.2kHz for the low pass filter. The different component choices were calculated from the 3dB cut-off equation, or:

$$f_c = \frac{1}{2\pi RC} \tag{5.1}$$

In order to find the component values required to obtain the cut-off frequencies of choice, different resistor and capacitor values were chosen, based on real world availability, and the resulting cut-off frequencies calculated. If the resulting frequency cut-off value was more than 10% higher or lower than the required cut-off, another resistor and capacitor combination would be chosen. The entire process was therefore based on educated guesswork and iteration. However, the resistor choices were kept below 100 kΩ and the capacitor choices below 1 μF, since it was known that small surface mount components were more readily available in values below the ones mentioned here.

Finally, the cut-off frequency choices were finalised after testing, since it was observed that choosing the different filter's cut-off frequencies too close to the 100 Hz centre frequency resulted in a significant amplitude attenuation. It was also found that although passive filters' outputs had little distortion, it had a very gradual cut-off characteristic, requiring a much larger bandgap to be chosen for the combined filter circuits than the theory would have suggested.

The values displayed in figure 5.2 will give the following cut-off frequencies:

- For the low pass filter: $f_c = \frac{1}{2.\pi.220.560.10^{-9}} = 1291.8$ Hz
- For the high pass filter: $f_c = \frac{1}{2.\pi.18.10^{3}.1.10^{-6}} = 8.84$ Hz

The buffer was an opamp from a LM358 dual opamp package. This opamp type was chosen for the following reasons:

- It could do ground sensing and have dual rail voltages - in this case ±6V.
- It was a common opamp and could be obtained as a surface mount package.
- High slew rates or large gains were not required, so this simple opamp type would work.
- Current consumption was the lowest when compared to the other common opamps available, such as the LM324 quad opamps and the LM351 single opamps.

Furthermore, the two 10 μF capacitors connected to the power pins of the opamp functioned as decoupling capacitors.

Testing of the entire pre-sensor circuit confirmed that the voltage amplitude was around 95% of the initial voltage amplitude generated by the microprocessor. However, during a close-up investigation of the voltage waveform, a triangular wave superimposed on the sinusoidal voltage was observed. Calculations determined that the triangular variations would not affect measured values, since it was in the single mV range, far below the minimum detectable voltage variations of the microprocessor A/D ability. Once again, more on these calculations can be found in the programming section (section 5.3).

5.2.4 Measurement circuitry

Figure 5.3 illustrates the measurement circuitry employed to measure the three different voltage peaks.

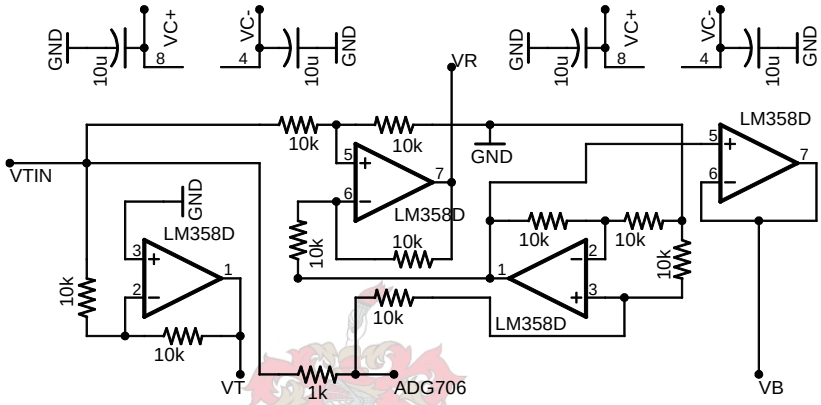

Figure 5.3: Measurement circuitry.

The three voltage peaks are indicated by VT, VR and VB respectively and the input voltage from the pre-sensor circuitry is indicated by $VTIN$. In addition, the 1 kΩ series resistor, mentioned in subsection 5.2.2, have been added for completion sake. The probes are not indicated, but all probes are connected via the ADG706 analog multiplexer, indicated by the $ADG706$ point in Figure 5.3. The "floating" connectors connected to $VC+$ and $VC-$ are the power pins for the different opamps. EAGLE (the PCB design program used by this thesis) remembers how many power connections there are per LM358 opamp package, so only two power pin connectors were needed for the four opamps used in this circuit.

From Figure 5.3 it can be seen that the measurement circuitry consisted out of two differential amplifiers, an inverting amplifier and a buffer. All the opamps were of the LM358 type. The reasons for choosing this opamp were the same as for the filter circuit and can be found under the previous heading.

The measured applied voltage, VT, was provided by an inverting amplifier with no amplification. The output voltage can be computed by the following equation:

$$V_o = \frac{-R_1}{R_2} V_{I1} \tag{5.2}$$

where V_o is the output voltage, V_{I1} the input voltage at the inverting input, R_1 the feedback resistor and R_2 the input resistor. In the case presented by Figure 5.3, V_o is VT, V_{I1} is $VTIN$, R_1 is the 10 kΩ resistor connected between pins 1 and 2 of the left-most opamp and R_2 is the 10 kΩ resistor connected to pin2 of the left-most opamp. From equation 5.2 it can be seen that the output voltage would have a 180 degrees phase difference from the input voltage. Luckily, this would not be a problem, since only the maximum positive

voltage amplitude, measured at any time, would be required by the phasor mathematics. The phase of the measured signal would not be required. A simple buffer was not built in case the signal had to be amplified, for reasons which will be given later.

The measured voltages VR and VB was provided by the two differential amplifiers and the buffer. The designs were obtained from *Electronic analysis and design* [46]. The design basically indicated the following:

$$V_o = \frac{R_2}{R_1}(V_{I2} - V_{I1}) \tag{5.3}$$

Where R2 is equal to the feedback resistance, which is also equal to the resistance to ground and R1 is equal to the value of any of the input resistances, which is also equal to each other. Furthermore, V_o is the output voltage, V_{I1} is the input voltage to the inverting input side and V_{I2} is the input voltage to the non-inverting side. In the case of Figure 5.3, starting with the opamp second from left, V_o is VR, V_{I1} is the output voltage of the opamp second from right (which should be VB) and V_{I2} is $VTIN$, or V_o is VB, V_{I1} is ground and V_{I2} is the output voltage from the ADG706 (representing the probe voltages). As for the resistances, their values are all 10 kΩ and their positions can be found from the desriptions given after equation 5.3. From equation 5.3 and Figure 5.3 it can be seen that the opamps put no amplification on the output voltage, since all the resistance values were equal.

The buffer providing VB was required in order to prevent the A/D circuitry of the microprocessor from causing loading effects on the output voltage of the opamp giving the input voltage to the differential opamp providing VR. The microprocessor's A/D ports had built in diodes that protected it from input voltage levels higher than its maximum rated input voltage abilities. This fact was used proactively, since the measured voltage signals were connected directly to the A/D ports and the ports were allowed to "chop off" the negative voltage cycles of the measured sinusoidal waves. In addition, the A/D sampling system could not resolve negative voltages, which meant that the minimum sampling value could only be 0 V, or the number 0. This meant, in turn, that the chopping effect had no consequence on the final positive A/D sampling values.

By using the diodes in this way, and by understanding that the only voltage measurements of interest were the sine wave's positive peak values, the measurement circuitry was greatly simplified. In addition, the A/D sampling results could be used "as-is", since a sampled peak value would resemble the exact peak value and calculation times could be minimised since no DC bias subtractions were required. The wave as it would be seen by the A/D pins will be illustrated by Figure 5.4.

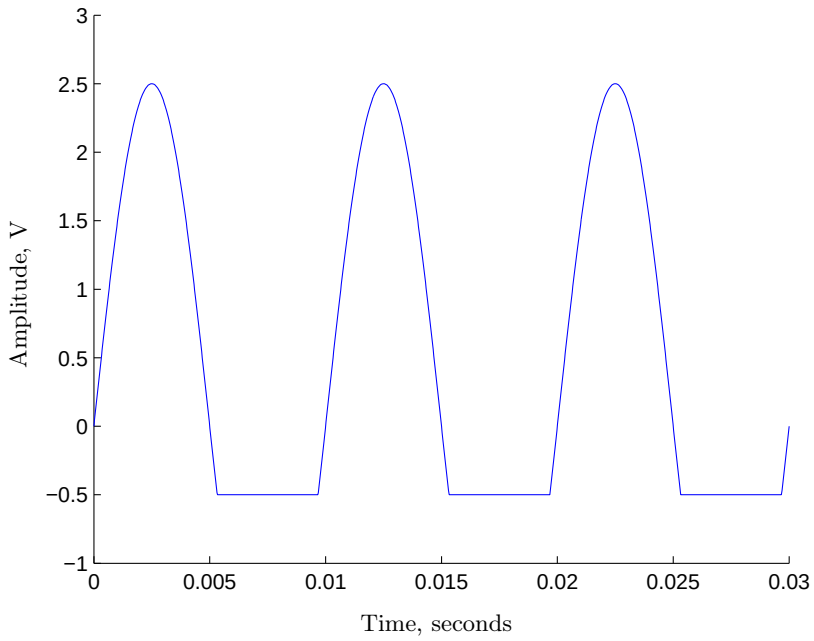

Figure 5.4: Sine wave shape as seen by A/D pins.

It must be noted that if the applied sine wave's maximum swing was less than 0.5 V, the diodes would not chop it off. Once again, this is not a problem since any value below 0 V will be given as 0 by the A/D sampling result. Finally, all the resistor value choices were based on the suggestions of *The art of electronics* [35].

It may be noted that the differential amplifiers gave no amplification to the signals. The reason was that any signal amplification had to be hard-coded into the programming, giving rise to the requirement that the voltage measured by the measurement circuitry had to be exactly as specified, or the law of cosines would not hold and the resulting impedance calculations would be completely erroneous. By building simple voltage following differential amps, and using the same components in all the circuit arms, the potential for erroneous signals were greatly reduced. In addition, the LM358 opamp could only amplify to about 1.5 V below its voltage rails. If the voltages on these rails dropped, as the case would be with batteries, the potential could exist that the signal might distort because the rail voltage was too close to the signal maximum. If it was absolutely essential to give amplification, it could be done by simply modifying the resistors, which is why some amplifiers were not changed to buffers.

5.2.5 Probe selection circuit

Figure 5.5 will give the probe selection circuitry.

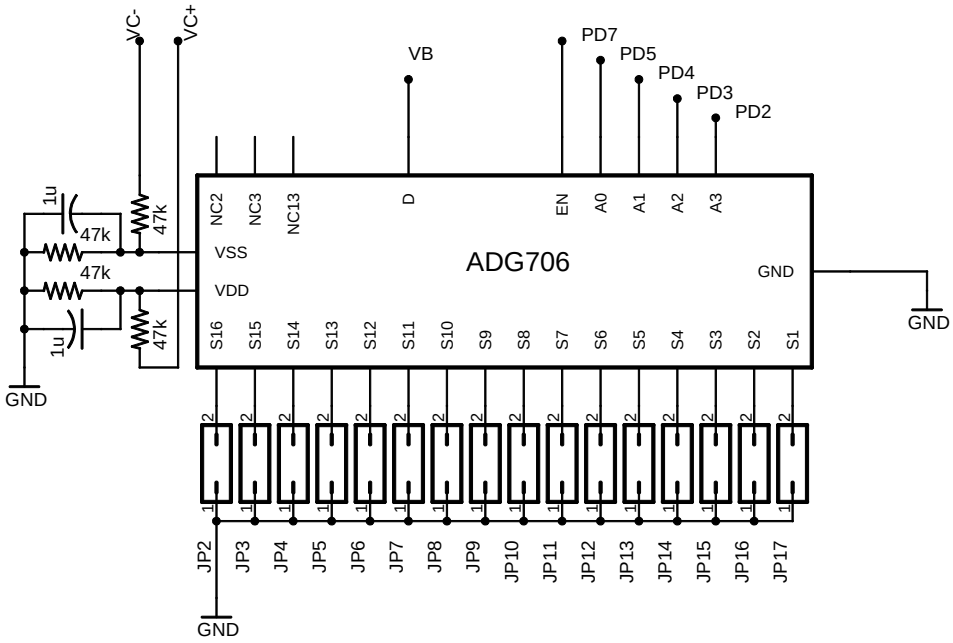

Figure 5.5: Probe selection circuitry.

The following elements can be seen in Figure 5.5: 16 jumper connectors, called JP2 to JP17, the ADG706 analog multiplexer and the power circuitry connected to VSS and VDD respectively.

The ADG706 is an analog multiplexer that is capable of switching between 16 different channels. In addition, its power consumption is very low, making it ideal for use in a battery powered device. However, the chip could only handle an absolute maximum differential power supply of 7V. Therefore, power divider circuitry had to half the initial analog voltage supplies in order to prevent over-voltage on the chip's supply pins.

The ADG706 switches to one of the 16 S-ports based on the address given at pins A0 to A3. It must also be enabled by making pin EN high. If all was done correctly, the probe of choice was connected to pin D which in turn connected to the 1 kΩ series resistor in the sensor circuitry. In addition, the resistance value that was added to the circuit by the ADG706 was around 0.6 Ω. This value was much smaller than the typical probe impedance value, so the effect on probe impedance was ignored. Therefore, as indicated in Figure 5.5, the value at pin D can be seen as the voltage over the probes, or VB.

The power divider circuitry mentioned earlier divided the ±6V supply to half that value by using two 47 kΩ resistors in series. The VDD and VSS pins were connected halfway between these circuits, as indicated in Figure 5.5. Two 1 μF capacitors were added to function as decoupling capacitors.

The power circuit was bound to be changed by loading effects, so tests were done in order to see how much, if at all, it changed. Tests revealed that although the voltage level that was obtained at each point changed as the S-pins were loaded, it was still well between the maximum differential voltage rating that the chip could handle. In addition, the voltages measured over the bottles were not affected by this change. The voltages changed to around 4.7V for VDD and -1.3V for VSS instead of the preferred 3V VDD and -3V VSS. However, the datasheet revealed that the maximum current required by the chip was around 60 times less than the current that could flow through the power divider circuitry, so the circuit was deemed functional.

Finally, the pin headers would connect the probes easily and effectively. In addition, an unused jumper would look like a very high impedance probe to the measurement circuitry and programming could be used to recognise this state and ignore if it was so desired.

5.2.6 Microprocessor circuit

Figure 5.6 will give the microprocessor circuit.

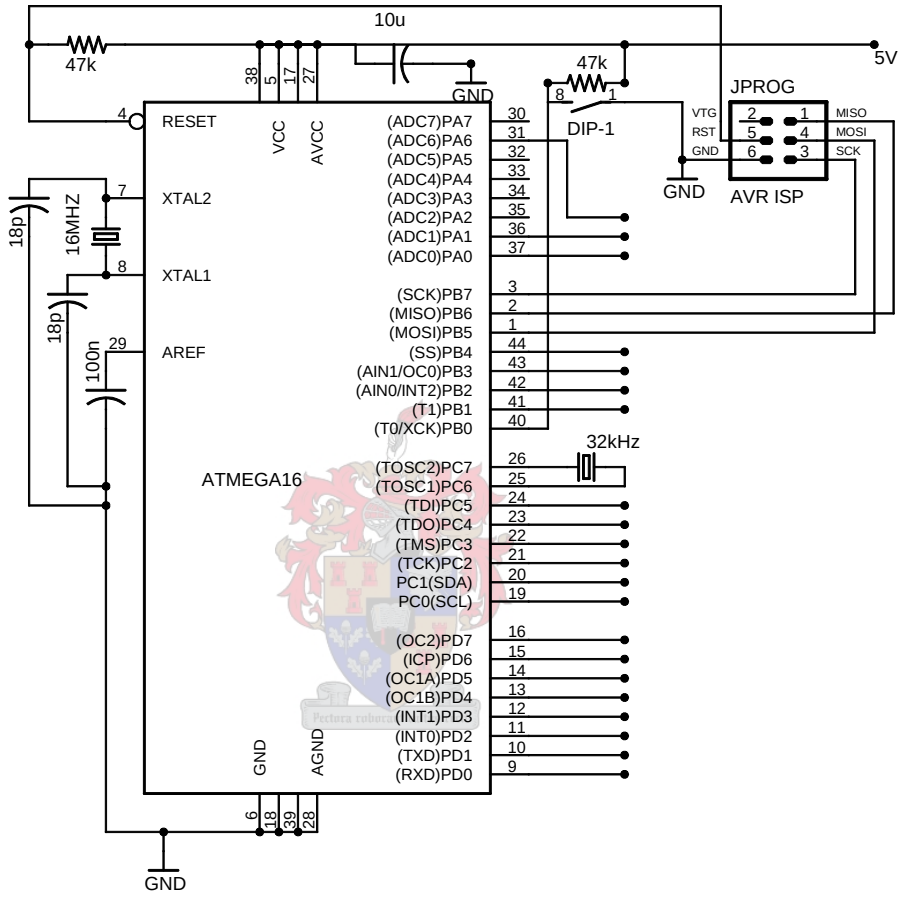

Figure 5.6: Microprocessor circuit.

In Figure 5.6 there are only two major circuit elements: The microprocessor, or ATMEGA16, and the ISP pin header, named the AVR ISP. Most of the other components were added to complete the microprocessor's hardware requirements.

The microprocessor chosen to control the entire AMD was the ATMEL ATMEGA16. It could provide all the functionality required by the AMD design. The functionality required will be summarised quickly:

- Sleep modes to limit power consumption during times when measurements were not taken.
- A/D ports to sample the measured voltages.
- D/A abilities, realised in this case by the PWM generation functions.

- Serial communication abilities.
- ISP capabilities, since the device must be adaptable to changing experimental requirements.
- Multiple pins for the control of various external chips.

The 16 MHz crystal provided the clock to the microprocessor. It was decided to use the fastest clock frequency the ATMEGA16 could handle in order to generate the smoothest possible sine wave with the PWM generator. In the case of the AMTEGA16, this frequency was 16 MHz. The two 18 pF capacitors connected to the crystal were required for the correct functionality of the ATMEGA16 clock.

The 32 kHz crystal connected to pins PC7 and PC6 acts as the external clock for the internal timer, called timer2. By using an external crystal to run timer2, timer2 could be used to bring the ATMEGA16 out of a deep sleep state. However, this function would only work with a so called "clock crystal", or the 32 kHz crystal, so this crystal frequency was the obvious choice. Finally, the true frequency of the clock crystal is 32.768 kHz, but it is generally referred to as a 32 kHz crystal.

The 47 kΩ resistors acted as pull-up resistors for the RESET and PB0 pins. The pull-up resistor value was specified in the datasheet for the RESET pin, but PB0 required no such resistor. However, PB0 was used as the detection pin for a communications-query. By switching the DIP1 switch to ground, the user indicated that the chip had to come out of sleep mode and enter into communications mode. The details behind this action is in the programming section. Therefore, the 47 kΩ resistor enabled a safe high to low pin transition.

The other capacitors acted as decoupling capacitors and was either added for proper power circuit constructions, or because the datasheet required it to be there. The 100 nF capacitor connected to the AREF pin was one such requirement of the microprocessor's A/D functionality.

The other important facet of the circuit was the ISP pin header. The ATMEGA16 can be reprogrammed through in-system-programming. However, it was decided to dedicate the SPI pins of the ATMEGA16 to this purpose and therefore no other SPI chips were connected to the MOSI, MISO and SCK pins of the ATMEGA16. The ISP pin header connections were based on the programmer's hardware and for that reason, VTG was not connected to any 5V supply voltage. If VTG was connected to 5V, it could damage the programmer circuit. The programmer and programming procedure will be discussed under the programming section.

As a final detail, all the pins, their connections and their intended use will be given by table 5.1.

Table 5.1: Different pin connections of the ATMEGA16

Pin name	Connection	Function
VCC	5V supply	Chip power
AVCC	5V supply	A/D reference voltage
RESET	ISP header reset pin	Chip external reset
XTAL1	16 MHz crystal	Clock
XTAL2	16 MHz crystal	Clock
AREF	100 nF decoupling capacitor	Secondary A/D reference voltage
PA6	V_t measurement	A/D sampling pin
PA1	V_b measurement	A/D sampling pin
PA0	V_r measurement	A/D sampling pin
PB7	ISP header SCK pin	Programming pin, clock
PB6	ISP header MISO pin	Programming pin, data in
PB5	ISP header MOSI pin	Programming pin, data out
PB4	Temperature sensor SI/O pin	LM74 data in/out pin
PB3	Temperature sensor SC pin	LM74 chip select pin
PB2	Temperature sensor ~CS pin	LM74 clock pin
PB0	Communications detection switch	User interface detection
PC7	32 kHz crystal	Timer2 external clock
PC6	32 kHz crystal	Timer2 external clock
PC5	MOSFET gate	LED activation
PC4	EEPROM S\ pin	EEPROM select pin
PC3	EEPROM Q pin	Data from EEPROM
PC2	EEPROM W\ pin	EEPROM write protect pin
PC1	EEPROM D pin	Data towards EEPROM
PC0	EEPROM C pin	EEPROM clock pin
PD7	ADG706 EN pin	Probe signal enable pin
PD6	Both ADG619 pins 6	Activation of ADG619 switch
PD5	ADG706 A0 pin	Probe channel select
PD4	ADG706 A1 pin	Probe channel select
PD3	ADG706 A2 pin	Probe channel select
PD2	ADG706 A3 pin	Probe channel select
PD1	MAX232 T1IN pin	Transmit serial data pin
PD0	MAX232 R1OUT pin	Receive serial data pin
AGND	Circuit gound	A/D ground
GND	Circuit ground	Chip ground

5.2.7 Temperature sensor circuit

Figure 5.7 will give the temperature sensor circuit and its connections.

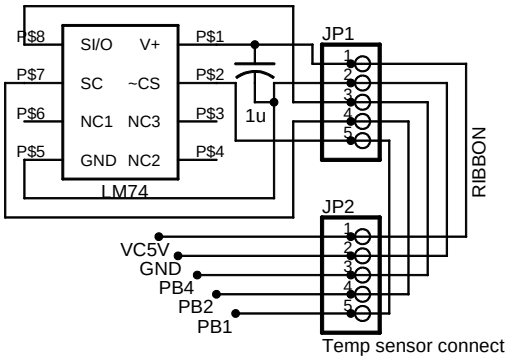

Figure 5.7: Temperature sensor circuit.

Figure 5.7 shows how the temperature sensor would be connected to the pin header on the automatic measurement device PCB. The temperature sensor's connection is a single row 5-pin header (JP2). The temperature sensor chip was connected via a ribbon cable and appropriate connector. The chip's type was the LM74 and provided temperature info via the SPI standard. In turn, this info was interpreted as a temperature (in degrees Celsius) in the programming.

The range of temperatures that the LM74 could detect was well beyond the range that the typical milk fermentation experiments would take place in. A small PCB circuit was designed for the sensor and the ribbon cable was soldered directly onto the pin header holes represented by JP1 in Figure 5.7. Finally, the 1 μF capacitor functioned as the decoupling capacitor for the LM74 power supply.

5.2.8 EEPROM circuit

Figure 5.8 will give the EEPROM circuit:

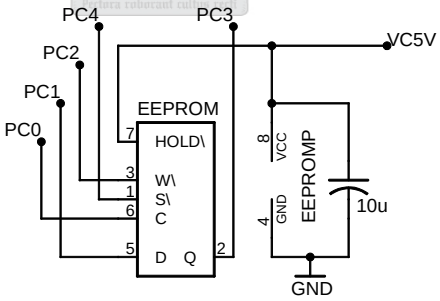

Figure 5.8: EEPROM circuit.

The EEPROM circuit is quite simple. The only extra component that was added was the 10 μF decoupling capacitor connected to the power pin. The rest of the connections were connected as required by the chip's datasheet and these connections are indicated in Figure 5.8.

The EEPROM chip type was the 25AA256 from Microchip. It used the SPI standard and had 256 kbit memory. The choice of memory size requirements was based on the average experimental sampling rate, which was based on the following criteria:

- The average length of a probe measurement would be 3 days. The maximum was determined to be 10 days if the measurements were done in cold storage. These lengths were based on the average time it would take for milk, containing the correct bacteria types, to ferment and become sour.
- The typical measurement intervals would be an hour. Therefore, in a single day, 24 measurements would be taken for one single probe.
- A further three values would be stored per probe and a fourth value per measurement cycle. These values would be the calculated probe resistance, the calculated probe capacitance and the calculated probe current density and once every probe has been measured, the ambient temperature value would be stored.
- The measurement device had to measure 16 probes.
- The size allotted per measured variable was decided to be 16 bits, or two bytes. This would allow sufficient resolution per variable, since the variables would essentially be converted into integer numbers before storage.

Based on the criteria, the calculated maximum storage size was (in bits) $10.24.(16.3.16 + 16)$ which gave 188160 bits, or 23520 bytes, or 183 kbits. Therefore, the first chip able to provide enough memory was the 256 kbit size.

A final circuit connection that needs to be discussed is the HOLD\ pin of the 25AA256 EEPROM. This pin could be used to hold data transferring if it was pulled low. This function was not required, so the pin was connected to the 5V supply in order to keep it high throughout its active time.

5.2.9 Serial communications circuit

Figure 5.9 will give the circuit for the serial communications connections.

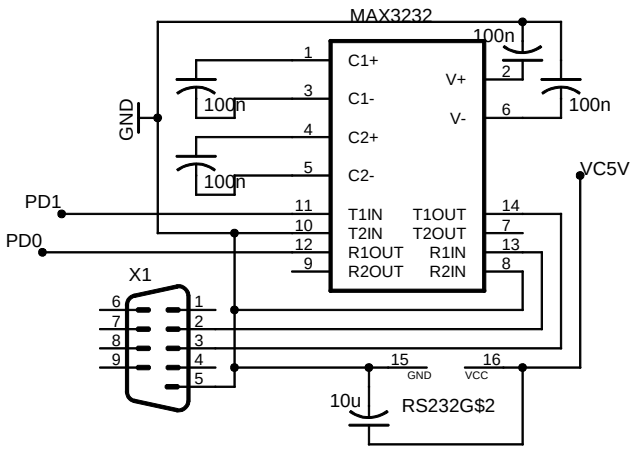

Figure 5.9: Serial communications circuit.

The two major components present in Figure 5.9 are the DB9 serial port connector, named X1, and the MAX3232 serial communications chip. The MAX3232 chip's power connections are represented by the RS232G$2 connections. The MAX3232 enabled the microprocessor to send and receive serial communication

data. Only one channel was used, so the other channel's input pins were grounded (R2IN and T2IN). The only connections required to enable serial communications were the send, receive and ground signals from the MAX3232 chip.

The chip's four 100 nF capacitors functioned as its charge pumps and allowed the chip to provide the ±12V serial port voltage signals from its own 5V supply. The 10 μF capacitor acted as the decoupling capacitor and the power supply was the switching 5V supply.

The communication required the transmit and receive signals and the serial cable to be connected as follows:

- The transmit signal was received from the PD1 (or TXD) pin from the microprocessor. This pin was connected to the T1IN pin on the MAX232 chip. In turn, the MAX232 T1OUT pin was connected to pin 3 of the DB9 connector.
- The receive signal was received from pin 2 on the DB9 connector. This pin was connected to the R1IN pin on the MAX232. In turn, the MAX232 R1OUT pin was connected to pin PD0 (or RXD) on the microprocessor.
- The final piece was the serial cable. The two sides of the serial port had pin two of the one connector connected to pin 3 of the other and vice versa. The ground pin (pin 5) was connected to pin 5 of the other connector. These connections was sufficient to enable the communications required by the AMD.

5.2.10 Light emitting diode circuit

The final circuit is the light emitting diode (LED) circuit and will be given by Figure 5.10.

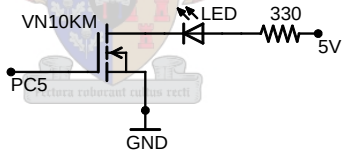

Figure 5.10: LED circuit

The LED circuit consisted out of a 330 Ω resistor, a surface mount LED and a VN10K n-channel enhancement-mode MOSFET. The LED circuit would be pulsed every 8 seconds by the microprocessor. The reason for the specific time will be discussed in the programming section.

The microprocessor turned on the LED by making the MOSFET's gate high. When the gate became high, the MOSFET switched on and current flowed through the LED. The current that flowed through the LED can be computed as follows:

$$I = \frac{V_{5V} - V_{LED} - V_{DS}}{R}$$

The datasheets give the average drain to source saturation voltage (V_DS) for the MOSFET's on condition as 0.2 V and the voltage drop over the LED at around 1 V. Measurements confirmed this. The current that would flow through the LED was chosen to be below 15 mA, but above 10 mA. Therefore, the total current that flowed through the circuit with a 330 Ω resistor in series with the LED was:

$$I = \frac{5 - 1 - 0.2}{330}$$

Which gives around 11.5 mA of current. In addition, in order to keep the current drawn per hour at an absolute minimum, it was decided to blink the LED for 10 ms only. If it is assumed that a battery could give 11.5 mA for one hour, then the total current that it could give in 1 ms is $11,5/(60.60.1000) = 3.2$ μA. Therefore, if the LED blinked every 8 seconds for 10 ms, the total current it would draw would be $3,2.10^{-6}.10.(3600/8)$ or 0.014375 mA. The battery's life could be extended $11,5/0.014375 = 800$ times by this method. The reason the LED had to blink every 8 seconds was because 8 seconds was the maximum time the microprocessor could be asleep before it had to wake up. Consequently, it was decided to use this cycle to indicate if the microprocessor was working or not.

5.2.11 Complete system tests

After the different circuits were built and tested independently, the entire measurement device had to be tested. In order to do this, the programming was adapted to test the various aspects of the measurement device. The programming flow was written out via serial port to a PC and the resulting debug code was scrutinized. Finally, the reliability of the device was tested by allowing the device to run continually for two weeks.

Once the test results showed that device performed according to specifications, the milk experiments could begin in earnest.

5.3 Software Design

The software design formed the brains of the AMD, since it was responsible for controlling the microprocessor's various responsibilities. These responsibilities included functions such as the voltage measurements, data storage and measurement timing.

The software design section will begin with an explanation of how the microprocessor was programmed and how the program was coded. Afterwards, the major functions and procedures will be discussed. All of the major decisions that were taken before implementing certain code sections will also be discussed. The different discussion will centre around the written code, which can be found in Appendix D.

5.3.1 Programming the microprocessor

Method of programming

As mentioned in section 5.2, the microprocessor that controlled the entire measurement device was the ATMEGA16. This chip was programmable and could be reprogrammed with different programming methods. In addition, with the help of a bootloader program residing withing its first section of internal memory, the ATMEGA16 could be programmed through the serial port.

It was decided, however, that the ISP programming method would be the simplest option. These decisions were based solely on the programmer - the STK500 development board from AVR. The STK500 contained different types of programming ports, making it capable of serial or parallel high voltage programming and

ISP programming. Amongst all these options, the ISP programming method was the least amount of hassle to implement.

The program used to communicate with the STK500 was AVR Studio. The programming procedure was done as follows:

- The AMD was switched on and the ISP pins on the device connected via a ribbon cable to the corresponding ISP programming pins on the STK500.
- The STK500 was then connected to the PC via serial cable and switched on.
- AVR Studio was then started up and told to connect to the development board. The AMTEGA16 chip was selected as the target and the "connect" button pressed. If all was done right, AVR Studio detected the chip and was ready for programming.
- No other options were changed on the board, since the programmer's default options proved to be sufficient to program the chip.
- The hex-file of choice was then programmed onto the ATMEGA16, but only after the previous contents were erased.

Code creation

The programs used to create the hex-file were obtained from the open-source community. These programs were packaged under the WINAVR signature. The program used to compile the hex-file was Programmer's Notepad. This program used a Makefile to compile the programming language of choice into a hex-file and AVR Studio programmed this hex-file onto the ATMEGA16.

A high level language was used to code the program that ran on the microprocessor. The language used was *C*. The reason was that the WINAVR bundle contained specific Atmel libraries that defined the ATMEGA16 registers and functions in the *C* language.

In the next few subsections, an overview of the most important coding decisions will be given. Code will not be discussed line by line, unless it is required to explain certain functions. In addition, as far as it is possible, the code will be detailed in the order that the chip would typically run it.

5.3.2 Main procedure

The *main* procedure was responsible for the correct chronological execution of the different program steps. Figure 5.11 will give a flow diagram illustrating the major decisions:

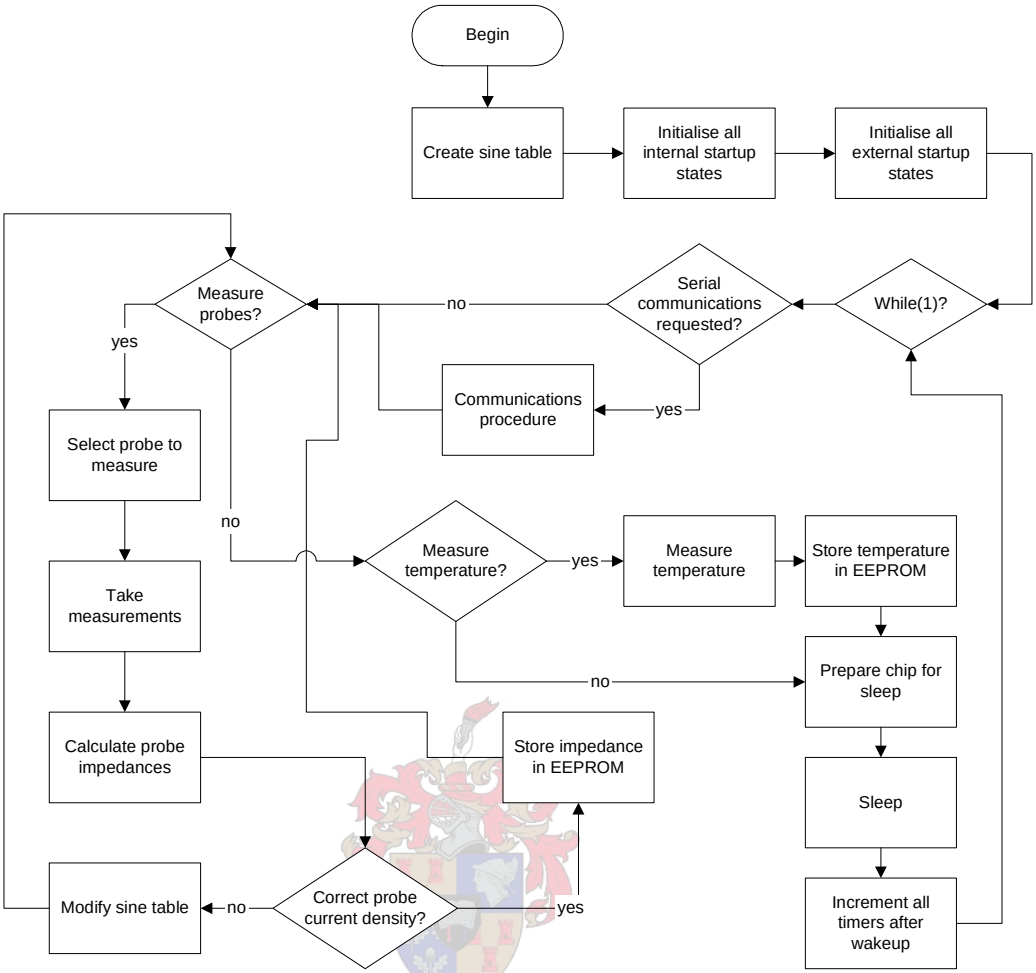

Figure 5.11: Flow diagram of *main* procedure.

The flow chart in Figure 5.11 should be fairly self-explanatory. Every block represents either a procedure call, or a sequence of code executions and every diamond a decision (such as an if or while test). Some detail about the microprocessor's timers, or more specifically timing, is not present in the flow chart and will be discussed under the seperate procedure discussions. It must also be remembered that each step in the *main* flow chart resembles a number of decisions and steps and the ones shown here is the broad overview.

Initialisations

The *main* procedure started out by calling the sine wave generation procedure in order to create a default sine table for the PWM generation. The default value for the sine table was chosen based on probe impedance values obtained in a 1% salt solution. The detail behind the sine table and PWM generation will be discussed under a seperate heading. The procedure then proceded to call the pin initialisation procedure, since certain pins were required to be a certain value at startup. Then, all the timer initialisation procedures were called. These procedures made sure that every timer and their corresponding interrupts were correctly set up. Following this, the A/D registers' and USART (serial communications) registers' initialisation procedures were called. The sleep mode registers were then set and only after all these procedures were called, was the

global interrupt flag enabled. By doing it in this order it was ensured that absolutely no interrupt could occur whilst critical setups were done.

After the interrupts were enabled, the overhead procedure was called. Overhead served a very important role in the AMD's program flow, since this procedure alone was responsible for recognising the different states that the microprocessor would next move in to. Finally, the external EEPROM initialisation procedure was called.

Main loop

The main loop is the one that took place within the while(1) loop. A broad overview of the basic procedures and processes will be given here.

The serial communications procedure was called if the microprocessor detected a low at the input pin connected to the DIP-1 switch. The following must be noted:

- Serial communication detection is only done at the start of every new program cycle. The cycle is enterd into after a chip reset or after a chip wakeup.
- Serial communication detection is never performed in any other position than in the position indicated in the flow chart in Figure 5.11. Therefore, if the probe measurement cycle has started, the chip will not enter into serial communications until after the entire measurement cycle has completed and the chip has reawakened from the sleep that followed the measurement.
- Once serial communications has started, the communications procedure keeps the chip in this mode until the corresponding DIP-1 pin reads a high. This situation is not indicated in the flow chart, since it is not caused by the main procedure.

The probe measurement and temperature measurement sections were only started if a control variable allowed it. This control variable represented the number of probes that were already measured. The overhead procedure controlled this variable and would reset it to zero if a new measurement sequence was required.

Before any of the above tests were done, a global variable was changed that indicated to the timers that controlled the LED flashing speed that the speed had to increase. This helped the user to recognise the measurement state once it started. If no measurements were done, the LED's flashing condition changed back to normal too quickly for the user to notice anything. After a measurement cycle the condition was also reset to normal.

The basic measurement procedure involved enabling the ADG706 chip, calling the probe selection procedure, calling the sampling procedure, calling the calculations procedure and then disabling the ADG706 chip. The calulation procedure then sent back a variable that indicated whether the probe current density values were within parameters. If not, the overhead procedure was called to modify the sine table's values and the measurement procedure was restarted. However, during the milk measurements, the current density was not checked since it was decided to limit the amount of on-time that the chip had to make. Therefore, Figure 5.11 needs to remove the "correct probe current density" diamond and have a line directly from the "calculate probe impedance" block to the "store impedance in EEPROM" in the case where the current density is not checked. Once one set of probe values were stored, the global sampling variables were reset and the measurement sequence continued. Once all the probes were measured, the temperature would be measured and the chip would move on to its pre-sleep code sections.

Before the chip was allowed to go into sleep mode, the EEPROM was polled to make sure that the data was written to it succesfully and after this check, the overhead procedure was called. On wakeup, the overhead procedure once again checked on the chip's current program state and the loop restarted from the serial communications test.

5.3.3 Sine wave generation

In order to explain how the sine wave was generated by the ATMEGA16, a few programming sections will need to be discussed simultaneously. These discussions will include the internal timer functionalities, the PWM generation function, the sine wave generation theory and the sine table creation procedure. A broad overview of the program flow will also be given in a flow chart.

Theory behind PWM generated sine waves

The method chosen to generate the required sine wave was chosen to be the PWM generation scheme. PWM, or pulse width modulation, provided the D/A ability that was required to change the generated digital sine wave into an analog sine wave. However, the PWM alone could not completely provide the required sine wave and the PWM generated wave had to be filtered in order to obtain the final sine wave. The filter was described in section 5.2.3.

A PWM signal is a square wave that is on for a certain length of its period and off for the remainder of its period. The square wave is generated by switching an output pin high and low based on the requirements of a digital signal. The square wave is considered on when the output of the digital pin is high and off when the output of the digital pin is low.

An analog load will only see the average power delivered by a PWM wave. If the wave is on for long periods of time and off for short periods of time, the average power delivered to the load will be high. The inverse is also true. A PWM wave that is off for long periods of time and on for short periods of time will result in a low average power being delivered to a load. Now, if a PWM signal was modulated so that the time it was high had a sinusoidal variation with a certain frequency, thereby causing the average power delivered to a load to have a sinusoidal curve at that frequency, then a sine wave would effectively have been created. This was the method that was used to create a sine wave of a 100 Hz. However, this is only half the story. The true output is far from a sinusoidal shape and the PWM output contained a DC as well as various other unwanted frequency components, which is why an external hardware filter was required.

In order to change the PWM generated wave with a sinusoidal shape and at the correct frequency, a sine table had to be created that would tell the PWM signal what shape to take on and at what time. In addition, the maximum sine wave amplitude that could be obtained with a 5 V digital signal was 2.5 V, since the signal would contain a 2.5 V DC offset if a complete sine wave was generated by the PWM signal.

A simple PWM wave will be given by Figure 5.12. This is not the wave generated by the AMD, since that wave will not display well. Instead, the PWM signal that will be displayed will resemble a wave being generated at a speed of around 16 times slower than the real device's speed. The wave was generated in Matlab using the same program code concept as that which was used in the microprocessor.

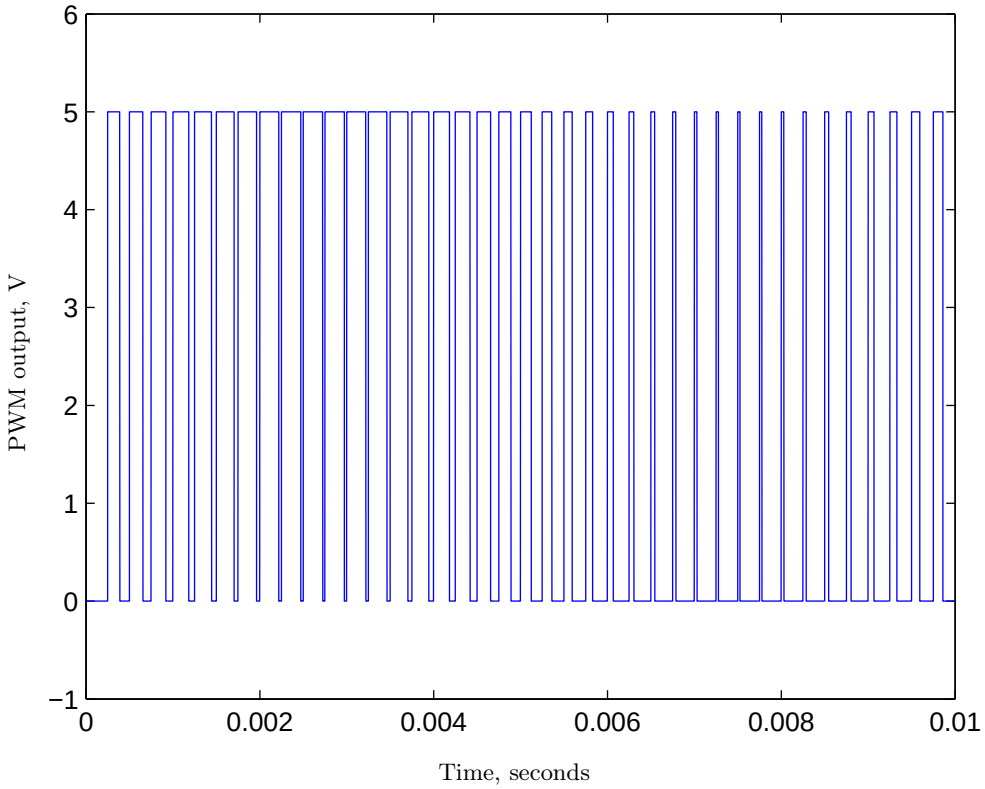

Figure 5.12: PWM signal of 100 Hz sine wave.

Finally, the resulting sine wave found after the PWM signal (generated by at the real microprocessor clock speed) is filtered is given by Figure 5.13.

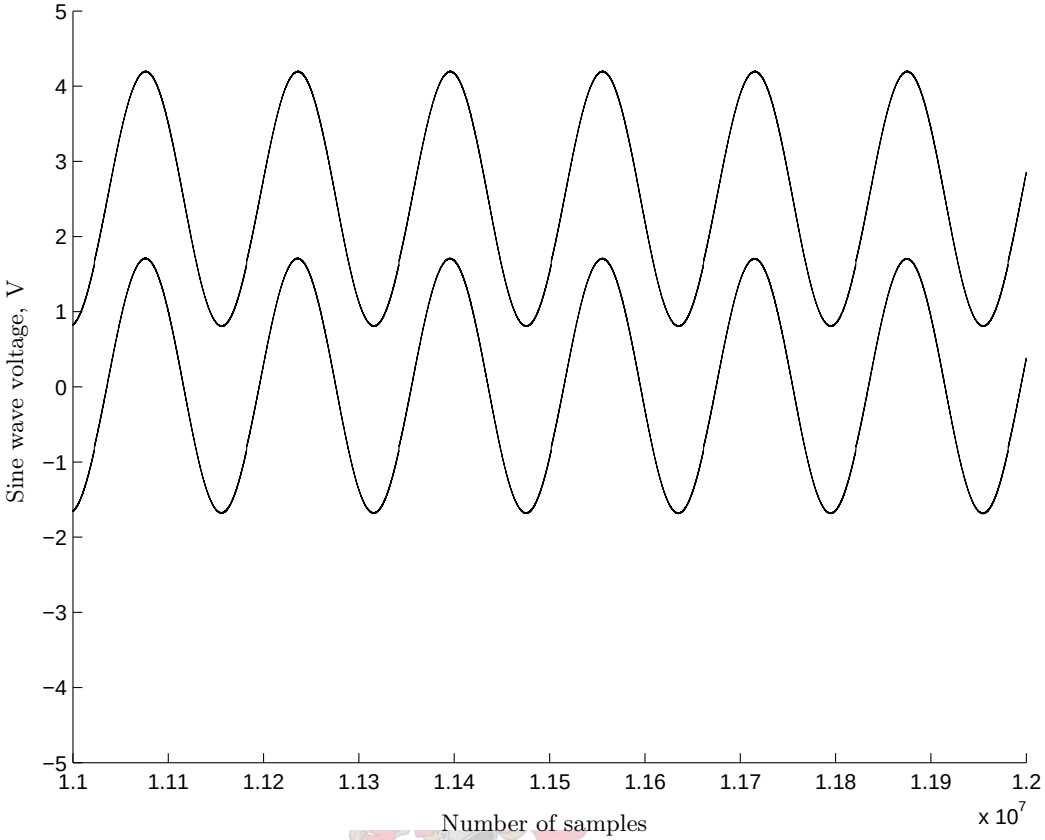

Figure 5.13: Resulting sine waves of filtered PWM signal as measured after different filter stages.

Figure 5.13 shows the two outputs of the different filter stages. The sine wave swinging around a DC voltage value is the output of the low pass filter and the sine wave swinging around 0 V is the output of the high pass filter. The PWM was generated to give a final peak sine wave output voltage of 2 V, but the simulation indicated that the expected output voltage would be more like 1.8 V peak. However, measurement taken from the completed AMD revealed that the method was sound, since the expected voltage amplitude value was indeed measured at the output of the filter. Therefore, the simulation results confirm the proof of concept, not the exact values.

The graphs in Figure 5.13 were generated by Matlab's simulink tool. The code used to generate the different PWM waves, as well as the simulation options, block diagrams and final outputs can be found in Appendix C. Finally, the values on the x-axis were determined by the simulation parameters and the time values can be found in the same Appendix.

Sine table generation

The sine table theory was obtained from reference [13]. The basic steps that were required to generate a sine wave through a sine table was implemented as suggested therein.

The sine table was responsible for providing the PWM function with a value that would indicate to it how long it should be on and how long it should be off. However, the sine table had to give enough compare values within a specific timeframe in order for the PWM generation function to create the correct sine wave

frequency. In other words, by the time the PWM is supposed to generate the value of the sine wave at 90 degrees (or a quarter of the sine wave period), the sine table should also be at the point where a quarter of it's values have already been compared, assuming it contained the values for an entire sine wave.

It can be understood, therefore, that an integral part of the sine table generation was the clock speed and timer overflow lengths within the microprocessor. The ATMEGA16 had a clock crystal of 16 MHz. Therefore, all the clocks driving the different chip functions had a frequency of 16 MHz, if they were not scaled. In turn, the different timers that would drive the PWM was set to have a maximum counting length of 8 bits, or a value of $2^8 - 1$=255, for reasons that will be given later.

Based on the above information, the following steps were taken to calculate the length of the sine table:

- Firstly, the amount of clock cycles that could take place within the timerframe presented by a 100 Hz wave had to be calculated. For a 16 MHz clock frequency, the amount of cycles were: $\frac{1}{100}/\frac{1}{16.10^6} = \frac{16.10^6}{100} = 16.10^4$ cycles.
- Next, the amount of timer cycles had to be calculated in order to know how many PWM generation cycles there would be for a single 100 Hz period. We know that a single timer cycle takes 256 clock cycles to reach overflow, so the value would be: $\frac{16.10^4}{256} = 625$.
- Finally, if it is understood that the first quadrant of a sine wave contains all the information needed to create a complete sine wave, then the amount of time cycles required to describe the first 90 degrees of a sine wave would be :$\frac{625}{4} = 156.25$, which an integer system would take as 156. This value would be the length that the sine table needed to be in order to provide enough information for a PWM clock speed of 16 MHz to generate a sine wave of a 100 Hz.

The sine table has two more aspects to it: sine wave amplitude and DC offset information. The values stored within each sine table position was not limited to one sine wave amplitude, as long as the values following each other exhibited a sine wave shape. Therefore, the sine table could be modified in order to allow the PWM to create a sine wave with an amplitude signal based on the requirements of the probes. In addition, the sine table had to cater for an entire sine wave, not just the positive section. Therefore, in order to create an entire sine wave, a DC offset had to be added into the final PWM compare values. This meant that all sine table values were given a bias of 2.5 V.

The amplitude and bias values were based on the following understanding: If the ideal PWM signal could take on 255 different values (based on the 255 timer counts), then the average output voltage should be able to take 255 different values between 0 V and 5 V. If we assume that a high valued digital number equals a high analog voltage level, then in order to generate an analog voltage level of 4 V, the PWM signal had to be high for $\frac{4}{5}.255 = 204$ counts and low for $255 - 204 = 51$ counts. Now, if sine wave peak values of ± 1 V were desired, as measured at the output of the filters, then the sine wave swinging around the DC offset of 2.5V would need to have a 3.5 V maximum and 1.5 V minimum peak value. Therefore, the sine table values would be computed based on the final peak value ($\frac{1}{5}.255 = 51$) added onto the bias value ($\frac{2.5}{5}.255 = 127.5 = 128$).

The sine table was generated by the *sin_table* function. An array was generated that would contain the values that the timer would use to generate the PWM wave. The radian values were computed by dividing the value of $\frac{\pi}{2}$ with the length of the sine table array and multiplying that value by the sine table array number that the value was being calculated for. Therefore, position 0 was at 0 rads, position 79 was at $\frac{\pi/2}{157}.79 = 0.79$ rads and position 157 was at $\frac{\pi/2}{157}.157 = 1.57$ rads. An imported sin-function would then use these radian values to calculate a float value between 0 and 1. In addition, only the first 90° of sine values

were stored by the sine table. Finally, the sin-function's answer was multiplied with the desired amplitude value, the DC offset added and the result stored in the sine table array.

PWM and timer setups

The microprocessor's PWM generation function was directly connected to its timer function, since the speed of the timer directly determined the speed of the PWM generation. The PWM wave was generated based on compare values stored within a special compare register. The values stored in these compare registers were compared to the count value of a specific timer. In addition, a variety of options within other specific registers would determine the inital output value, output shape and speed of change.

The timers within the ATMEGA16 had a specific PWM setup that allowed for quick PWM generation. This option is called fast PWM mode. Fast PWM mode allows the microprocessor to generate a cyclic PWM signal.

The fast PWM mode functioned as follows:

- The timers are set to count upwards from a minimum to a maximum value and once the maximum value is reached, it will restart at the minimum value. These values can be specified by the programmer.
- The PWM output starts at the top or bottom value (0 or 5 V) based on the register setups.
- During counting, the value of the timer is constantly compared with a value in a compare register. If these values coincide, the PWM output is reversed from its start value.
- Once the timer has reached its maximum, an overflow interrupt is generated on overflow and the PWM output is reset to its start value. If the interrupt is serviced, another compare value can be entered into the compare registers during the interrupt service routine, which will allow for a dynamic change to the PWM output.

The timer registers that could be used to generate PWM waves from the ATMEGA16 were the *timer0* and *timer1* registers. Both these registers were set to fast PWM mode, but only the output connected to the *timer0* register was used. In addition, *timer0* could only be a maximum size of 8 bits, so *timer1*, which could be 16 bits, were limited to 8 bits as well. This meant that the absolute maximum number of counts any of the timers could give were 0 to 255, or 256 counts, before it overflowed and restarted at 0.

The reason for using both registers was to limit the amount if code that would be executed by the timer's interrupt service routine. The timers were not used solely for the PWM generation, so to limit the amount of time the processor would spend in any one interrupt routine, it was decided to split the load between two timer interrupts. It was further decided to use *timer0* as the general delay timer and to dedicate *timer1* as the PWM compare value calculation timer. Any of the two timers could perform any of these functions, so no merit must be placed on the specific choices.

The timers were initialised by the *init_timer0* and *init_timer1* procedures. For detail, refer to the ATMEGA16 datasheet mentioned in Appendix E and the code in Appendix D. The interrupt service routine that was responsible fot the correct PWM output was called *ISR(TIMER1_OVF_vect)*. The other timer interrupts will be discussed in the sections where they were critical.

Timer interrupt service routine

The *timer1* ISR was responsible for determining to what point the sine table was already compared and for loading the next sine table compare value into the PWM compare register. In addition, since only the first 90 degrees of information was kept in the sine table, the *timer1* interrupts had to calculate the remaining 270 degrees of information from the first 90 degrees of information.

The complete sine wave was calculated based on the following: For the first 90 degrees, use the sine table from beginning to end. If the sine wave lies between 90 and 180 degrees, load the values of the sine table in from end to beginning. If the sine wave lies between 180 and 270 degrees, use the sine table from beginning to end and multiply the values by -1. Finally, if the sine wave lied between 270 and 360 degrees, load the values of the sine table from end to beginning and multiply the outputs by -1.

Since the sine wave that would be described by the sine table would swing around an offset of 127, it meant that the mathematical concepts had to be modified to work in the mircoprocessor environment. Therefore, in order to describe a complete sine wave in the microprocessor environment, the first 180 degrees would use the value of the output provided by the sine table to compute the positive sine wave, but the last 180 degrees would be subtracted from the value of 255 to compute the negative cycle of the sine wave.

Program flow for sine wave generation

To summarize the sine wave generation, the program flow will be given by the flow chart in Figure 5.14.

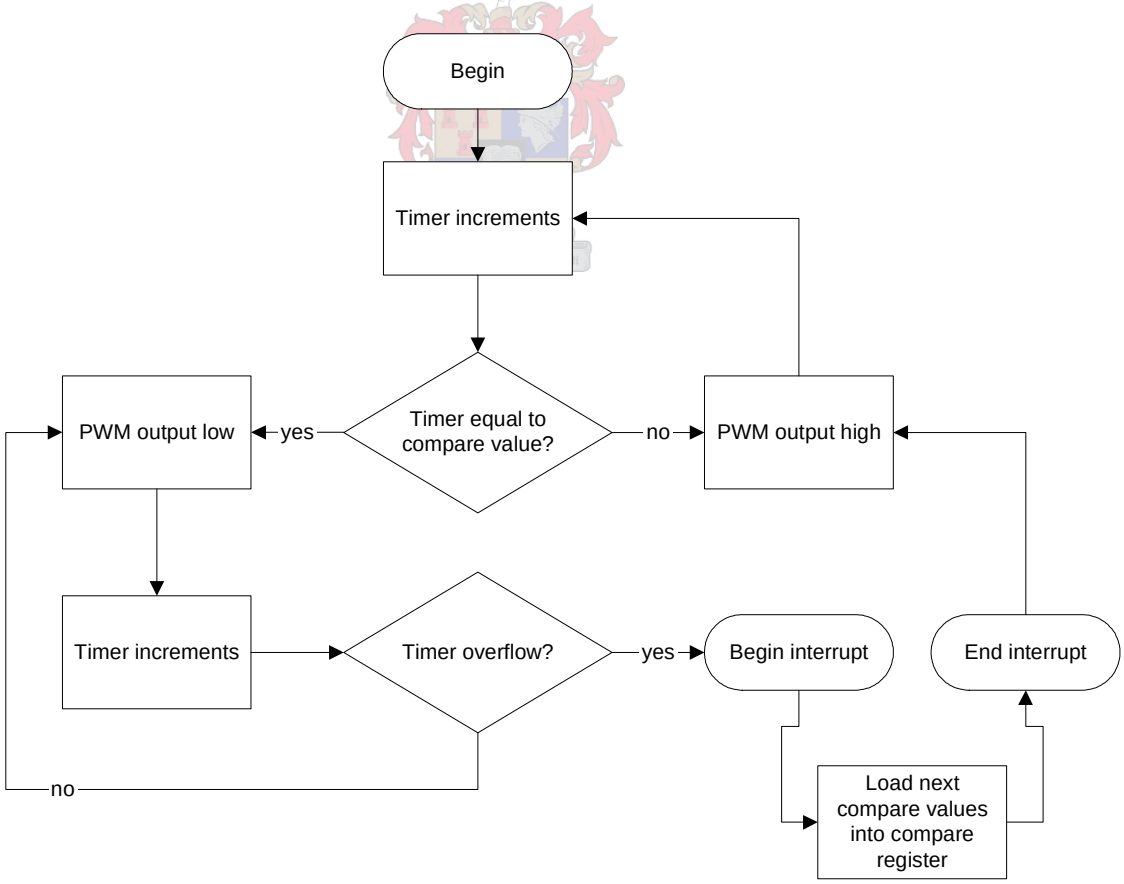

Figure 5.14: Sine wave generation flow chart.

The reader must keep in mind that most of this process happens in the background and that the only time the program flow of the main chip process is interrupted is during the interrupts service routine. In addition, the sine table creation and timer initialisations is assumed to be done by the main procedure. Finally, note that the procedure is cyclic and the only way that the PWM output could be stopped was to change the timer setup registers or to change the PWM output pin to an input pin. The latter was chosen and controlled by the overhead procedure.

5.3.4 Voltage measurement procedures

The voltage measurements required an understanding of two aspects: What to measure and how to measure it with the microprocessor. The probe theory and initial measurements revealed that the mathematical solutions required the peak value of the applied sine wave. The time at which that peak value is measured does not matter, as long as the peak value is fairly accurate. In order to measure these peak values, the microprocessor's A/D functions would be used extensively.

Characteristics of measured signal

The typical signal that would be expected on the A/D pins were already simulated for the sine wave generation discussion and can be found in Appendix C. To summarise, the typical measured signal would be a 100 Hz sine wave swinging around 0 V. It would be stable after around 0.75 seconds and remain stable for the duration of the measurement time. However, when a closeup of the sinusoidal wave was made, it was observed that the sine wave shape consisted out of a fast triangular oscillating frequency that could cause a measure of uncertainty over the exact value of the sinusoid at any time. See Figure 5.15 for a graphical representation.

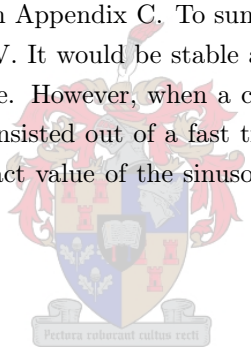

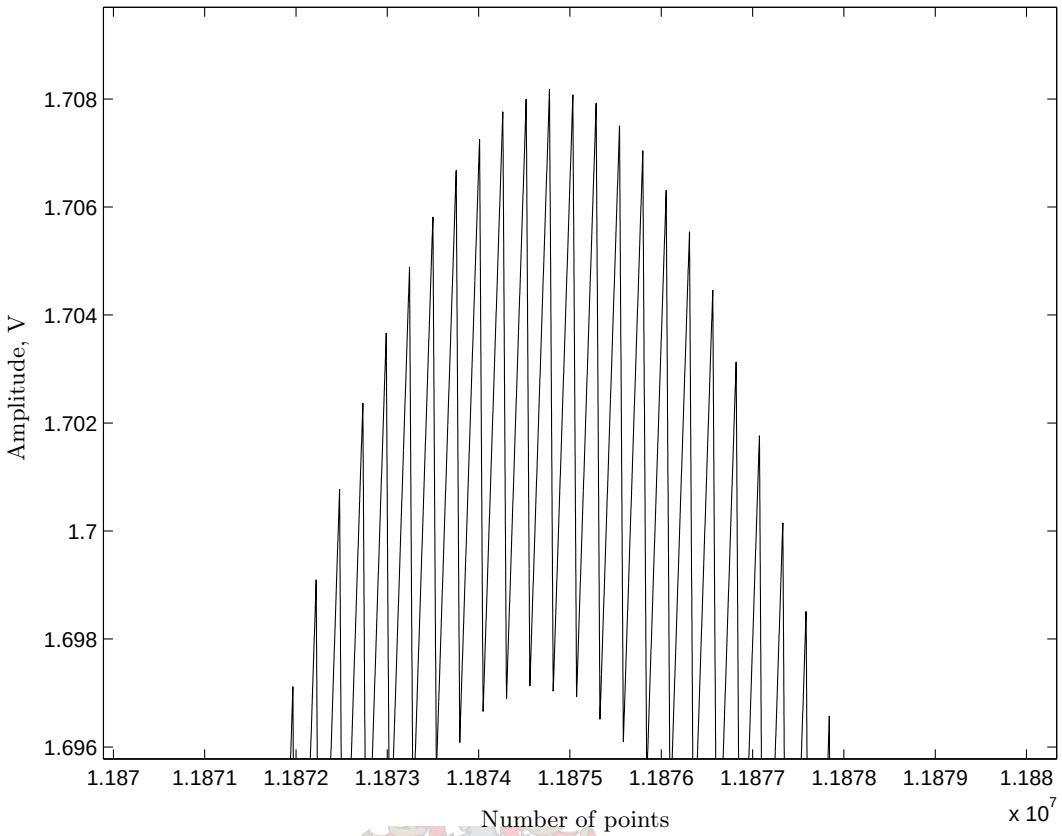

Figure 5.15: Close-up of sine wave peak.

Two major options were available for handling the triangular oscillation: Improve the filter or cater for it in the sampling method. The filter could not be improved much, since measurements revealed that the simple RC filters started to attenuate the output too much. However, the A/D procedures could be programmed to measure the average of a number of samples and that average value would be used in the calculations.

In addition to the triangular aspects of the measured sinusoids, the final measured shape of the sine wave was changed by the microprocessor's pins. This fact and the resulting sine wave shape was already discussed under subsection 5.2.4. The only voltages of interest were the positive peak values, so the chopped sine was more than adequate as a measurable voltage signal.

The typical voltage peak amplitudes that would be measured ranged around 1.1 to 1.4 V over the resistor and probes for an applied voltage of 2 V. These ranges were determined during the manual measurements of multiple salt and a few rudimentary milk experiments before the device's design was finalised. In addition, the maximum that the applied voltage could be was 2.5 V, which meant that the reference voltage of the A/D system could be modified to increase the measurement resolution.

The last aspect is the frequency of the sine wave. At 100 Hz, the frequency should be slow enough to allow an accurate A/D representation of the sine wave, since the A/D sampling rate should be fast enough to sample it accurately.

A/D setup and capability

Based on the characteristics described above, the ATMEGA16 A/D procedure was set up in the following way:

- The A/D sampling rate was set as fast as possible, whilst still retaining an accurate sampling result. A/D measurements done on a clean 100 Hz sine wave determined that an accurate sine wave representation could still be achieved with an A/D clock frequency of 2 MHz.
- In order to obtain the fast sampling rate, the A/D result bit size was set to 8 bits.
- The A/D conversion method was set to free running mode, a special capability of the ATMEGA16. In this mode, the A/D sampling process was a continuous one and no time was lost between the completion of one sample's conversion and the start of the next sample's conversion.
- The A/D reference voltage was set to the internal 2.56 V reference.

The ATMEGA16 A/D sampling rate used a different clock source than the microprocessor's. The microprocessor's clock was prescaled by a value and the resulting clock frequency was used by the A/D functions. In order to obtain the 2 MHz clock frequency, the microprocessor's 16 MHz clock was prescaled by 8.

The sampling resolution was determined by two factors: The choice of the conversion result's bit size and the choice of the A/D reference voltage. For the choices mentioned above, the resolution for a 8 bit result measuring between 0 and 2.56 V would be $\frac{2.56}{2^8} = 0.01$ volts per bit. In other words, the voltage being sampled must increase 10 mV before the A/D result would increase by 1 bit.

The sampling resolution choices were guided by two major problems: The stability of the A/D function's reference voltage and the characteristics of the sine wave peak that was being measured. The first problem was directly caused by the nature of the microprocessor's supply voltage. As was mentioned in subsection 5.2.1, the supply voltage was battery powered and tended to drop with time. This meant that if the reference voltage was connected to the battery supply, the A/D sampling result would an inaccurate representation of the true measured voltage, since the reference voltage changed with time. This problem was solved by using the ATMEGA16 internal reference voltage that is guaranteed to be nominal at 2.56 V, regardless of the supply voltage. Another reason this reference voltage was ideal was the fact that the measured voltage peaks would never be more than 2.5 V, since this is the absolute maximum output swing that the generated sine wave could have. The second problem was also solved by the choice of reference voltage. The triangular oscillations that formed the sine wave peak displayed by Figure 5.15 had a peak to peak difference of around 0.11 V. Therefore, the potential existed that the oscillations could cause an incorrect sample result. However, the choice of reference voltage forced this bit error to be one bit at the most and by using averaging this error would be further reduced.

With the setups as above, the A/D sampling procedure would take around 13 A/D clock cycles to complete one sampling conversion. If the first sampling conversion is ignored (which takes around 25 A/D clock cycles), the number of points that can be sampled for a 100 Hz sine wave is $\frac{2.10^6}{13}/100$ which equals 1538.46, or an interger number of 1538. In addition, the A/D results will give the same values for measured voltages in between its digital resolution range. For instance, if the value required to increase the A/D result one bit is 0.01 V, then all values that lie, for example, between 1.0095 and 1.014 V will yield a result of 1.01 V and a voltage value of 1.015 will yield a result of 1.02 V.

Figure 5.16 will display the typical sampling results of the abovementioned A/D setup as it would measure a 2.5 V peak, 100 Hz sine wave.

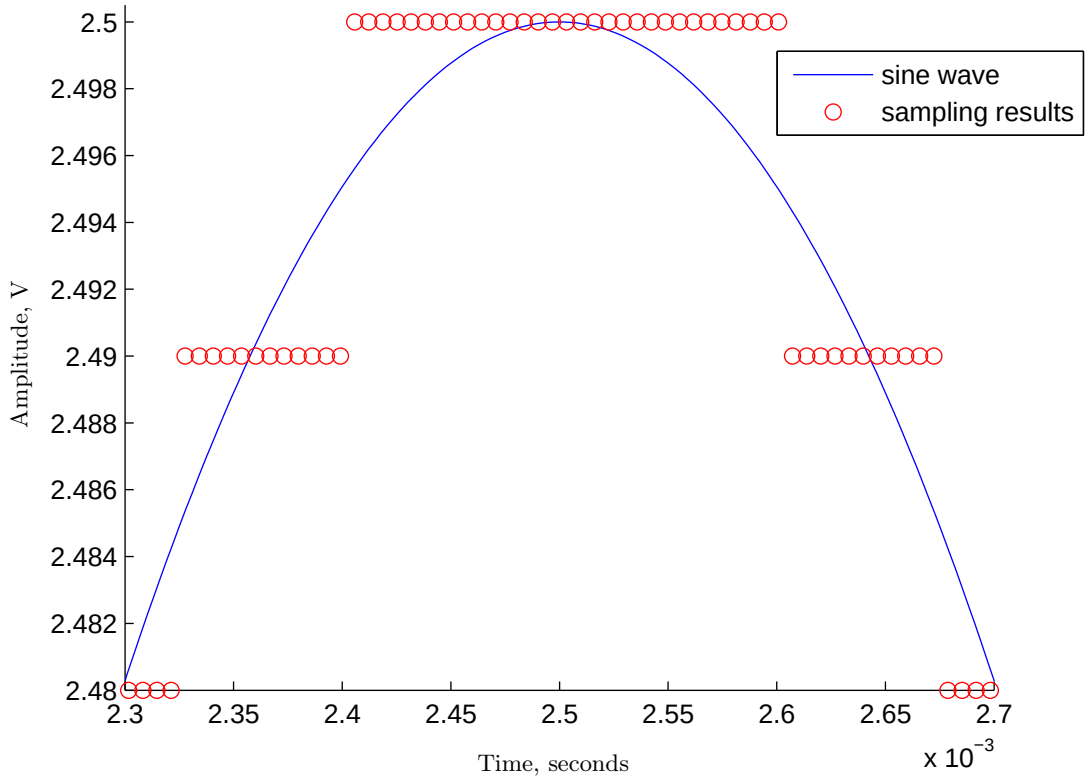

Figure 5.16: Sampling results of 100 Hz sine wave.

The number of times the sine peak was incorrectly picked up is not a problem, as long as the true peak value was always sampled.

The A/D registers was set up by calling the *init_ AD* procedure. In addition, a variety of safety delays and transient disipation delays were used to ensure that the measured A/D values were correct. The delays themselves were controlled by the *timer0* ISR and the length of delay computed by various delay procedures that will be discussed later. The *timer0* initialisation was done by the *init_ timer0* procedure, as mentioned before.

Probe selection procedure

The probe selection procedure, called *select_ channel*, would take the current probe number as an input and would write the correct address to the ADG706 analog multiplexer. The multiplexer would then switch in the correct probe into the circuit. The speed at which the multiplexer switched to the different probes was faster than the internal clock speed of the microprocessor, which meant that by the time the different lines of code was executed for the selection procedure, the probes would be ready for measurement.

Sampling procedure

The sampling procedure was the control procedure for the different voltage measurements. The procedure was called *sample* and was executed only after the correct probe was selected for measurement by the *select_ channel* procedure. The sampling procedure relied heavily on the A/D interrupt service routine. The basic sampling procedure involved the following steps:

- Select the correct A/D pin for sampling.
- Enable the A/D sampling functions and wait for the internal reference voltage to reach a steady state.
- Activate the A/D sampling function and wait until the A/D interrupt service routine has completed all the measurements by checking if the required amount of peaks were measured.
- Store the results in a global variable and reset the A/D result variable.

This routine would be done for all three required voltage measurements before the procedure would jump back to the *main* procedure.

A/D interrupt service routine

If the sampling procedure can be described as the control function of the voltage measurement procedure, then the A/D interrupt service routine can be described as the direct interface. The A/D interrupt service routine is called the *ISR(ADC_ vect)*.

The A/D ISR was directly connected to the conversion complete interrupt flag. However, since the A/D system was set up to run in free running mode, time would not be wasted between sampling results because of the time spent executing the interrupt code. This meant that the interrupt could be used to do various checks before the result was handled.

In order to ensure that the A/D would not miss the sine wave peak, the A/D code would simply save the highest of all the A/D results into a variable for a period of time slightly longer than an entire sine wave period. Once the number of samples required to measure one sine period has passed, the A/D interrupt service routine would check if the required amount of peak measurements have been done and if not, the result would be added to the previous results, the current peak value reset and the compare process restarted. Once the required number of peaks were measured, the A/D interrupt service routine would shut itself down. All conversions would therefore be stopped immediately and no more samples would be taken once the A/D function is stopped.

Based on preliminary measurement results, it was decided to take the average of 128 peak values before the A/D sampling could stop. All the 128 peak values would be added together in one 16 bit integer value and this value would be handled later by the calculation procedure. In addition, it was known that an entire sine wave required, at worst, 1538 A/D conversion results before it was completely described so a total amount of 1540 conversion results would cover slightly more than an entire sine wave period. Based on these values, the minimum amount of time that would be required to complete one voltage measurement would be $128.0.01 = 1.28$ seconds. However, in practice this time was longer, since the different delay procedures called in between each measurement forced this time to increase per voltage measurement.

Additional program code

An integral part of the voltage measurement procedures were the delay functions. The use of these delay functions varied from allowing transient responses to stabilise to indicating to the user that a measurement sequence has begun.

As mentioned before, the main interrupt service routine responsible for handling the different delay variables was the *ISR(TIMER0_OVF_vect)*, or *timer0* interrupt service routine. Within this interrupt routine, the following was done:

- The time delay variable used by the various delay functions was incremented.
- The output connected to the MOSFET was switched on or off, based on comparisons made to a 10 ms time delay period, to indicate to the user if the AMD was still active. If a measurement sequence was being done, the switching speed was doubled and this too was handled by the *timer0* interrupt service routine.

The time that passed between every *timer0* overflow was exactly the same as the time that would pass for the *timer1* overflow, since the two were set up in exactly the same way. Refer to subsection 5.3.3 for the reasons. *Timer0* would therefore be 8 bits in length and take around $256.\frac{1}{16.10^6} = 16$ μs to complete one counting cycle, which meant that every one of the delays would be incremented every 16 μs.

The delay procedure used by the *sample* procedure was called *stabilise*. This procedure would be called to allow the A/D internal reference voltage to stabilise before sampling was started. A waiting time of 70 μs would have been sufficient to allow the reference voltage to stabilise, but extra time was added as a safety precaution. This step had to be performed before every A/D measurement procedure, since switching off the A/D converter disconnected the internal reference voltage which meant that upon re-initialisation of the A/D converter, the reference voltage had to restabilise itself.

Program flow for voltage measurement

The complete program flow describing the voltage measurement procedure will be given by Figure 5.17. The basic measurement procedure has already been presented by the flow diagram in Figure 5.11. However, the flow diagram will elaborate on the measurement processes and ignore the cycle that controls it.

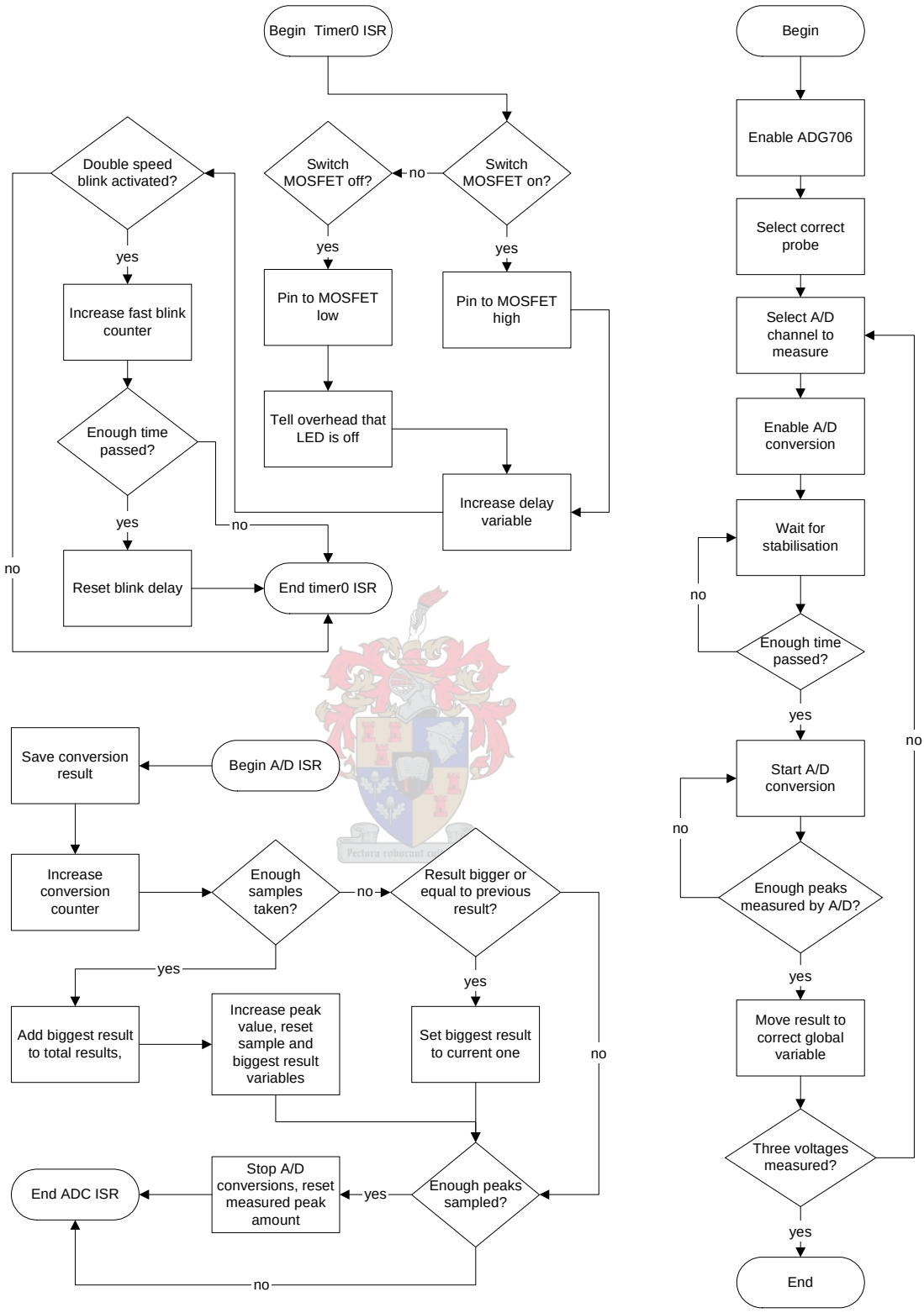

Figure 5.17: Flow diagram of voltage measurement process.

5.3.5 Calculation procedure

The calculation procedure was responsible for calculating the measured probe impedance values. The different calculations that were required to compute the impedance values were already discussed under subsection 3.1.

In order to obtain the best calculation accuracy possible with the ATMEGA16, all calculations were done with floats. Floats proved to have the best accuracy for the different calculation results, but a compromise was the fact that float values took a long time to calculate. Once all the calculations were completed, the resulting float values could be scaled and rounded off into a final answer in integer format. These answers would be the ones used by any internal checks and would also be the ones that would be stored in the external EEPROM.

The calculate procedure made use of the knowledge of the typical probe measurement results by applying a few simplifications to the calculations. These were the following:

- Only positive angles were used for the real part of the impedance calculations. The reason was that the typical measurement results would never have a phase difference of more than 90 degrees because of the inherent system parameters. Therefore, the answer of the cosine of negative angles between 0 and 90 degrees is the same as the answer of the cosine of positive angles between 0 and 90 degrees.
- The answer of the sine of the negative angles between 0 and 90 degrees will give an equal but negative result when compared to the answer of the sine of positive angles between 0 and 90 degrees. However, since it is already known that the impedance has a capacitive component, the sign of the imaginary impedance is not important, only the size. Therefore, positive angles could be used to calculate the reactance value.

The calculation process involved the following steps:

- Convert all integer numbers into float numbers
- Calculate the measured voltage levels from the average of the 128 A/D peak samples for all three voltages. These voltage levels would lie between 0 and 2.56 V.
- Do all the impedance calculations
- Convert probe impedance, probe resistance and probe current density into readable integer values. The resistance was simply cast into an integer, the capacitance was multiplied with 1.10^9 before it was cast into an integer and the current density was multiplied by 1.10^6 before it was cast into an integer. This meant that the values being tested were in Ω, nF and mA/cm^2 for each variable respectively.
- Check if the correct probe current density was being applied. If not, modify the sine table in order to close the difference between the measured current density and the required current density.
- If the current density was within limits, return a true to the external measurement program cycle. If the current density required change, return a false to the external measurement program cycle.

The sine table modification was done in simple bit increment or decrements, based on the test results. If the current density was too high, the sine table amplitude was decreased, and vice versa. The use of the current density test could cause the measurements to take up a lot of time if the probe's levels differed considerably,

which is why it was not used in the milk experiments. The reason was that the on time was limited in order to save battery power. However, during the times the device was powered by a bench, the sine table modifications were brought back in during measurements.

As an overview, Figure 5.18 will give the flow diagram of the calculation procedure. The program flow is quite straight forward, so only the broad idea will be summarised here. In addition, the optional battery program flow is indicated by a dashed line.

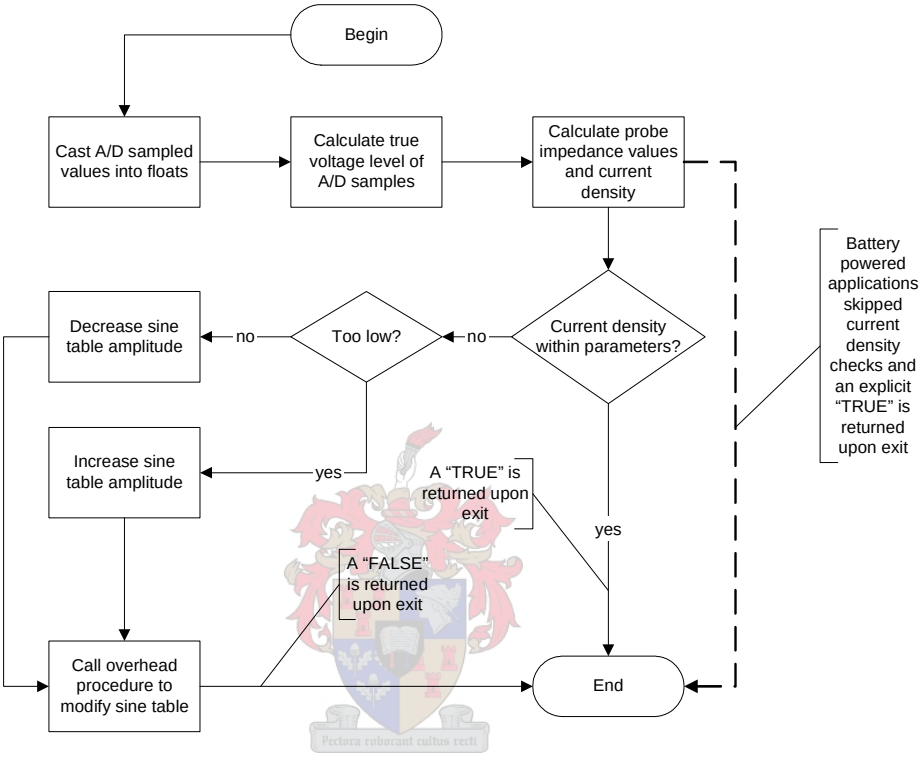

Figure 5.18: Flow chart of calculation procedure.

5.3.6 EEPROM procedures

The decision to dedicate the SPI pins to ISP programming meant that all the SPI code had to be written explicitly for the external EEPROM. Therefore, the EEPROM procedures did not only handle the main storage and retrieval sections, but the exact bit-by-bit clocking functions that would normally be handled by the SPI functions of the microprocessor.

External EEPROM programming requirements

Studies into the different 8-pin EEPROM SPI chips and their different command codes revealed that a standard existed around the value of these command codes. This meant that a command code was not limited to one type of SPI EEPROM. In addition, the SPI standard meant that the typical clock cycles required to transmit and receive data from the chip was the same for all the EEPROM types.

Based on these findings, the different EEPROM command codes were hardcoded into the microprocessor's program and used whenever needed. Furthermore, the code generated for the SPI transmit and receive

sections could be re-used for any chip that worked with the SPI standards, since the clock system had to be the same. This was applied to the SPI temperature chip that will be discussed later.

EEPROM SPI procedures

The SPI code was implemented line by line as the EEPROM datasheets required it. Therefore, the different SPI procedures will not be handled in detail, only their basic functions mentioned. It must be noted that the clocking system required by the SPI standards did not need to have a rigid period. As long as the maximum time that could pass between each clock pulse was not exceeded, the ATMEGA16 could clock in the different bits as it pleased. The clocking process was simulated by making the clock pin high and then low with consecutive lines of code within the SPI program sections.

The procedures that provided the SPI transmit and receive functions were *transmit_EEPROM* and *receive_EEPROM*. *Transmit_EEPROM* took an unsigned integer and a char as inputs. The char was the instructions and the integer the data to be transmitted. Based on the value of the instruction, the transmit function would transmit a command code, an address value or data. The size of the command code differed from the address and data sizes, which meant that the EEPROM transmission had to check how many times to clock before the entire variable's size was transmitted.

Receive_EEPROM took a char as an input and returned an unsigned integer. The char was once again an instruction and would tell the reception to either receive the EEPROM's status register value, or receive the data stored at a adress position. As with the transmit procedure, the receive procedure had to check how many clock cycles to make before either variable has been wholly received.

EEPROM control

The EEPROM SPI transmit and receive procedures formed the foundation of all the EEPROM control procedures. The control procedures created and used by the AMD will be discussed in short:

- *Read_status_EEPROM* returns the value of the EEPROM's status register. The status register is used to determined if the EEPROM is busy with a write, if writing is enabled and if certain memory sections have been blocked.
- *Poll_EEPROM* uses the *read_status_EEPROM* procedure to check if the EEPROM is ready to receive the next instruction or write cycle. This procedure will only exit once that is the case.
- *Write_status_EEPROM* writes to the status register of the EEPROM. It takes an integer as an input. The integer represents the desired codes that should be written to the status register.
- *Write_enable_EEPROM* enables the EEPROM for a write instruction. This needs to be done before every single write cycle, since the EEPROM disables any writing functions once a write cycle has completed.
- *Write_EEPROM* writes data to a specific EEPROM address. The procedure takes the data to be written and the address to be written to as inputs. The procedure first calls *write_enable_EEPROM* and *poll_EEPROM* to set the EEPROM up for a write sequence, then proceeds to transmit the write instruction, then address position and then data.

- *Read_EEPROM* reads the data from a specific address in the EEPROM. The procedure takes the addres to be read from as an input and returns the data stored at that section of memory. To read the EERPOM, the procedure first transmits the read instruction, then the address position, after which it reads the data shifted onto the EEPROM pins through the *receive_EEPROM* procedure.

Finally, every time an EEPROM procedure was called, the procedure would start off by selecting the EEPROM chip, then do whatever was required with the chip, then deselect the chip. It was done this way in order to provide a greater flexibility when using the different control procedures.

EEPROM initialisation

The EEPROM initialisation procedure, called *init_EEPROM*, was called by the main procedure before entering into the while(1) loop. The initialisation procedure was responsible for performing a variety of checks and setups before the EEPROM chip could be used. The different steps and reasons for those steps were the following:

- Certain pins connected to the EEPROM were set to an initial state. These pins were the clock pins and write protect pins. The clock pin was set to a low state and the write protect pin to a high state. By setting the write protect pin to a high state, the status register could be written to.
- The initial state of the EEPROM was then obtained and if it differed from the required state, the status register was written to. The status register was set to be write protectable and to allow all memory blocks to be written to.
- The write protect pin was made high, which allowed the status register to be changed. At the end of the procedure, the write protect pin was made low in order to put write protection on the status register contents.
- The value of the first memory position was then obtained. It was decided to use this position to store the address position to which the EEPROM store procedure last wrote to.
- If the value of the first memory position was not zero, it meant that the memory contained previously stored impedance values. This situation could only occur if the chip experienced a premature power failure or if the chip was switched off and back on again without clearing the memory's contents. In this situation, the EEPROM initialisation procedure would proceed by writing a garbage value (randomly chosen as 55555) to the next open address value (if one existed) and then store the next open address position into the first EEPROM memory space.

EEPROM storage

The EEPROM storage procedure, called *store_EEPROM*, was used to store the different calculated variables into the external EEPROM memory. It was also responsible for checking how much memory space was available before the EEPROM was written to. The reason was that the external EEPROM's internal writing functions simply wrapped around during writes and could therefore write over previously save data if not kept in check.

Store_EEPROM took a char as input. This char only indicated whether or not the store procedure was used to store a temperature value, or the measured probe impedance and current density values. In addition,

the biggest address that could be written to was limited to 2 address positions below the absolute maximum size of the EEPROM memory. This was simply done as a safety, since it was absolutely critical that no rewrites of the positional value stored in address position 0 was done. By limiting the maximum address position to 2 below the maximum, we effectively had a "one variable buffer" at the end of the EEPROM memory space. Finally, the value of the address stored in memory address 0 was always the last position where data was written to.

The store procedure did a sequential storage of the probe resistance value, then the probe capacitance value, then the probe current density during a "store probe impedance" run. Otherwise, it only stored the temperature value. The different values that were stored were contained within global variables that were given their values in either the calculate or temperature measurement procedures. One of the variables, called *impRes* in the code, were used to either store the temperature data, or the probe resistance data.

Figure 5.19 will give a flow diagram of the EEPROM store procedure.

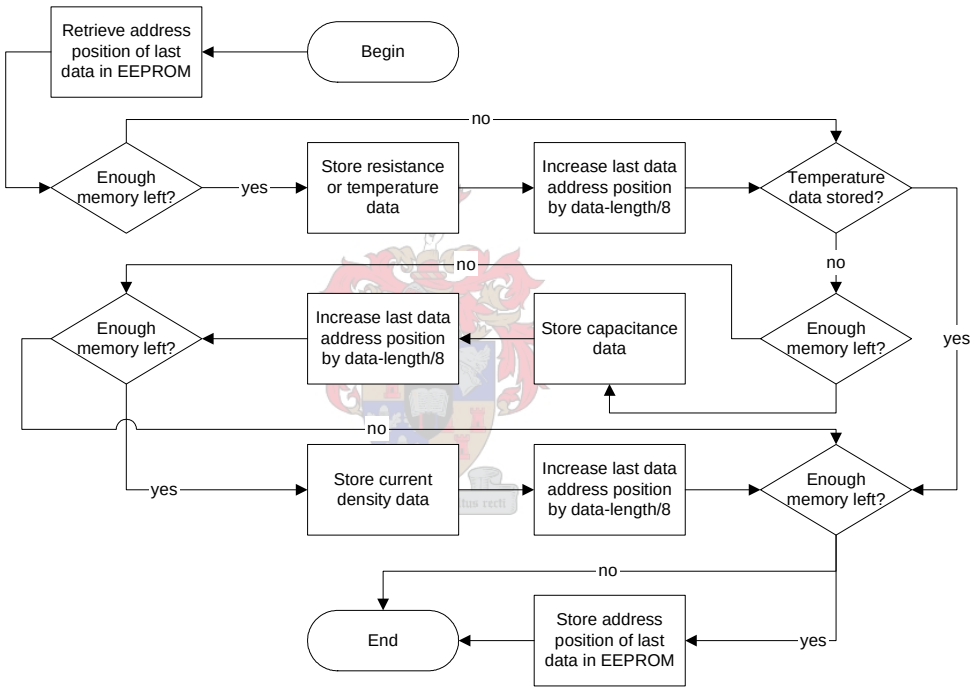

Figure 5.19: Flow diagram of EEPROM store procedure.

It must be noted that the memory space check is performed per variable and not per probe. This means that the situation can exist where the last parts of the probe measurement data can be missing if the memory space is filled before all the different variables could be stored. However, in the typical experimental runs, the data present at these positions will only be useful to determine minimum probe impedance values and should not be critical to the experimental results. The critical data points would be where the probes start to detect the bacterial growth and where the probes follow a gradient towards the minimal values.

EEPROM retrieval

The EEPROM retrieval procedure was a simple one to implement. This procedure, called *transmit_ mem*, was called by the serial communications procedure. The *transmit_ mem* procedure started at the beginning of the EEPROM memory, retreived the data stored there, transmitted the data with the microprocessor's serial transmission function, then incremented the address position to the next data. This cycle would continue until the data stored at the final address position was retrieved.

The detail behind serial communications will be discussed later. However, it must be mentioned that the retrieved data was transmitted over the serial port as a string of characters. Each string of data was seperated by a space character. The result of this transmission system was a long list of number characters separated with spaces. Matlab was used to detect the space and divide the different values into corresponding groups of matrixes before the values were plotted. Although this was a very raw approach to data retrieval, it proved effective and reliable.

5.3.7 Temperature measurements

The temperature measurements were handled by one single procedure, called *temp_ measure*. This procedure was designed to do the following:

- Control the flow of the temperature measurement process
- Transmit and receive correct data via the SPI standard
- Control the LM74 temperature chip according to specified command codes
- Calculate the temperature data from 10 temperature samples
- Store the temperature data through the *store_EEPROM* procedure

The result of the *temp_ measure* procedure call would therefore be a temperature average of 10 measurements stored in the external EEPROM.

Temperature chip control

The LM74 communication had two phases, called the transmit and receive phases, which followed each other during a single communications cycle. The LM74 is capable of SPI communications, so the clocking system could be implemented in the same way as it was done for the external EEPROM. Both the transmit and receive phases consisted out of 16 clock cycles.

Another facet of the LM74 temperature communication is the way in which its registers are accessed and updated. During its transmit phase, the temperature register data will be shifted out to the input/output pin, which is an output in this phase. The temperature data is contained in the first 13 bits, starting at the MSB. During the receive phase, the configuration register can be accessed by the microprocessor and the chip can be put into various states. Certain predefined codes, specified in the datasheet, can be used during this phase in order to change the states. The temperature pin automatically changes into an input during this phase and data can be shifted onto this pin by the microprocessor.

The default state of the LM74 was the continuous conversion mode upon startup. In addition, once the LM74 completed its first conversion, the temperature register conversion complete flag was not reset. This

meant that any subsequent conversions had to be timed, based on the typical conversion times specified in the datasheet, before the temperature register contained new temperature values. Finally, the LM74 was kept in continuous coversion mode by writing 16 zeros to the configuration register during the receive phase of the LM74 communications.

Temperature measurement

The temperature measurement was performed with the help of two while loops. The first while loop constantly checked the conversion complete flag in the temperature register in order to determine the exact time that the first conversion was completed. After the first while loop completed, the second while loop ran until 10 temperature measurements were sampled. The measurements were timed with a separate wait procedure and the timing was based on the first conversion complete time.

Once all ten measurements were completed, the value was divided by ten, cast into an integer and stored in the external EEPROM.

Time delay procedure

The delay procedure is called *temp_ delay*. It uses the time delay variable incremented by the *timer0* counter to keep track of time. *Temp_ delay* waits until 500 ms have passed before it exits, allowing more than enough time for the temperature sensor to have taken new temperature samples. The timer speed and *timer0* interrupt service routine was already discussed under subsection 5.3.4.

Flow chart of temperature measurement

To underline the temperature measurement procedure, a flow chart will be given by Figure 5.20.

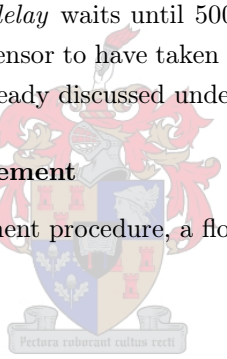

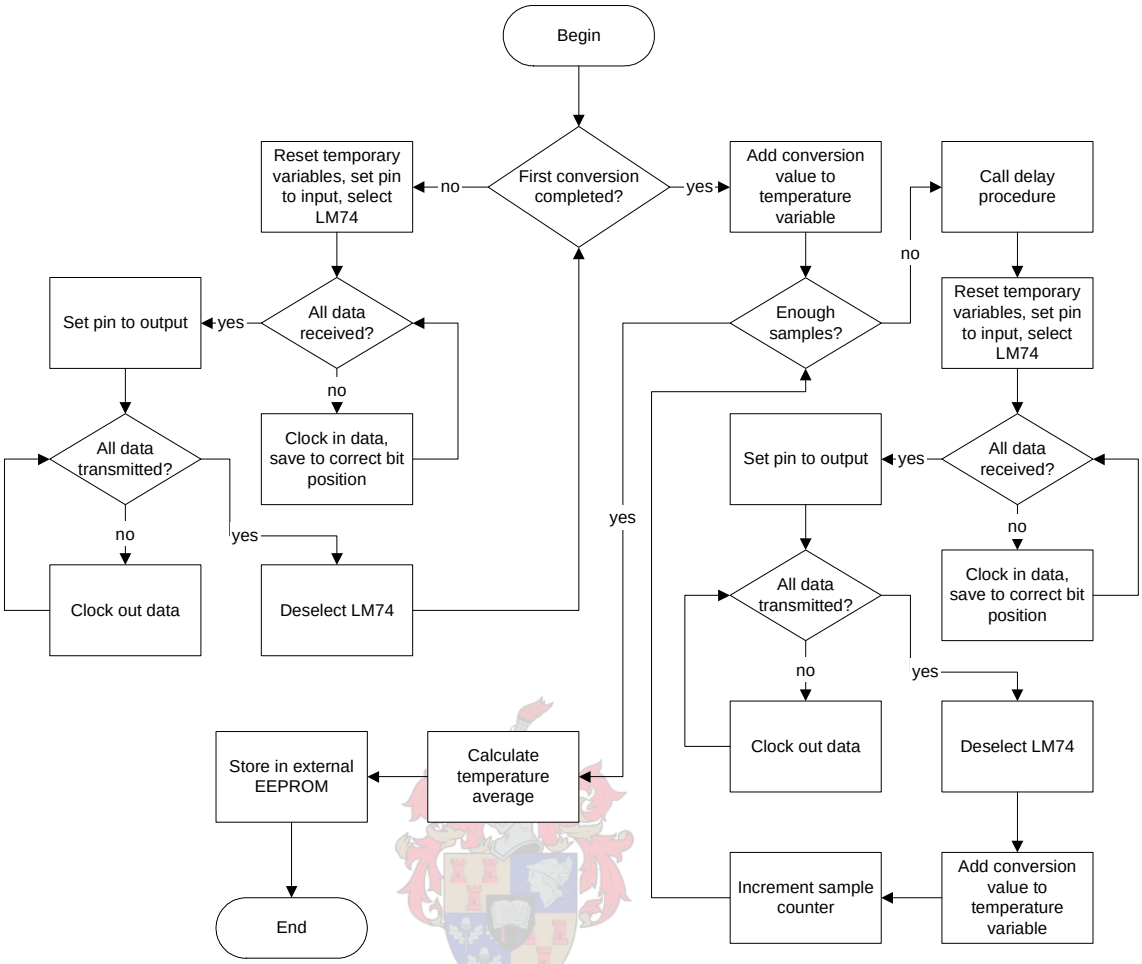

Figure 5.20: Flow chart of temperature measurement procedure.

5.3.8 Serial communications

Serial communications were used for two purposes: To write out debug data during program testing and to implement the EEPROM memory data retrieval system. All of these communications fall under the "human interface" criteria, since it allows a user to monitor and interact with the AMD.

Serial communications setup

The ATMEGA16 serial communications required various internal USART registers to be set up according to the requirements of the serial communications protocols. In addition, the speeds at which data transmission would be transmitted needed would also need to be set up in these registers.

The procedure used to set up the USART registers was called *init_ USART*. *Init_ USART* set up the registers according to the following criteria:

- Transmission error rates had to be good to ensure reliable data retrieval. To that end, the microprocessor's double speed USART clock function was implemented to decrease the error percentage at higher baud rates.

- The USART asynchronous mode was used. Only in this mode could the double speed USART clock function be used.
- It was decided to make the baud rate 57.6 kbps. At this baud rate, with the double clock speed active, the error rate was -0.8% for a 16 MHz clock frequency. Faster rates were not implemented since the PC side of the communications did not have faster options than 57.6 kbps.
- The communication protocols were set to have 1 stop bit, no parity bits and 8 bit characters lengths.
- Internally, the program would be set to use interrupts for reception, but no interrupts for transmission. This would simplify communication implementations since character reception would not waste time as the program waits for it and character transmissions would not use an unnecesary interrupt if all that needed to be done was to transmit a character at the time and place of the programs choosing.

The values that were written to the registers controlling the baud rate were calculated from values hardcoded at the beginning of the entire AMD's program. Therefore, by simply changing the baud rate at the beginning, the correct values would be computed and added into the USART registers by the *init_ USART* procedure.

Basic serial communication procedures

The serial communications were implemented with the help of a few small procedures. These were called *putchr*, *printstr*, *testfunc* and the USART reception interrupt service routine *ISR(USART_ RXC_ vect)*.

The core serial communications transmission procedure was *putchr*. This procedure took the character to be transmitted as input. It then polled the transmission ready bit in the *UCSRA* register to check if the transmission buffer was ready for the next character. If so, the character was written to the transmission buffer and the procedure exited.

Printstr took a string as input. It ran through the entire length of the string, called *putchr* for every character, and exited when the entire string was transmitted.

Testfunc was the debug procedure. It took the value to be transmitted over serial port as an input, then used an imported function *itoa* to transform the integer to a string. The *printstr* procedure would then be called to transmit the string over the serial port.

Finally, the interrupt service routine, *ISR(USART_ RXC_ vect)*, performed one function only. As soon as a character received interrupt was generated by the USART, the interrupt service routine would simply load the value of the character stored in the USART buffer into a global variable.

User-EEPROM interaction

The procedure that allowed the user to access the external EEPROM memory was called *comms*. This procedure performed two functions: It either allowed the user to recall the data stored in the external EEPROM memory or allowed the user to delete the entire external EEPROM memory space. It was also assumed that the user would use a keyboard to send various characters to the microprocessor.

The implementation was done as follows:

- The procedure started by switching on power to all external chips. This was necessary, since it might happen that serial communications were requested at a time when the chip was between measurement cycles and in low power mode. The power on process involved some time delays which will be discussed under subsection 5.3.10.

- The entire serial communications process would take place within a test loop. This loop would check the pin activating the serial communications for a change in its state. If it returned to a low, the serial communications would stop.
- The procedure would check every incoming character for a command recognition. If a character was recognised, it would transmit that character back to the user, followed by whatever data the command may have requested. Any other characters would be ignored.

The following characters would be recognised by the comms procedure: “q”, “t”, “d”, “e” and “l”. However, a certain sequence had to be followed for some of the characters to be recognised. To elaborate:

- “q” would query the microprocessor to check if it has woken up (if it was asleep) and if it was ready for serial communications. “Awake” will be transmitted if it was ready.
- “t” would tell the microprocessor to transmit the entire contents of the external EEPROM memory over serial port. “Transmitting EEPROM contents” would be transmitted first, followed by the *transmit_mem* procedure call.
- “d” would be the first letter that would be required to delete the entire EEPROM memory. This letter had to be followed by “e” and “l” within the time it took for the *timer2* counter to finish one complete time cycle. *Timer2* will be discussed later, but for now it will be mentioned that it would take 8 seconds to complete a time cycle of 255 bits. If any other character was pressed after the “d” character, the deletion command would be cancelled and “del Command Cancelled” would be transmitted. The same would be displayed if the time ran out. If the delete procedure was succesfully completed, “Deleting EEPROM!” would be displayed and the address value stored at memory address 0 would be reset to 0. This elaborate deleting system was implemented as a precaution against accidental deletions.

As a final word, it must be mentioned that the EEPROM access procedures were implemented with windows hyperterminal in mind. This external program would run on the PC and would allow easy access to the microprocessor’s serial communication functions. In addition, hyperterminal could save all incoming serial data into a text file that could be used by Matlab. In turn, Matlab extracted the data in the text file, grouped it together as required by the user, and plotted all the values obtained from these data points.

Flow diagram of user-EEPROM interaction

Figure 5.21 will give the flow diagram of the *comms* procedure.

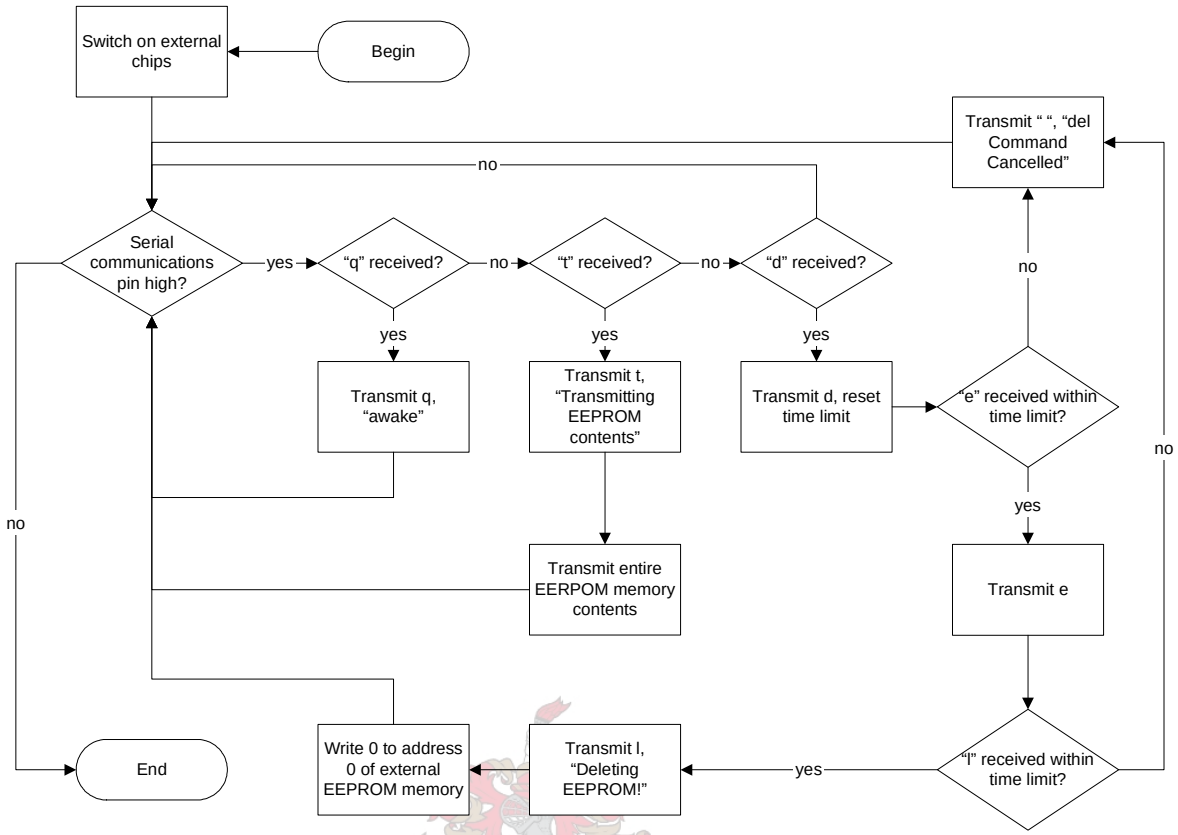

Figure 5.21: Flow diagram of user-EEPROM interaction.

5.3.9 Procedures surrounding sleep mode

The low power requirements set by the device criteria at the beginning of this chapter required the microprocessor to go into a low power mode during the times it was not active. Therefore, a sleep mode was implemented into the AMD's program in order to force it to draw less power during these inactive times. The specific implementation of the sleep mode that took the device into sleep required the use of *timer2*. Therefore, in order to discuss the sleep mode, *timer2* and its function needs to be discussed as well.

Power save sleep mode

The ATMEGA16 had several sleep modes, but only one was able to go into a very low power mode and still be able to wake without the use of an external interrupt source. This was the "power save" mode. The power save sleep mode brought the microprocessor into a low power state by stopping all clock sources, with the exception of the *timer2* clock. By setting the *timer2* clock source to asynchronous mode, an external "clock crystal", connected to pins PC6 and PC7, could be used to drive the *timer2* clock.

The *timer2* counter would therefore continue to function during the microprocessor's sleep. After the *timer2* counter overflowed, the *timer2* overflow interrupt could be used to wake up the device from sleep. This wakeup procedure was an excellent function for the AMD, since the AMD had to time the interval length between measurement cycles and could not be allowed to lose track of time during sleep modes. By

using this sleep mode, the sleep mode itself was subject to exact timing and the program could be centered around the sleep mode's wakeup times.

The microprocessor's sleep mode registers had to be set up before the correct sleep mode could be used. An imported library, created by the AVR community, was used to do the setups. The procedure *set_sleep_mode(SLEEP_MODE_PWR_SAVE)* set up the sleep mode registers into power save mode. The procedure *low_power* was then used to put the device into safe mode.

The procedure *low_power* was not an imported procedure. It was created to ensure that the ATMEGA16 did not enter sleep mode prematurely. If the AMTEGA16 entered sleep mode before the *timer2* interrupt flag was reset, the device may enter sleep mode indefinitely, since another overflow interrupt will never be picked up. The *timer2* interrupt flag would only be reset after one *timer2* clock cycle and since the *timer2* clock speed was 500 times slower than the ATMEGA16 clock speed, the probability of a premature sleep mode was more than likely. The ATMEGA16 datasheet gave excellent steps to prevent such a situation and the preventative steps were implemented exactly as suggested therein.

Timer2 setup

As mentioned previously, the *timer2* timer could be used in an asynchronous mode. This mode was a prerequisite for the power save sleep mode if the sleep mode was to be woken up with a *timer2* overflow interrupt. However, in order to set up *timer2* in asynchronous mode, specific steps had to be taken to ensure a correct *timer2* clock function. These steps were laid out in the datasheet and will not be explained here.

The procedure used to initialise the *timer2* timer into the correct mode was *init_timer2*. This procedure set the *timer2* timer into asynchronous mode, divided the clock speed by 1024 and enabled the *timer2* interrupt on overflow. By dividing the external clock frequency by 1024, the *timer2* frequency was now $\frac{32{,}768.10^3}{1024} = 32$ Hz and since *timer2* was an 8 bit counter, the length of time it would take for *timer2* to overflow would be $\frac{1}{32}.256 = 8$ seconds. This was the slowest possible clock frequency that could be obtained from the 32 kHz clock crystal. It was decided to go as slow as possible in order to stretch out the length of time that the ATMEGA16 would be asleep, thereby conserving power.

Timer2 ISR

The *timer2* interrupt service routine would be the first thing that the ATMEGA16 ran after it woke up from sleep mode. It performed a myriad of little functions, but the main function of the *timer2* interrupt service routine was to increment the voltage measurement time variable. This variable was checked by the program in order to determine if it was time for a new measurement cycle to be started.

The timer2 interrupt service routine can be summed up as follows:

- Firstly, all the other timer's counting registers are set to 0 and any of their interrupt flags cleared. This step is done to ensure that all timers are synchronised with the external asynchronous *timer2* clock source. This synchronisation was not a prerequisite, but a safety, since it could not be predetermined what the state of all the different timers would be after the device woke up from sleep mode. By forcing it to a certain start state, this uncertainty was removed.

- Certain variables would then be reset and the voltage measurement variable incremented. The variables being reset was used by the overhead procedure that will be explained in subsection 5.3.10. The *timer2* ISR was also responsible for resetting the LED "blink" counter in order to allow it to blink every 8

seconds. However, if the AMD was busy with a measurement, the blinking was solely controlled by the *timer0* ISR, which meant that *timer2* had to check this fact before it reset the variable to prevent possible erratic blinks.

- The ISR would then check if the voltage measurement variable has reached the correct value for a new measurement cycle. If so, a global variable "time" would be set and the voltage measurement variable would be reset to 0. Once again, this variable is checked by the overhead procedure.
- Finally, a variable "passed" would be reset to 0 in order to indicate to the serial communications procedure that too much time has passed between keypresses for the "delete EEPROM memory" command. Of course, this would only be of use if the serial communications procedure was being run.

Once the ISR completed, it would return to the line directly following the sleep command and the program flow would continue.

Flow diagram of sleep mode procedures

Figure 5.22 will give a flow diagram of the all the processes that were involved with the sleep mode process.

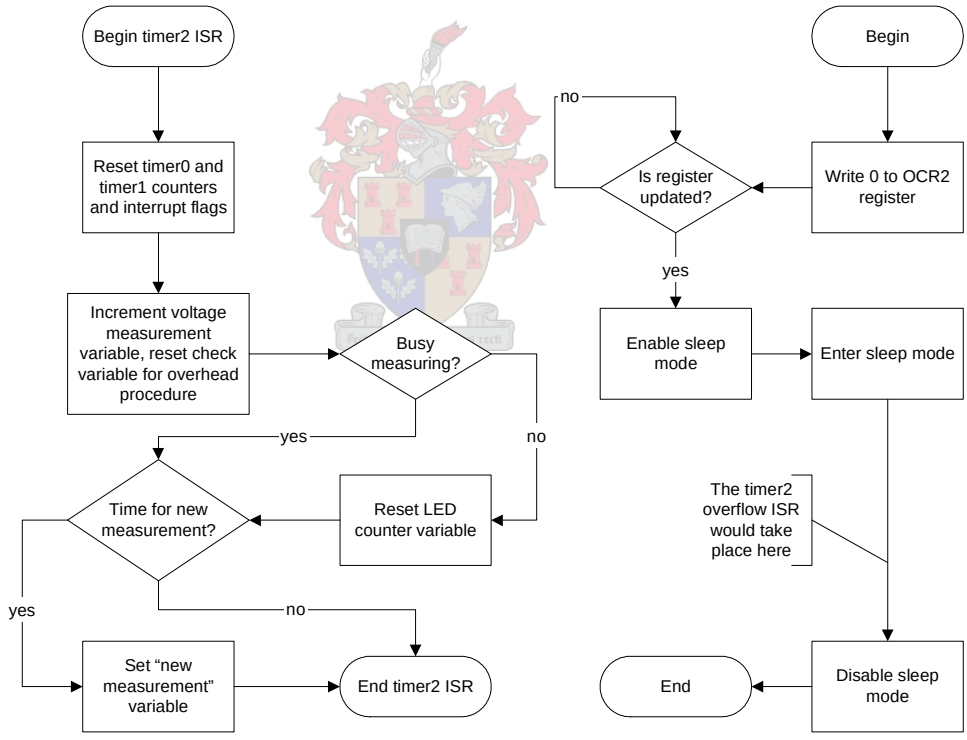

Figure 5.22: Flow diagram of surrounding sleep mode procedures.

5.3.10 Overhead procedure

The final procedure that will be discussed here is the overhead procedure. This procedure was responsible for overseeing correct microprocessor startup and shutdown procedures, depending on the different control variables. These control variables were changed by the different timer interrupt service routines. Finally,

the overhead procedure itself changed certain variables that the main procedure used during its different measurement cycle checks. Please refer to Appendix D for exact variable names.

Overhead procedure

The overhead procedure did one of three things:

- Ensure that the microprocessor was in the correct startup state after waking up from sleep mode.
- Ensure that the microprocessor was ready for sleep mode after either a measurement cycle or a simple wakeup loop.
- Facilitate the safe change of the sine table values without causing sporadic outputs or timer malfunctions.

After the microprocessor woke up from sleep, overhead would determine if it was time for a new measurement cycle. If not, the procedure would simply exit to the rest of the program flow. If it was time for a new measurement cycle, overhead would ensure that the external power feeding the measurement circuitry was switched on and that enough time passed before the chip continued with the measurement cycle. It would also re-enable the PWM output pins.

The overhead procedure would always start by checking if the timer0 ISR has switched off the pin that switches on the LED (pin PC5). If that was not the case, overhead would wait until the LED has been switched off before continuing. In addition, the only time the LED "blink" variable was reset was during a *timer2* ISR. If one remembers that the *timer2* ISR always took place after the chip woke up, it meant that the "LED off" check would be done on startup as well.

The shutdown procedure would ensure that no unnecessary output pins, such as the PWM pins, were active before the chip went into sleep mode. If this was not done, the power consumption would climb drastically during sleep mode. In addition, it was absolutely critical that the LED did not remain on during sleep mode, since the amount of current that it would drain for these long periods of time would deplete the batteries too quickly. For this reason, the "LED off" check was done every time overhead was called. Finally, before proceding to the sleep mode procedures, overhead would switch off all the external chips' power supplies.

During the sine table updating process, overhead would switch off all PWM outputs, then disable the global interrupts, then change the sine table with the new amplitude setting, then re-enable the global interrupts and finally switch the PWM outputs back on. If this was not done, the sine table update would take too long and the output would follow a gradual change instead of a sudden one. The reason was that the sine table update took longer to calculate than it took the timers to overflow. This meant that if the timer interrupts were not switched off, the sine table calculations would constantly be interrupted, which increased the time the sine table took to update itself.

Finally, the overhead procedure took a char and an integer as inputs and returned a char. The inputs were the current bottle number being measured (char) and the scale value of the next sine table amplitude (integer). Overhead will either return the current bottle number, or a zero, depending on where the overhead procedure was called. During normal shutdown and startup situations, the scale integer would be 0, overhead would do whatever was needed in the situation, and the bottle number would be returned. However, if automatic scaling was used, the calculate procedure could call overhead, together with the new sine table

scale value as input, and overhead would change the sine table and return 0. This 0 would be used as a check for the EEPROM storage procedure and would tell it to skip the storage of the unwanted probe impedance values.

External supply switch delay

The procedure that was responsible for ensuring that the power up and power down states did not happen too quickly was *relay_ act*. *Relay_ act* was a simple time delay procedure that used the same delay variable as the *stabilise* and *temp_ delay* procedures. *Relay_ act* took a char as input and this char would indicate whether *relay_ act* was used as the shutdown or startup waiting time. The application was critical, since during a startup, the delay had to happen before the external supplies were switched on and during a shutdown, the delay had to happen before the supplies were switched off.

The reasons were simple: External chip transients. During the startup process, enough time had to pass after the supplies were switched on to allow the different chips to reach a steady state. The time it took for the different chips to stabilise varied, so a long time delay was allotted to the startup procedure. Testing showed that 750 ms were more than enough time for all the chips to start up and stabilise.

During the shutdown process, all the external chips had to be ready for a shutdown. It was found that something like the serial communications would be interrupted if a delay was not placed before the shutdown, since the last transmission may still be in the buffer and be busy transmitting by the time the MAX3232 chip lost its power. The same delay was given, since it was not possible to know the exact time required for the chips to be ready for a shutdown. In this case, longer time delays were better than shorter time delays.

Flow diagram of overhead procedure

Figure 5.23 will give a flow diagram of the overhead procedure's decisions and processes. The delay procedure is very straightforward and will not be given here.

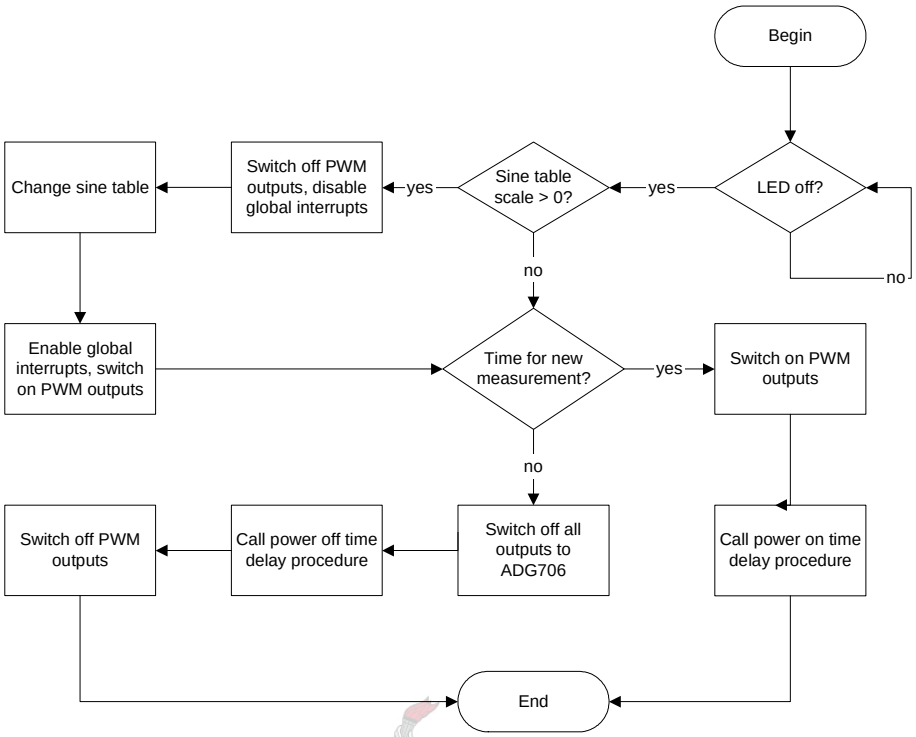

Figure 5.23: Flow diagram of overhead procedure.

5.3.11 Summary

As a summary of the entire software design, the different procedures and interrupts, together with a description of their main function, will be given by Table 5.2.

Table 5.2: Table of program procedures and their functions

Procedure name	Function
main	Initialises microprocessor, steers program flow
low_power	Provides correct sleep mode sequence
comms	Serial communications for EEPROM memory access
sample	Measures the voltage peaks on the A/D pins
temp_measure	Obtains the temperature from the LM74 temperature sensor
select_channel	Selects a probe channel in the ADG706 multiplexer
calculate	Calculates the probe impedances and current densities
init_EEPROM	Initialises external EEPROM into correct state
transmit_mem	Transmits entire external EEPROM memory via serial port
store_EEPROM	Stores impedance, current density or temperature data in external EEPROM
read_EEPROM	Reads external EEPROM memory
write_EEPROM	Writes to external EEPROM memory
write_enable_EEPROM	Enables external EEPROM to be written to
write_status_EEPROM	Writes to the external EEPROM status register
poll_EEPROM	Checks if the external EEPROM is ready for a new write sequence
read_status_EEPROM	Reads the external EEPROM status register
receive_EEPROM	Receives data from the external EEPROM via SPI processes
transmit_EEPROM	Transmits data to the external EEPROM via SPI processes
overhead	Oversees correct microprocessor startup and shutdown processes
init_USART	Initialises serial communications registers
init_AD	Initialises A/D registers
init_timer2	Initialises *timer2* registers
init_timer1	Initialises *timer1* registers
init_timer0	Initialises *timer0* registers
temp_delay	Time delay procedure for temperature measurement
stabilise	Time delay procedure for voltage measurements
relay_act	Time delay procedure for shutdown and startup processes
initports	Initialises microprocessor pins to correct initial states
sin_table	Calculates sine table values
ISR(USART_RXC_vect)	Place newly received character in global variable
ISR(TIMER2_OVF_vect)	Tests if its time for new measurement, increments time variables
ISR(TIMER1_OVF_vect)	Loads new PWM compare values into compare registers
ISR(TIMER0_OVF_vect)	Increments delay variables, flashes LED
ISR(ADC_vect)	Samples 128 peak values of sine wave voltage on A/D pin
testfunc	Debugging procedure - writes out integer values in decimal
printstr	Transmits a string of characters via serial port
putchr	Transmit a single character via serial port

Chapter 6

Probe experiments, results and discussions

This chapter will discuss the experimental setups as well as the results of the milk fermentation measurements as it was measured by the automatic probe measurement device. Most of the results can be found in Appendix F, so only a summary of the results will be given here.

6.1 Experimental setup

All of the final experiments were done in the Department of Microbiology at the University of Stellenbosch. They provided the regulated temperature environments and the different bacterial samples used in the different fermentation runs.

The initial experimental setup was done as follows:

- Two days in advance, three different bacterial concentrations were created. The bacterial types suggested for use in milk were Enterococcus spp. HKLHS (HKLHS for short), sakei DSM 20017 (Sakei for short) and Lactobacillus plantarum 423 (423 for short). These bacteria were "friendly" gram positive bacteria.

- A day in advance, the milk's glass containers (Erlenmeyer flasks), cotton, aluminium foil and 2 litres of water were autoclaved. The autocalving procedure was done according to standard laboratory methods. The autoclaved water would be used to rinse the probes.

- The rest of the steps were taken on the day that the experiment started. In addition, all of the different substances were put together in sterile conditions.

- Enough milk (200 ml) was then poured into the autoclaved flasks so that the exposed probe areas would be completely covered with milk. However, the probes were not yet inserted into the containers. The milk was Clover 2% long life milk and the best before date was 09-06-2007.

- A 2% bacterial concentration was then added to every milk sample. The solutions created for use in the experiments had a cell/ml concentration of around 10 million cells per 1 ml. Therefore, a 2%

solution of a 200 ml milk sample would result in a total bacterial addition of around 4 ml, or 40 million cells. All of the bacterial types were added at this concentration.

- Once all the bacterial samples were added, the probes were inserted into ethanol. After about 3 minutes, one probe would be removed, rinsed with autoclaved water, then inserted into the flask containing the contaminated milk. This process would be repeated until 15 probes have been placed into milk samples. The openings of the flasks were then closed with cotton wool and the cotton wool covered with aluminium foil. This allowed the probes to be inserted into the flasks without potentially damaging the probes. One more probe was inserted into a 1.6% salt solution and would serve as the control measurement.

- Three of the 18 flasks, one of each bacterial type, were kept aside for pH measurements and would not be measured by the probes. The rest of the flasks contained the probe sensors.

- All the samples were then carried to a 27 degree Celsius room and the experiments were carried out there.

The different probes in the different samples were now connected to the automatic measurement devices. In order to ensure that the measured results were constant, regardless of the measurement device, both the prototype and final version of the AMD were used in the experiments. The final device could measure 16 probes, but the prototype could only measure 3 probes. Furthermore, the devices were powered with a bench power supply, in order to determine what the measurements would look like when the devices were powered by an ideal power source. Finally, the devices were programmed to measure every half-hour, but to refrain from adapting the applied sine wave in order to obtain a specific current density through the probes.

To summarise the setup: A total of 18 contaminated milk samples were made, for a total of 6 samples per bacterial type. Three (1 of each bacterial type) of the flasks remained without probes. The other 15 were connected to the automatic measurement devices. Twelve (4 sets of each bacterial type) were connected to the 16-pin device and three (1 of each bacterial type) to the prototype device. The probe inserted into the 1.6% salt solution was also connected to the 16-pin device.

The experimental run would then proceed as follows:

- Once all the different probes were connected to the measurement points, the devices were switched on and left alone. The devices would measure the probes every half hour for the duration of the experiment.

- The milk in the probeless flasks' pH was tested every morning (at around 10:00) and every afternoon (at around 16:00) until one of the flasks of milk curdled up.

- The experiment was ended after approximately 72 hours, since it was observed that this was the time it took for most of the milk to become curdled.

The different measurement devices were then removed from the labs, connected to a PC via serial cable, and the stored measurement data retrieved from the EEPROM via hyperterminal. The retrieved numbers would be stored in a text file and this file would be opened by Matlab and the data sorted and plotted as needed. The results can be found in the next section.

6.2 Measurement results

The major results presented here will be those measured by the 16-pin automatic measurement device. The reason was that the 16-pin device had less noise on the measured impedance values, since the device was small and stray signal noise was kept to a minimum. The 3-pin device was effectively only used to double check the curve of the impedance changes and to eliminate the chance that an error in one device will give false results for the entire experiment.

The first major result is the average probe resistance change as measured over three days, given by Figure 6.1.

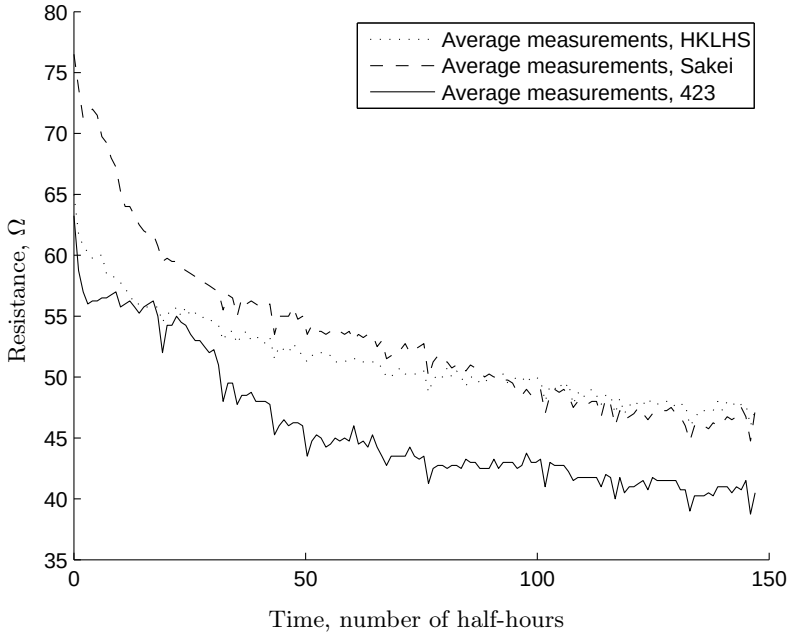

Figure 6.1: Average of measured probe resistance vs time for the milk fermentation process as a result of the three different bacterial types' activities.

The next major result is the average probe capacitance change as measured over three days, given by Figure 6.2.

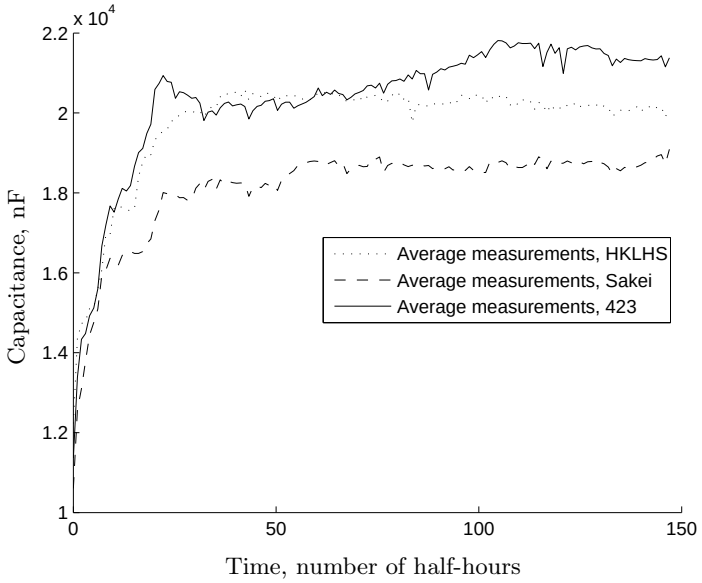

Figure 6.2: Average of measured probe capacitance vs time for the milk fermentation process as a result of the three different bacterial types' activities.

The last major result is the average probe impedance change as measured over three days, given by Figure 6.3.

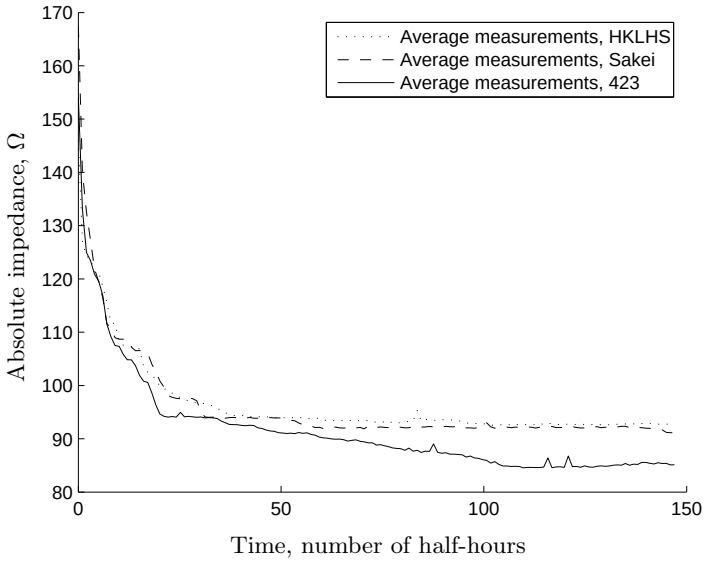

Figure 6.3: Average of measured probe impedance vs time for the milk fermentation process as a result of the three different bacterial types' activities.

The resistance vs reactance change of the average of all the milk measurements will be given by Figure 6.4. This is done to find the average linear change for the milk fermentation process. The figure will represent

the average of the twelve probes connected to the 16-pin AMD, since all twelve probes changed at more or less the same rate with time.

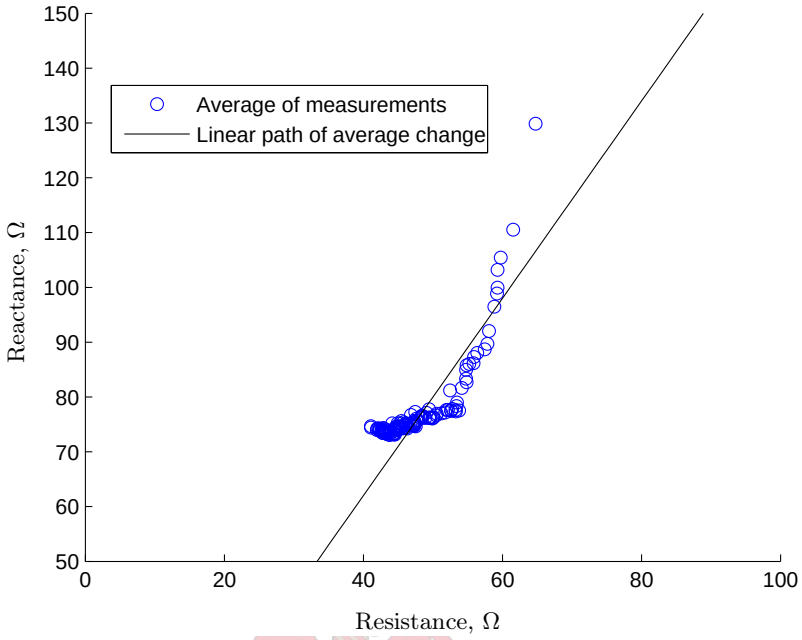

s

Figure 6.4: Resistance vs reactance for the milk fermentation process. The measurements start top right and move towards bottom left with time. Every point represents a half-hourly measurement.

Finally, Figure 6.5 will give a comparison between the probe impedance measurement and the pH measurements.

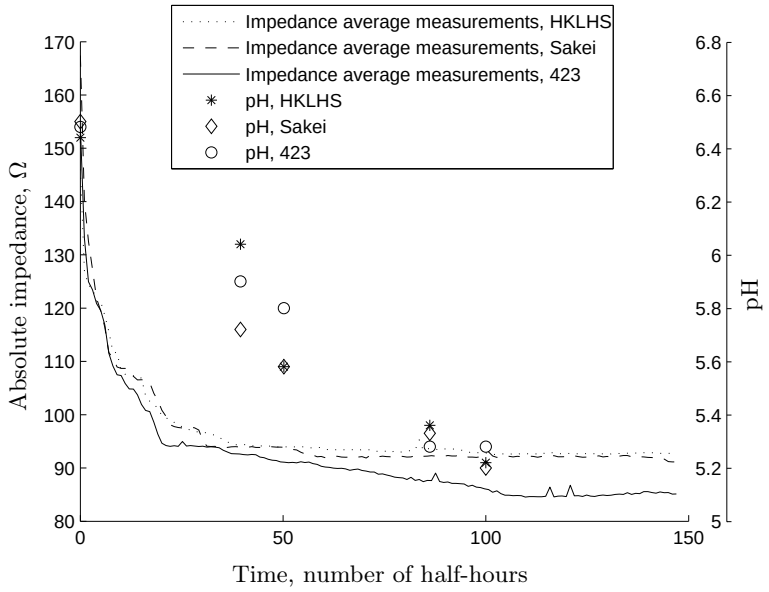

Figure 6.5: Comparative plot of Impedance and pH over time. Take care to note the different scales.

6.3 Result discussions

The results of the milk fermentation experiments contain a lot of data that must be interpreted correctly. As mentioned under the literature study's conclusion section (section 2.3), the interpretations will be guided by knowledge of bacterial growth.

The results clearly show that the surgical stainless steel probes had a change in impedance as the milk fermented. Indeed, if the measurements of the probes in milk are compared to the measurements of the probe in salt, the difference is clear. Both environments start the probes off at more or less the same impedance level, but they quickly go into opposite directions because of the fermentation processes. Refer to Appendix F for the data obtained from the probe in the 1.6% salt solution.

Before the results are investigated, a few things must be mentioned in order to remove any potential interpretation bias:

- The average probe measurements give excellent results for all three bacterial contaminations. However, the reader must not forget that the probes used in the tests had different initial impedances and that each probe did not necessarily follow the average graph's line. Indeed, some probes changed very little after the initial 12 hour drop, whilst others showed impedance changes well into the second day of measurements. These changes could either be ascribed to the specific sample of milk, or to the specific probe used in the milk and since it is known that the changes in milk are complex, none of the arguments can be confirmed or ruled out.

- The specific values of each average measurement, as seen for each bacterial type, should not be interpreted as a bacterial identification value. Because the probes had varying initial impedances, it could be that the specific probes used in, for example, the 423 measurements had inherently smaller resistances and larger capacitances than the probes in, for example, the Sakei measurements.

- The reason that the different probe could not be identified by their impedances in these experiments is that the probe used in salt had a different initial impedance in the 1.6% solution at the time the milk experiments were started than it had when the probes were screened. Since no correlation existed between the probe then and now, any attempts at identification was abandoned, which is why nothing can be said of the exact impedance values for the different bacterial types. The reason for the change will be given later.

- The pH measurements should be seen as a general indication of the changes that takes place in milk because of the different bacterial activities. The different flasks' pH were not tested to see if all the milk followed the same rate of change in pH as the sample without the probes. This means that the different rate of changes exhibited by some of the probes could be because the milk (and therefore bacteria) had a slower rate of change than other milk samples. The incomplete pH data also means that no precise conclusion can be drawn concerning the exact abilities of the probes to predict the point at which milk is sour. However, observations made during the cleaning process revealed that all the coagulated milk had the same "consistency", which suggests that the milk had more or less the same rate of change as the samples used for the pH measurements. For this reason, the average graphs are a better representation of the probe's abilities in measuring the fermentation process and a general conclusion can be drawn from the results.

The impedance values of the probe in the salt solution seen in the results are much lower than the impedance values seen at the time the newly manufactured probes were screened. Investigations into possible reasons for the impedance changes revealed that the probes were left in the 1.6% saline solution, used during the screening process, for almost a month. It was assumed that the surgical stainless steel probes would only be minimally affected by the prolonged exposure in the saline solution. However, the measurements suggest differently. The corrosion of surgical stainless steel is a well known phenomenon in the medical profession and a myriad of studies has been done around it. However, as far as the knowledge of the author goes, little study exists over the effect that corrosion has on stainless steel impedance components.

Measurements thus far, especially for roughened stainless steel probes, suggests that an increase in surface roughness causes a decrease in probe impedance. Oxidisation causes an increase in surface roughness, which could explain the decrease in the probe's impedances. However, why the capacitance would also decrease (and not increase as the surface roughness observations showed) remains unknown. What can be said is that stainless steel probes will lose their initial impedance values with extended use in corrosive environments. Fortunately for this thesis, all the probes were subject to the same corrosive environment during that month, which means that all the probe's impedances should be affected in the same way. The initial values seen by the milk experiments confirm this suspicion.

The probe measurement results are in agreement with the typical measurements done by the studied literature. To elaborate:

- The sharp decrease in impedance seen in the results have a similar shape as the typical drop in impedance seen by the probes used in the document by Hause et al. [32]. Their probes changes 40% from the original value whilst measuring E. Coli in about 5 hours, after the first initial probe impedance change. This thesis had the same percentage of change within 12 hours. However, there is a fundamental difference in the starting bacterial concentrations, which will be discussed later.

- The probe resistance and reactance values decreased with time, as the bacterial populations increased, then seems to reach a stable state. This also agrees with the literature.

- The angle between the line of change for reactance and resistance changes, as given by Figure 6.4, is between those presented by Geddes et al. and Hause et al.. Geddes et al. measured their impedances in saline and Hause et al. measured their impedances in Columbia solution contaminated with E.Coli. Therefore, the exact correlation may be subject to the different measurement environments.

With all of the above in mind, the results were scrutinised and the following was seen:

- The average absolute impedance components already reached their minimum value around 25 hours before the pH measurements reached their minimum point.

- The resistance drops quickly at first (a 30% change from its starting value), but then very gradually after the first 25 hours (another 8% of the original value over 50 hours).

- The capacitance increases quickly for the first 17 hours (a 50% increase from its original value), then seems to stabilise after 25 hours. No major increases or decreases are observed after this time.

- The average absolute impedance has a very smooth appearance (for every single probe impedance in the appendix as well).

Now, with the understanding of bacterial activity, the graphs can be interpreted as follows:

- Initial bacterial increase would be exponential at first, since the environment is suited to the bacterial groups used in the milk. The quick drops or increases of the impedance components testify to this.
- After a while, the bacterial population will reach a limit. This is indicated by the stabilisation in probe impedances.
- As the milk becomes more sour, the ionic mobility (simulated in the probe characterisations by an increase in salinity concentration) further decreases probe impedance. However, the changes are very little and it seems as if the resistance component is the only one that picks this up. Furthermore, at low frequencies, the electrode interface component in the Warburg model is dominant, which will minimise the effect that medium resistance will have on the measured impedances.
- All the pH and impedance curves indicate that every one of the bacterial types fermented the milk at the same pace. Based on this, it can be seen that the impedance drops lead the bacterial activities at the correct speed.

There is one final component that affect the measurements: Initial bacterial count. It is clear from the graphs that the impedances fall immediately after the probe have been put into the milk, unlike the measurements in the literature. However, this thesis used 100000 times more cells/ml than those of Hause et al. Therefore, in order to determine if the probes truly follow bacterial growth, a much smaller initial bacterial concentration should be used. If the probes work as they should, similar impedance curves should be seen as those in the literature.

Another promising element in the results is the fact that the measurements did not have much noise. This is a very important prerequisite for an accurate predictive system, since exact measurement values are required if the predictions are to be believed. Furthermore, the impedance components were smooth, which suggests that monitoring the impedance value will be the best way to indicate the keeping quality of milk. However, it is not known how much the bacterial growth leads the milk's acidification, so the predictive element may not be nearly as large as the probes suggests. This may be an advantage, since people may want to know when their milk will be sour an hour in advance, not a day in advance.

Finally, it can be seen from the discussions that there were a lot of unknown variables present at the time of the measurements. Before the author is confident in making statements about the accuracy and correctness of the sensor, these unknowns must be removed. However, for the purposes of bacterial detection, it is clear that the probes did change in the predicted way and that the data correlates well with existing literature. Probe sensors are therefore more than capable of being used in real time milk fermentation monitoring systems and if a standardised probe impedance can be implemented, probe impedance changes will give excellent frame of reference for any future milk sensor designs.

Chapter 7

Conclusion, contributions and future work

The electronic measurement of the fermentation of milk has proven to be a very interesting research topic. A myriad of measurement observations were made during the design and testing of the sensors investigated by this thesis. This has lead to the fact that many questions around the practical application of the different sensor types still remain unanswered. However, initial probe measurements results were promising and allowed basic conclusions to be made around the application of probes as milk fermentation sensors. This chapter will give the final conclusions, contributions by this thesis and suggested future work.

7.1 Conclusions

The milk fermentation process required a specific design methodology to be followed. The design methodology would be based on specific schools of thought around measuring the changes in milk. The following conclusions can be made concerning sensor choices:

- The fermentation of milk could theoretically be detected by measuring two major electronic phenomenon: Changes in milk's dielectric properties or changes in milk's conductive properties. The other detectable changes were chemical in nature and required a different sensor system, something that fell outside the scope of this thesis.
- The dielectric changes in milk will be dominated by bacterial growth and will reflect the growth pattern of the bacteria. By measuring bacterial growth, a predictive measurement system can be developed in order to indicate the point at which milk will be sour, since bacterial growth precedes milk acidification. The conductive changes of milk will be dominated by bacterial by-products. By measuring conductance changes, a real time indication of milk's acidification can be given.
- The two sensor types discussed in this thesis, namely the invasive probe sensors and non-invasive fringe capacitor, measured different components of the fermentation process. The probes measured both the conductance and dielectric changes, but the fringe capacitor would only measure the dielectric changes. Probes could therefore theoretically provide data on both the bacterial state and the milk's acidity,

but capacitors would detect only bacterial changes. However, probes were subject to both changes at once, whilst capacitors could be tuned into the dielectric changes.

The decision to use probe impedance sensors as the first prototype sensor device proved to be a challenging study, since a myriad of external and internal influences determined the probe's final impedance value. However, the studies also revealed that probes could be used very effectively, if properly designed. The following major conclusions were drawn from the probe investigations:

- Probe materials played a roll in the detection of bacterial changes. Out of the three metal types tested in this thesis (copper, brass and stainless steel), stainless steel probes were the only ones that detected a milk fermentation change. It was concluded that the only element that could cause the other probes to remain unchanged was the bacteria, since all probe types detected a change in salinity concentrations during the characterisations tests and milk's conductivity seemed to change little during the fermentation process.

- Probes are not passive electrical components. Instead, probe impedances are dependant on the working measurement frequency range as well as the current density that runs through the probe surfaces in contact with the medium being measured. Studies into the probe dependencies showed the following:

  - Lower frequencies gave the highest impedance values, but could suffer from polarisation effects. Higher frequencies were safer, but small impedance values would be measured. It was concluded that a probe measured at the lowest frequency, as suggested by the literature, would give the largest impedance changes in milk. In turn, the large variations would ease the constraints on the measurement system sensitivity.
  - The major criterion guiding the choice of current density was the linear working range. However, once the working range was determined, the current density choice was solely determined by the measurement system. Once again, the maximum and minimum current density choices were based on literature. The measurement system used in this thesis was dependent on relatively large variations in measured series resistor and probe voltages. Therefore, for such a measurement system to work well, the probes would be designed in order to provide the maximum comparable change between the different sensor components.

- Physical probe effects caused large variations in measured probe impedances. The greatest factor was surface roughness, since even a slight scratch could cause a large drop in measured impedance. Therefore, to ensure a repeatable probe manufacturing system, the probe surfaces would need to be polished in exactly the same way to exactly the same grade.

- Tests done around probe surface areas and distances revealed that probe impedances were highly dependant on the surface areas in contact with the liquid medium. However, a medium with a conductivity equal to, or higher than, a 1% saline solution would not cause the probes to measure a variation in distance. The standard probe experimental setup could therefore be modified to be more robust and practical, based on these findings.

The abovementioned conclusions allowed the development of a new probe sensor, specifically for milk. These sensors were measured by the newly developed automatic measurement device. The subsequent milk experiment's results gave rise to the following conclusions:

- The measurement device was sensitive and accurate enough to detect and follow probe impedance changes. In addition, the ATMEGA16 chip proved to be more than capable of controlling and monitoring the various measurement routines. The probes could also interface well with simple 5 V hardware systems, making it ideal for digital measurement designs.

- The probe sensors were effective at detecting the milk fermentation process. More specifically, it seemed as if the absolute impedance could predict the point at which milk was considered sour by around 24 hours. However, the prediction time was dependant on history, since a stable bacterial growth phase is required for the predictions to be accurate.

- The impedance curves generated by the milk fermentation experiments followed similar changes as the impedance curves found in literature that studied other bacterial systems. However, because of the high bacterial concentrations used in this thesis, there was no specific discernable impedance detection time that most literature pieces make mention of. It was concluded that more experiments need to be run before a true assessment can be made around the probes' abilities to follow bacterial growth.

- A large impedance variation existed between the different probes manufactured in this thesis. Although the reasons were not determined, it was concluded that calibrated probe averages could be used to detect the fermentation process. In addition, the averages were close to the values given by literature for smooth stainless steel probes. However, it was concluded that this result alone cannot be taken as fact and that more study must be done into probe manufacturing processes.

- Finally, the vastly lower impedance values measured in the salt and milk during the milk fermentation experiments were not caused by the measurement setup. Instead, it was concluded that since the probes were left in a 1.6% salt solution for almost a month, the probes' surfaces oxidised, which changed the characteristics of the probe impedances. Unfortunately, no literature could be found concerning the effects of the long term immersion of surgical stainless steel probes in saline solutions. The conclusion that can be taken from all of this is that probe sensors do not keep their base impedance values in a highly corrosive environment, if left there for long periods of time. Therefore, probes would need to be replaced often if such environments are measured in.

Finally, the brief study done into non-invasive sensors concluded that a fringe-fields capacitor would be capable of detecting impedance changes. However, these changes may be very small, which may require sensitive measurement circuitry in order to give sufficient measurement resolution to the sensor system.

7.2 Contributions by this thesis

This thesis gave the following contributions:

1. Research around the typical electric characteristics of milk, and how they could change as milk ferments, were performed. A broad overview of the major electric parameters that would determine sensor designs were given.

2. Copper and brass probes were ruled out as milk fermentation monitoring sensors, since their impedances did not change as the milk fermented.

3. Though probes impedances may change with changes in saline concentrations, it does not mean that they will pick up changes in biological environments. This was observed for copper and brass probes.

4. Studies were done into the effect of probe surface area variations on probe impedances and an ideal surface area parameter was presented for probes working in a CMOS driven, 5 V system. It was shown that large surface areas in contact with the medium of choice had low impedance values and vice versa.

5. The potential use of sandblasted probes as milk fermentation sensors was ruled out, since sandblasted stainless steel probes did not detect a change in milk as it fermented, even though it detected the difference between different saline concentrations.

6. Extensive study into probes and their potential use as milk sensors allowed the standard manufactured impedance cells, or precise probe insertion methods, to be replaced with an easy to used stainless steel wire probe application and the manufacturing method was given. The "classic" probes were modified as follows:

   (a) Heat shrink was applied to the probes in order to limit the amount of open surface area in contact with the medium being measured. Tests showed that the measurements were not adversely affected by the addition of heat shrink.

   (b) Probes were made flexible so that cleaning was easy. The addition of the heat shrink made it vulnerable to normal autoclaving methods. However, by making it flexible, other cleaning methods could be applied.

   (c) It was shown that distance variations did not matter in the highly conductive salt environment, or the milk environment, for the probe sensor designed in this thesis. Therefore, probes could be inserted into the milk containers without paying attention to the exact probe shape, location or depth.

7. Observations made during the different probe characterisation tests showed that there are various unexplained probe effects that still require research. These effects were voltage wave distortions, dissimilar probe impedances measured from newly constructed probes and the effect of probe oxidisation on impedance measurements. No specific mention was made around these effects by the studied literature.

8. Temperature measurements revealed that probe impedances were measurably affected by changes in temperature and a very basic correlation was given.

9. A potential non-invasive fringe-field milk fermentation sensor was investigated and presented. The expected capacitance was theorised and hypothetical development procedures were given, based on literature works.

10. An automatic measurement device was developed for the probe sensor, based on the one created by Hause et al. [32]. The following major additions and modifications were contributed by the device developed in this thesis:

    (a) The applied sine wave, usually generated by analog systems, were generated digitally by means of PWM signals and a band pass filter. The sine wave amplitude could be modified, allowing for adaptive measurements to be done.

(b) A digital sine wave peak detection system was implemented, removing extra analog components and extra power drain. The system automatically measured the average of 128 peaks in order to limit the effect of false peak value samples.

(c) The device was designed to measure 16 probes at once, creating an effective averaging measurement system for any specific measurement setup.

(d) The ambient temperature measurements were taken together with the probe measurements, in order to determine if a correlation existed between probe impedances and ambient temperature and to allow the chip to make internal corrections if such a correlation could be removed mathematically.

(e) The measurement system was autonomous and automatically calculated and stored the measured impedance values onto an external EEPROM, eliminating the potential for lost data. It could therefore function for days on end without adversely affecting measurements, if run from a power source.

(f) The device could make decisions about the measured impedances based on current density calculations. Based on these decisions, the applied sine wave may be changed in order to keep the current density value at precisely the required value. This implementation will remove the added problem of "false" lowered impedance values, because of a current density increase caused by the decrease in the probe impedances, if the current densities fell in a non-linear region. In other words, it could allow probes to function in the non-linear regions of current density.

(g) The device was designed to be portable and battery driven. Therefore, the foundation for a production-ready field-measurement device is already present.

11. Data for probe measurements in 2% low fat milk for three different types of bacterial contaminations were presented, adding to the knowledge base of impedance detection systems.

12. Probe impedance, capacitance and resistance changes, as measured during the milk fermentation experiments, were correlated against pH changes and conclusions drawn around the practical applications of probe sensors.

7.3 Future work

Throughout this thesis, unknown variables, strange observations and lack of data riddled the development and evaluation of the probe sensors. This thesis suggests that the following future work be done:

1. Investigate potential calibration constants for probe surface roughness and temperature influences on measured probe impedances.

2. Investigate the deleterious effects observed in this thesis during the probe characterisation tests, specifically the voltage distortion effect.

3. Investigate the reason for the diverse initial probe impedance values as measured for the probes created by this thesis and if possible, find a calibration coefficient to cater for any inherent probe impedance differences.

4. Investigate stainless steel probe oxidisation, specifically with the focus on impedance changes.

5. Find an easily applicable, easily reproducible probe manufacturing system, especially as far as probe roughness is concerned.

6. Do a lot more measurement with probes. The different measurements can be subdivided into:

   (a) Measure the impedance of probes in different milk types, such as full cream and skim milk.

   (b) Use probes to measure changes in milk in a cold environment, to simulate fridge conditions.

   (c) Use smaller initial bacterial samples in order to find if the probe impedance components follow bacterial growth in milk as well as the results in thesis suggests.

   (d) During milk fermentation runs, use bacterial samples that will have different growth rates in milk, in order to test the probe's bacterial growth detection abilities. In addition, until enough data is gathered, measure the pH changes in these runs in order to correlate pH, bacterial growth, conductivity and impedance to each other.

   (e) Do measurements in real-world environments, to test the effect of temperature on bacterial growths and impedance detection abilities.

7. Test the automatic measurement device capabilities when powered with batteries. Modify the device so that the user can change certain measurement parameters in the labs, if so desired. To this end, a simple keyboard interface and a small liquid crystal display (LCD) screen is recommended. Furthermore, batteries could be built in and a recharge function added, to reduce battery costs.

8. To simplify data extraction, add universal serial bus (USB) capabilities and interfaces to the automatic measurement device, so that the data could be placed on a USB disk, instead of across a serial port.

9. Investigate and develop the non-invasive fringe capacitor.

Once the two sensors investigated and suggested by this thesis give consistent and accurate results, this thesis suggests investigating the feasibility of simple infrared sensors to detect the keeping quality of milk.

Bibliography

[1] (2006 September). Lesson 3: Bacteria. University at Albany School of Public Health web site. Available at: `http://www.albany.edu/sph/coned/lesson3.pdf` (Cited on page 6.)

[2] Asami, K., Gheorghiu, E. *&* Yonezawa, T. (1998). Dielectric behaviour of budding yeast in cell seperation. *Biochimica et Biophysica Acta*, vol. 1381, pp. 234 – 240. (Cited on pages 11 and 48.)

[3] Asami, K. *&* Yonezawa, T. (1995). Dielectric analysis of yeast cell growth. *Biochimica et Biophysica Acta*, vol. 1245, pp. 99 – 105. (Cited on pages 11, 48, and 49.)

[4] Asami, K. *&* Yonezawa, T. (1995). Dielectric behaviour of non-spherical cells in culture. *Biochimica et Biophysica Acta*, vol. 1245, pp. 317 – 324. (Cited on pages 11 and 48.)

[5] Austin, G.D., Watson, R.W.J. *&* D'Amore, T. (1994). Communications to the editor: Studies of on-line viable yeast biomass with a capacitance biomass monitor. *Biotechnology and Bioengineering*, vol. 43, pp. 337 – 341. (Cited on page 13.)

[6] Barnard, J. (2003). The use of electrical conductivity and capacitance for shelf-life prediction of liquid milk. Laboratory Project 478, final report. (Cited on page 12.)

[7] Baro, J.A., Perez, M.A. *&* Grillo, G.J. (2005 May). Method comparison for diagnose of subclinical mastitis and milk quality determination in raw milk. *IEEE Proceedings, Instrumentation and Measurement Technology Conference*, vol. 1, pp. 240 – 243. (Cited on page 13.)

[8] Baxter, L.K. (1997). *Capacitive Sensors: Design and Applications*. IEEE Press. (Cited on page 51.)

[9] Bergey, D.H. (1994). *Bergey's Manual of Determinative Bacteriology*. 9th edn. Baltimore : Williams & Wilkins. (Cited on page 6.)

[10] Bishop, J.R., White, C.H. *&* Firstenberg-Eden, R. (1984 June). Rapid impedimetric method for determining the potential shelf-life of pasteurized whole milk. *Journal of Food Protection*, vol. 47, no. 6, pp. 471 – 475. (Cited on pages 2 and 13.)

[11] Braithwaite, N. *&* Weaver, G. (1998). *Electronic materials: inside electronic devices*. Materials in action series, 2nd edn. Butterworth-Heinemann. (Cited on page 10.)

[12] Cady, P., Hardy, D., Martins, S., Dufour, S.W. *&* Kraeger, S.J. (1978 April). Automated impedance measurements for rapid screening of milk microbial content. *Journal of Food Protection*, vol. 41, no. 4, pp. 277 – 283. (Cited on pages 2 and 13.)

[13] Dattalo, S. (2006 November).
Available at: `http://www.dattalo.com/technical/theory/sinewave.html` (Cited on page 77.)

[14] DeRosa, J.F. *&* Beard, R.B. (1977). Linear ac electrode polarization impedance at smooth noble metal interfaces. *IEEE Transactions on Biomedical Engineering*, vol. BME 24, no. 3, pp. 260 – 268. (Cited on page 19.)

[15] Dickert, F.L., Lieberzeit, P. *&* Hayden, O. (2003). Sensor strategies for microorganism detection - from physical principles to imprinting procedures. *Analytical and Bioanalytical Chemistry*, vol. 377, pp. 540 – 549. (Cited on page 13.)

[16] du Toit, P.A. (2004). Capacitance vs. counductance for the shelf life prediction of milk. Laboratory Project 478, final report. (Cited on pages 12 and 49.)

[17] Ebina, Y., Ekida, M. *&* Hashimoto, H. (1989). Origin of changes in electrical impedance during the growth and fermentation process of yeast in batch culture. *Biotechnology and Bioengineering*, vol. 33, pp. 1290 – 1295. (Cited on page 12.)

[18] Felice, C.J., Madrid, R.E., Olivera, J.M., Rotger, V.I. *&* Valentinuzzi, M.W. (1999). Impedance microbiology: Quantification of bacterial content by means of capacitance growth curves. *Journal of Microbiological Methods*, vol. 35, pp. 37 – 42. (Cited on page 13.)

[19] Felice, C.J. *&* Valentinuzzi, M.E. (1999 December). Medium and interface components in impedance microbiology. *IEEE Transactions on Biomedical Engineering*, vol. 46, no. 12, pp. 1483 – 1487. (Cited on page 12.)

[20] Felice, C.J., Valentinuzzi, M.E., Vercellone, M.I. *&* Madrid, R.E. (1992 December). Impedance bacteriometry: Medium and interface contributions during bacterial growth. *IEEE Transactions on Biomedical Engineering*, vol. 39, no. 12, pp. 1310 – 1313. (Cited on page 12.)

[21] Firstenberg-Eden, R. (1984 September). Collaborative study of the impedance method for examining raw milk samples. *Journal of Food Protection*, vol. 47, no. 9, pp. 707 – 712. (Cited on pages 2 and 13.)

[22] Firstenberg-Eden, R. *&* Tricarico, M.K. (1983). Impedimetric determination of total, mesophilic and psychrotrophic counts in raw milk. *Journal of Food Science*, vol. 48, pp. 1750 – 1754. (Cited on pages 2 and 13.)

[23] Geddes, L.A. (1997). Historical evolution of circuit models for the electrode-electrolyte interface. *Annals of Biomedical Engineering*, vol. 25, pp. 1 – 14. (Cited on pages 12, 15, and 19.)

[24] Geddes, L.A., da Costa, C.P. *&* Wise, G. (1971). The impedance of stainless steel electrodes. *Medical and Biological Engineering*, vol. 9, pp. 511 – 521. (Cited on pages 16, 18, 19, 20, 31, 36, 44, and 45.)

[25] Geddes, L.A., Foster, K.S., Reilly, J., Voorhees, W.D., Bourland, J.D., Ragheb, T. *&* Fearnot, N.E. (1987). The rectification properties of an electrode-electrolyte interface operated at high current density. *IEEE Transactions on Biomedical Engineering*, vol. BME 34, pp. 669 – 672. (Cited on page 19.)

[26] Gheorghiu, E. (1993). The resting potential in relaion to the equivalent complex permittivity of a spherical cell suspension. *Physics in Medicine and Biology*, vol. 38, pp. 979 – 988. (Cited on page 11.)

[27] Gnan, S. *&* Luedecke, L.O. (1982 January). Impedance measurements in raw milk as an alternative to the standard plate count. *Journal of Food Protection*, vol. 45, no. 1, pp. 4 – 7. (Cited on pages 2 and 13.)

[28] Goff, D. (2006 September). Dairy science and technology education series. University of Guelph web site.
Available at: `http://www.foodsci.uoguelph.ca/dairyedu/home.html` (Cited on pages 4 and 6.)

[29] Grillo, G.J., Perez, M.A., Anton, J.C. *&* Ferrero, F.J. (2002). Direct-evaluation of the fresh-milk somatic cell concentration (scc) through electrical permittivity measurements. *IEEE Proceedings, Instrumentation and Measurement Technology Conference*, vol. 1, pp. 153 – 157. (Cited on page 13.)

[30] Harris, C.M., Todd, R.W., Bungard, S.J., Lovitt, R.W., morris, J.G. *&* Kell, D.B. (1987 March). Dielectric permittivity of microbial suspensions at radio frequencies: a novel method for the real-time estimation of microbial biomass. *Enzyme and Microbial Technology*, vol. 9, pp. 181 – 186. (Cited on pages 11, 48, and 49.)

[31] Haus, H.A. *&* Melcher, J.R. (1989). *Electromagnetic Fields and Energy*, vol. 1. Prentice-Hall Inc. (Cited on page 46.)

[32] Hause, L.L., Komorowski, R.A. *&* Gayon, F. (1981 May). Electrode and electrolyte impedance in the detection of bacterial growth. *IEEE Transactions on Biomedical Engineering*, vol. BME-28, no. 5, pp. 403 – 410. (Cited on pages 13, 16, 19, 20, 28, 111, and 116.)

[33] Hazarika, D., Laskar, S., Sarma, A. *&* Sarmah, P.K. (2006 October). Pc-based insturmentation system for the detection of moisture content of tea leaves at its final stage. *IEEE Transactions of Instrumentation and Measurement*, vol. 55, no. 5, pp. 1641 – 1647. (Cited on pages xi, 52, and 53.)

[34] Heerens, W.C. (1986). Application of capacitance techniques in sensor design. *Journal of physics E: Scientific instruments*, vol. 19, pp. 897 – 906. Review Article. (Cited on pages 52 and 54.)

[35] Horowitz, P. *&* Hill, W. (1989). *The Art of Electronics*. 2nd edn. Cambridge University Press. (Cited on page 63.)

[36] Hui, Y.H. (ed.) (1993). *Application Science, Technology, and Engineering*, vol. 3 of *Dairy Science and Technology Handook*. VCH Publishers, Inc. (Cited on pages 7 and 8.)

[37] Hui, Y.H. (ed.) (1993). *Principles and Properties*, vol. 1 of *Dairy Science and Technology Handook*. VCH Publishers, Inc. (Cited on pages 4, 5, 7, 8, and 9.)

[38] Hui, Y.H. (ed.) (1993). *Product Manufacturing*, vol. 2 of *Dairy Science and Technology Handook*. VCH Publishers, Inc. (Cited on pages 5, 7, and 8.)

[39] Karatzas, C.N. *&* Turner, J.D. (1997). Toward altering milk composition by genetic manipulation: Current status and challenges. *Journal of Dairy Science*, vol. 80, no. 9. (Cited on page 4.)

[40] Lake, J.R., Hillerton, J.E., Ambler, B. *&* Wheeler, H.C. (1992). Trials of a novel mastitis sensor on experimentally infected cows. *Journal of Dairy Research*, vol. 59, pp. 11 – 19. (Cited on pages 12 and 13.)

[41] Li, X., Zyuzin, A.S. *&* Mamishev, A.V. (2003 October). Measuring moisture content in cookies using dielectric spectroscopy. *IEEE CEIDP Conference*.
Available at: `http://www.ee.washington.edu/research/seal/publications.html` (Cited on page 52.)

[42] Liu, J. *&* Spiegel, M.R. (1999). *Mathematical Handbook of Formulas and Tables*. Schaum's Outline series, 2nd edn. McGraw-Hill. (Cited on page 23.)

[43] Markx, G.H. *&* Davey, C.L. (1999). The dielectric properties of biological cells at radiofrequencies: Applications in biotechnology. *Enzyme and Microbial Technology*, vol. 25, pp. 161 – 171. (Cited on pages 11 and 48.)

[44] Marth, E.H. *&* Steele, J.L. (eds.) (2001). *Applied Dairy Microbiology*. 2nd edn. Marcel Dekker, Inc. (Cited on pages 4, 5, and 8.)

[45] Mucchetti, G., Gatti, M. *&* Neviani, E. (1994). Electrical conductivity changes in milk caused by acidification: Determining factors. *Journal of Dairy Science*, vol. 77, no. 4, pp. 940 – 944. (Cited on page 12.)

[46] Neamen, D.A. (2001). *Electronic Circuit Analysis and Design*. 2nd edn. McGraw-Hill. (Cited on page 62.)

[47] Nielen, M., Deluyker, H., Schukken, Y.H. *&* Brand, A. (1992). Electrical conductivity of milk: Measurement, modifiers, and meta analysis of mastitis detection performance. *Journal of Dairy Science*, vol. 75, no. 2, pp. 606 – 614. (Cited on page 12.)

[48] Nilsson, J.W. *&* Riedel, S.A. (2001). *Electric circuits*. Sixth edn. Prentice-Hall, Inc. (Cited on page 21.)

[49] Noble, P.A., Dziuba, M., Harrison, D.J. *&* Albritton, W.L. (1999). Factors influencing capacitance-based monitoring of microbial growth. *Journal of Microbiological Methods*, vol. 37, pp. 51 – 64. (Cited on page 13.)

[50] O'Mahony, F. (1988). *Rural dairy development : experiences in Ethiopia*. ILCA (International Livestock Centre for Africa) manual no. 4. Addis Ababa : ILCA; Dairy Technology Unit. (Cited on page 8.)

[51] Ong, K.G., Bitler, J.S., Grimes, C.A., Puckett, L.G. *&* Bachas, L.G. (2002). Remote query resonant-circuit sensor for monitoring of bacteria growth: Application in food quality control. *Sensor*, vol. 2, pp. 219 – 232. (Cited on pages 2 and 13.)

[52] Paquet, J., Lacroix, C., Audet, P. *&* Thibault, J. (2000). Electrical conductivity as a tool for analysing fermentation processes for production of cheese starters. *International Dairy Journal*, vol. 10, no. 5, pp. 391 – 399. (Cited on page 12.)

[53] Radke, S.M. *&* Alocilja, E.C. (2004 August). Design and fabrication of a microimpedance biosensor for bacterial detection. *IEEE Sensors Journal*, vol. 4, no. 4, pp. 434 – 440. (Cited on page 13.)

[54] Ragheb, T. *&* Geddes, L.A. (1991). The polarization impedance of common electrode metals operating at low current density. *Annalytical Biomedical Engineering*, vol. 19, pp. 151 – 163. (Cited on page 16.)

[55] Robinson, R.K. (ed.) (1981). *The Microbiology of Milk*, vol. 1 of *Dairy Microbiology*. Applied Science Publishers, Ltd. (Cited on pages 4, 5, and 7.)

[56] Schwan, H.P. (1968). Electrode polarization impedance and measurements in biological materials. *Annals of the New York Academy of Sciences*, vol. 148, pp. 191 – 209. (Cited on page 19.)

[57] Schwan, H.P. (1985). Analysis of dielectric data: Experience gained with biological materials. *IEEE Transactions on Electrical Insulation*, vol. EI-20, no. 6, pp. 913 – 922. (Cited on page 48.)

[58] Schwan, H.P. *&* Ferris, C.D. (1968 April). Four-electrode null techniques for impedance measurement with high resolution. *Review of Scientific Instruments*, vol. 39, no. 4, pp. 481 – 485. (Cited on page 12.)

[59] Serway, R.A. *&* Beichner, R.J. (2000). *Physics For Scientists and Engineers*. 5th edn. Saunders College Publishing. (Cited on page 47.)

[60] Siano, S.A. (1997 July). Biomass measurement by inductive permittivity. *Biotechnology and Bioengineering*, vol. 55, no. 2, pp. 289 – 304. (Cited on page 13.)

[61] Ur, A. *&* Brown, D.F.J. (1975). Impedance monitoring of bacterial activity. *Journal of Medical Microbiology*, vol. 8, pp. 19 – 28. (Cited on page 13.)

[62] Walz, D., Berg, H. *&* Milazzo, G. (eds.) (1995). *Bioelectrochemistry of Cells and Tissues*. Basel; Boston : Birkhäuser Verlag. (Cited on page 11.)

[63] Webb, B.H., Johnson, A.H. *&* Alford, J.A. (eds.) (1974). *Fundamentals of Dairy Chemistry*. 2nd edn. AVI Publishing Co., Westport, CT. (Cited on page 4.)

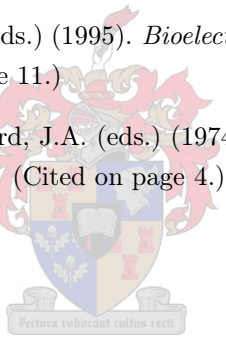

Appendix A

Probe characterisation measurements

The Probe characterisation measurements can be found in this appendix. The information herein is divided into three groups, namely:

- Tables of results containing data of measured voltage and series resistor values used.
- Three-dimensional plots of all the resulting probe impedances. The plots will show the resulting calculations for absolute impedance, resistance and capacitance per probe type.
- Two-dimensional (x-z axis when compared to the three-dimensional graphs) of probe absolute impedance vs. current density per salinity concentration, together with the linear approximations. Only the centre depth (2 cm) will be extrapolated.

The initial milk measurement test results can also be found here.

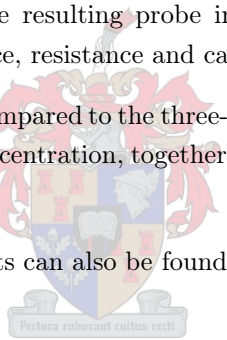

Tables of results

Tables A.1 to A.12 will tabulate the measured results as measured for applied voltage (V_t), resistor voltage (V_r) and probe voltage (V_b) at a frequency of 100 Hz.

Table A.1: Stainless steel probe, 0.5% salt solution.

Depth	Voltage	Current density level (mA/cm^2)						
		0.5	0.75	1.0	1.25	1.5	1.75	2.0
5 cm	V_t	1.480	2.160	2.920	3.520	4.160	4.720	5.360
	V_r	1.000	1.540	2.060	2.580	3.100	3.600	4.120
	V_b	0.682	0.920	1.120	1.200	1.280	1.360	1.440
2 cm	V_t	1.380	2.020	2.640	3.160	3.720	4.240	4.800
	V_r	0.900	1.350	1.800	2.260	2.820	3.160	3.680
	V_b	0.600	0.860	1.040	1.160	1.240	1.320	1.360
5 cm	V_t	1.480	2.180	2.820	3.360	4.000	4.640	5.200
	V_r	1.030	1.540	2.060	2.580	3.100	3.600	4.080
	V_b	0.620	0.840	0.960	1.080	1.200	1.280	1.360

Table A.2: Stainless steel probe, 1% salt solution.

Depth	Voltage	Current density level (mA/cm^2)						
		0.5	0.75	1.0	1.25	1.5	1.75	2.0
5 cm	V_t	1.320	2.000	2.640	3.240	3.840	4.400	4.800
	V_r	1.000	1.540	2.080	2.600	3.120	3.600	4.160
	V_b	0.540	0.740	0.880	1.000	1.080	1.160	1.200
2 cm	V_t	1.120	1.740	2.320	2.840	3.520	3.880	4.480
	V_r	0.900	1.360	1.800	2.280	2.840	3.160	3.680
	V_b	0.420	0.620	0.760	0.880	1.040	1.080	1.160
0.5 cm	V_t	1.220	1.900	2.480	3.120	3.720	4.280	4.720
	V_r	1.000	1.540	2.080	2.600	3.120	3.600	4.080
	V_b	0.380	0.580	0.720	0.840	0.960	1.040	1.080

Table A.3: Stainless steel probe, 2% salt solution.

Depth	Voltage	Current density level (mA/cm^2)						
		0.5	0.75	1.0	1.25	1.5	1.75	2.0
5 cm	V_t	1.180	1.820	2.400	3.000	3.560	3.920	4.640
	V_r	1.000	1.540	2.080	2.600	3.120	3.600	4.160
	V_b	0.360	0.520	0.640	0.720	0.800	0.880	0.960
2 cm	V_t	1.020	1.600	2.100	2.600	3.240	3.600	4.160
	V_r	0.900	1.360	1.800	2.280	2.840	3.160	3.680
	V_b	0.280	0.420	0.540	0.620	0.720	0.780	0.880
0.5 cm	V_t	1.100	1.720	2.280	2.880	3.440	4.000	4.400
	V_r	1.000	1.540	2.080	2.600	3.120	3.600	4.080
	V_b	0.240	0.360	0.440	0.560	0.640	0.700	0.720

Table A.4: Stainless steel probe, 5% salt solution.

Depth	Voltage	Current density level (mA/cm^2)						
		0.5	0.75	1.0	1.25	1.5	1.75	2.0
5 cm	V_t	1.140	1.760	2.320	2.880	3.440	3.960	4.560
	V_r	1.000	1.540	2.080	2.600	3.120	3.600	4.160
	V_b	0.300	0.440	0.520	0.640	0.720	0.760	0.800
2 cm	V_t	1.020	1.540	2.040	2.520	3.160	3.560	4.120
	V_r	0.900	1.360	1.800	2.280	2.840	3.160	3.680
	V_b	0.240	0.360	0.460	0.560	0.640	0.720	0.800
0.5 cm	V_t	1.080	1.660	2.240	2.760	3.320	3.800	4.240
	V_r	1.000	1.540	2.080	2.600	3.120	3.600	4.080
	V_b	0.160	0.260	0.320	0.400	0.480	0.520	0.560

Table A.5: Copper probe, 0.5% salt solution.

Depth	Voltage	Current density level (mA/cm^2)						
		0.5	0.75	1.0	1.25	1.5	1.75	2.0
5 cm	V_t	1.200	1.820	2.360	2.960	3.560	4.160	4.640
	V_r	1.090	1.630	2.180	2.700	3.280	3.820	4.360
	V_b	0.220	0.320	0.400	0.420	0.440	0.480	0.500
2 cm	V_t	1.040	1.600	2.120	2.600	3.120	3.680	4.200
	V_r	0.960	1.450	1.920	2.400	2.900	3.400	3.840
	V_b	0.160	0.240	0.300	0.340	0.400	0.440	0.480
5 cm	V_t	1.220	1.860	2.400	3.120	3.640	4.280	4.800
	V_r	1.090	1.650	2.200	2.800	3.300	3.840	4.400
	V_b	0.220	0.300	0.360	0.440	0.520	0.560	0.560

Table A.6: Copper probe, 1% salt solution.

Depth	Voltage	Current density level (mA/cm^2)						
		0.5	0.75	1.0	1.25	1.5	1.75	2.0
5 cm	V_t	0.500	0.720	0.960	1.240	1.480	1.700	1.920
	V_r	0.440	0.640	0.860	1.080	1.280	1.500	1.720
	V_b	0.160	0.220	0.260	0.320	0.340	0.380	0.380
2 cm	V_t	0.500	0.740	0.960	1.240	1.480	1.720	1.980
	V_r	0.440	0.660	0.880	1.100	1.300	1.540	1.760
	V_b	0.120	0.160	0.200	0.260	0.280	0.340	0.360
0.5 cm	V_t	0.500	0.740	1.020	1.280	1.580	1.820	2.100
	V_r	0.440	0.660	0.880	1.100	1.320	1.540	1.760
	V_b	0.140	0.200	0.260	0.320	0.380	0.440	0.480

Table A.7: Copper probe, 2% salt solution.

Depth	Voltage	Current density level (mA/cm^2)						
		0.5	0.75	1.0	1.25	1.5	1.75	2.0
5 cm	V_t	0.460	0.680	0.960	1.200	1.440	1.720	1.920
	V_r	0.440	0.640	0.860	1.080	1.280	1.520	1.720
	V_b	0.100	0.160	0.200	0.240	0.300	0.340	0.360
2 cm	V_t	0.480	0.740	1.020	1.300	1.540	1.820	2.040
	V_r	0.440	0.660	0.880	1.120	1.320	1.560	1.760
	V_b	0.140	0.200	0.260	0.320	0.360	0.400	0.440
0.5 cm	V_t	0.500	0.740	1.020	1.260	1.540	1.820	2.080
	V_r	0.440	0.660	0.880	1.100	1.320	1.540	1.760
	V_b	0.140	0.180	0.260	0.300	0.360	0.420	0.460

Table A.8: Copper probe, 5% salt solution.

Depth	Voltage	Current density level (mA/cm^2)						
		0.5	0.75	1.0	1.25	1.5	1.75	2.0
5 cm	V_t	0.480	0.680	0.920	1.160	1.400	1.640	1.840
	V_r	0.440	0.640	0.860	1.080	1.280	1.520	1.720
	V_b	0.100	0.140	0.160	0.200	0.240	0.280	0.280
2 cm	V_t	0.460	0.680	0.960	1.160	1.400	1.640	1.880
	V_r	0.440	0.660	0.880	1.120	1.320	1.560	1.760
	V_b	0.080	0.120	0.160	0.160	0.240	0.260	0.280
0.5 cm	V_t	0.460	0.720	0.960	1.200	1.440	1.680	1.940
	V_r	0.440	0.660	0.880	1.100	1.320	1.540	1.760
	V_b	0.080	0.140	0.160	0.200	0.240	0.280	0.320

Table A.9: Brass probe, 0.5% salt solution.

Depth	Voltage	Current density level (mA/cm^2)						
		0.5	0.75	1.0	1.25	1.5	1.75	2.0
5 cm	V_t	1.800	2.640	3.440	4.280	4.880	5.680	6.400
	V_r	1.280	1.920	2.580	3.220	3.840	4.480	5.160
	V_b	0.660	0.880	1.040	1.160	1.200	1.300	1.360
2 cm	V_t	1.920	2.680	3.360	4.120	4.680	5.160	5.920
	V_r	1.130	1.700	2.260	2.900	3.400	3.960	4.520
	V_b	0.860	1.080	1.200	1.300	1.360	1.400	1.520
5 cm	V_t	1.740	2.600	3.480	4.400	4.880	5.760	6.400
	V_r	1.280	1.920	2.560	3.300	3.840	4.480	5.120
	V_b	0.540	0.800	1.000	1.160	1.240	1.360	1.440

Table A.10: Brass probe, 1% salt solution.

Depth	Voltage	Current density level (mA/cm^2)						
		0.5	0.75	1.0	1.25	1.5	1.75	2.0
5 cm	V_t	1.940	2.640	3.520	4.200	4.880	5.440	6.080
	V_r	1.280	1.920	2.600	3.220	3.880	4.480	5.200
	V_b	0.740	0.880	1.000	1.080	1.120	1.120	1.140
2 cm	V_t	1.600	2.440	3.120	3.920	4.440	4.960	5.600
	V_r	1.140	1.700	2.280	2.900	3.400	3.920	4.560
	V_b	0.520	0.800	0.960	1.080	1.160	1.120	1.200
0.5 cm	V_t	1.860	2.640	3.520	4.360	4.800	5.520	6.160
	V_r	1.280	1.920	2.560	3.300	3.840	4.480	5.120
	V_b	0.640	0.840	1.000	1.120	1.120	1.200	1.280

Table A.11: Brass probe, 2% salt solution.

Depth	Voltage	Current density level (mA/cm^2)						
		0.5	0.75	1.0	1.25	1.5	1.75	2.0
5 cm	V_t	1.520	2.260	3.040	3.700	4.400	4.960	5.680
	V_r	1.280	1.920	2.600	3.240	3.880	4.480	5.200
	V_b	0.390	0.500	0.600	0.640	0.720	0.720	0.800
2 cm	V_t	1.560	2.300	2.920	3.600	4.120	4.720	5.360
	V_r	1.140	1.720	2.280	2.920	3.400	3.920	4.560
	V_b	0.500	0.660	0.760	0.840	0.880	0.920	0.960
0.5 cm	V_t	1.600	2.480	3.200	4.080	4.680	5.200	5.920
	V_r	1.280	1.920	2.560	3.320	3.840	4.480	5.120
	V_b	0.400	0.620	0.760	0.880	0.920	0.960	1.040

Table A.12: Brass probe, 5% salt solution.

Depth	Voltage	Current density level (mA/cm^2)						
		0.5	0.75	1.0	1.25	1.5	1.75	2.0
5 cm	V_t	1.520	2.260	3.000	3.680	4.360	4.960	5.680
	V_r	1.280	1.920	2.600	3.240	3.880	4.480	5.200
	V_b	0.340	0.460	0.540	0.600	0.640	0.660	0.720
2 cm	V_t	1.300	2.000	2.600	3.320	3.840	4.400	4.960
	V_r	1.140	1.720	2.280	2.920	3.400	3.920	4.560
	V_b	0.260	0.360	0.440	0.560	0.600	0.640	0.720
0.5 cm	V_t	1.520	2.280	2.960	3.800	4.240	4.960	5.600
	V_r	1.280	1.920	2.560	3.320	3.840	4.480	5.120
	V_b	0.320	0.460	0.520	0.640	0.640	0.720	0.720

Tables A.13 to A.15 will give the measurement setup conditions for each probe type with regards to series resistor selection.

Table A.13: Measurement condition table for probe types, 0.5 cm depth.

		Measurement conditions			
Probe depth, cm		0.5			
Salt concentration, %		0.5	1	2	5
Series resistor	330Ω	-	-	-	-
	820Ω	-	-	-	-
	1800Ω	-	-	-	-
	3300Ω	-	Cu	Cu	Cu
	8200Ω	Br,Cu,SS	Br,SS	Br,SS	Br,SS

Table A.14: Measurement condition table for probe types, 2 cm depth.

		Measurement conditions			
Probe depth, cm		2			
Salt concentration, %		0.5	1	2	5
Series resistor	330Ω	-	-	-	-
	820Ω	-	Cu	Cu	Cu
	1800Ω	Br,Cu,SS	Br,SS	Br,SS	Br,SS
	3300Ω	-	-	-	-
	8200Ω	-	-	-	-

depth 4 (50 mm) solution 2, CU

Table A.15: Measurement condition table for probe types, 5 cm depth.

		Measurement conditions			
Probe depth, cm		5			
Salt concentration, %		0.5	1	2	5
Series resistor	330Ω	-	Cu	Cu	Cu
	820Ω	Br,Cu,SS	Br,SS	Br,SS	Br,SS
	1800Ω	-	-	-	-
	3300Ω	-	-	-	-
	8200Ω	-	-	-	-

Three-dimensional graphs

The following three-dimensional graphs show plots of absolute impedance, resistance and capacitance changes as calculated from the data in the tables. The three different planes show values for depths of 0.5, 2 and 5 cm respectively. The impedance and resistance plots have the 5 cm plane on top, the 2 cm one in the middle and the 0.5 cm one at the bottom. The capacitance plot is the inverse of this order.

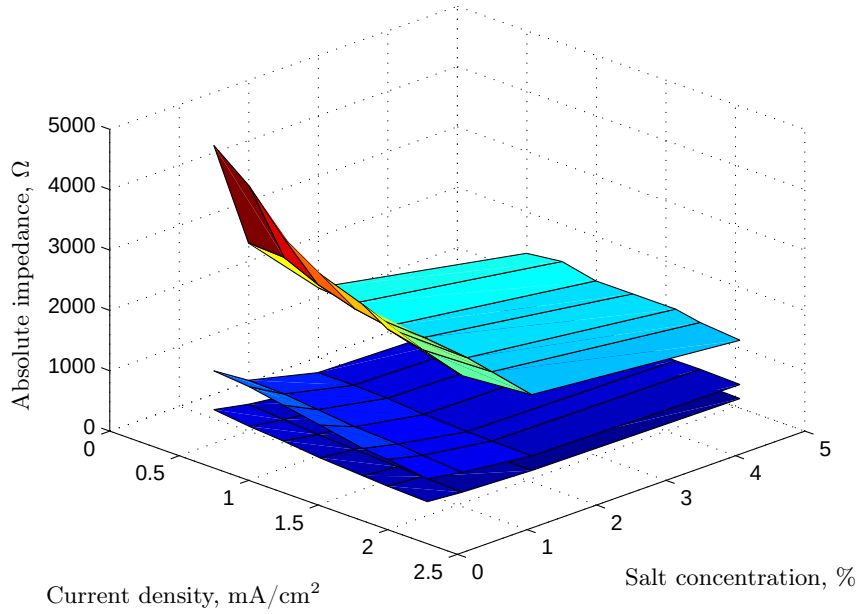

Figure A.1: Calculated data for stainless steel probe.

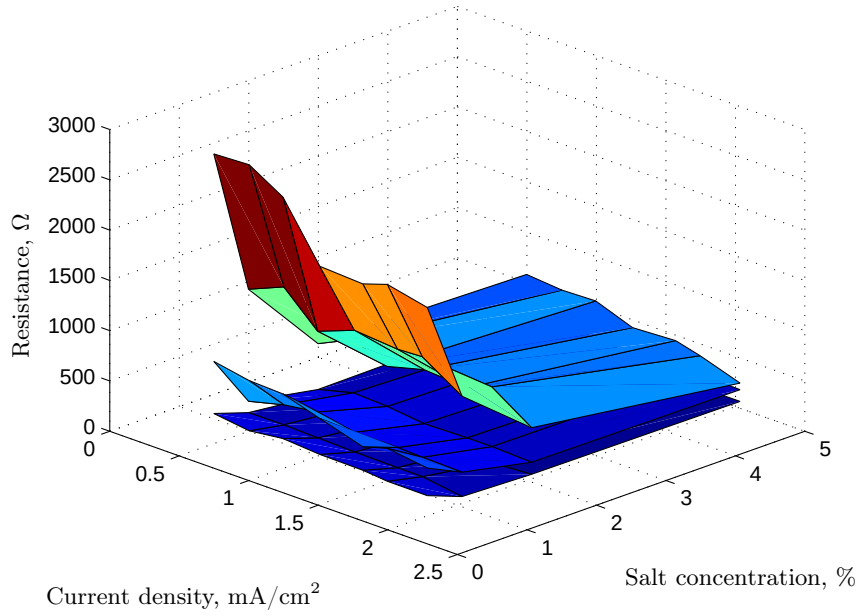

Figure A.2: Calculated data for stainless steel probe.

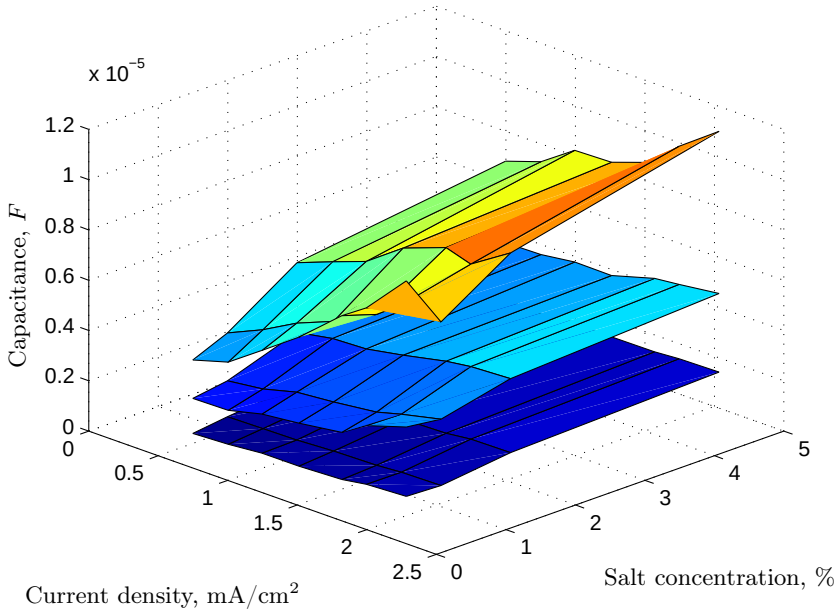

Figure A.3: Calculated data for stainless steel probe.

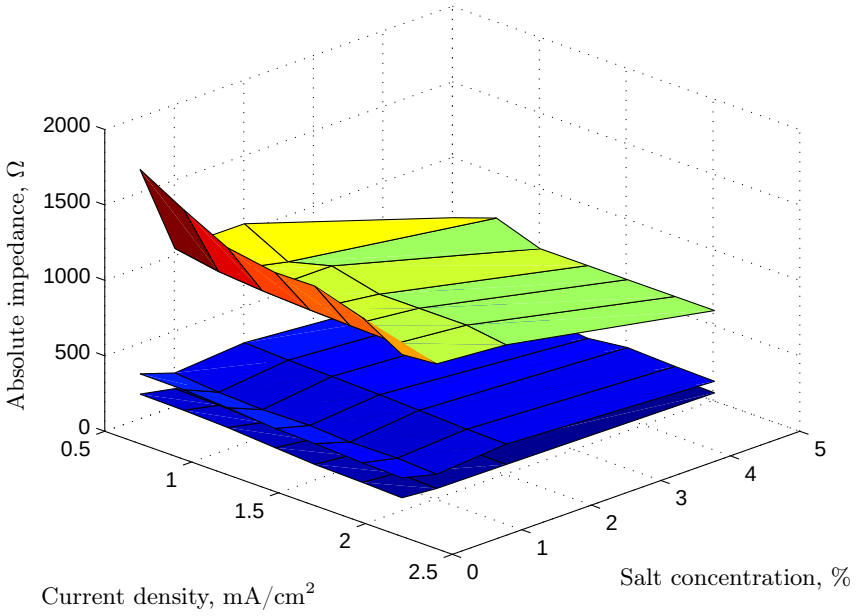

Figure A.4: Calculated data for copper probe.

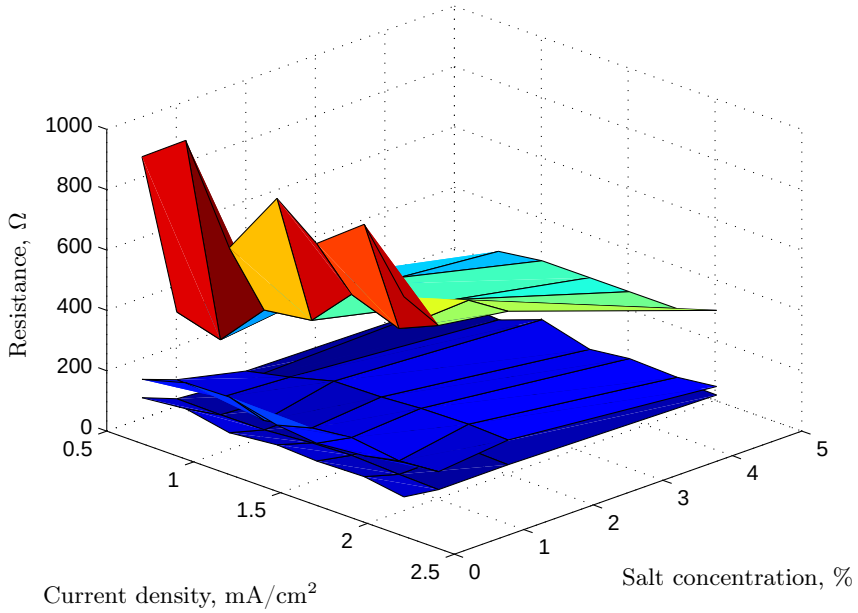

Figure A.5: Calculated data for copper probe.

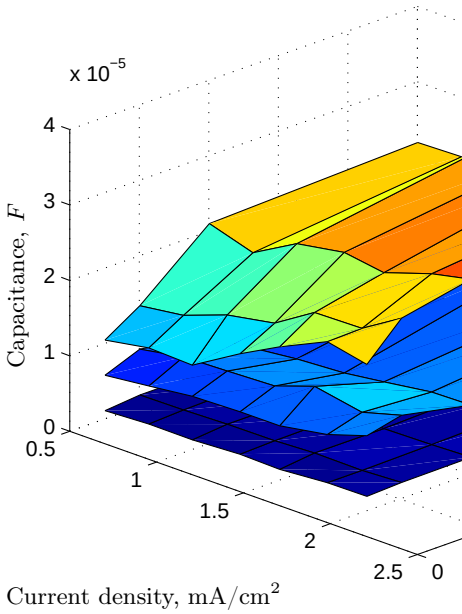

Figure A.6: Calculated data for copper probe.

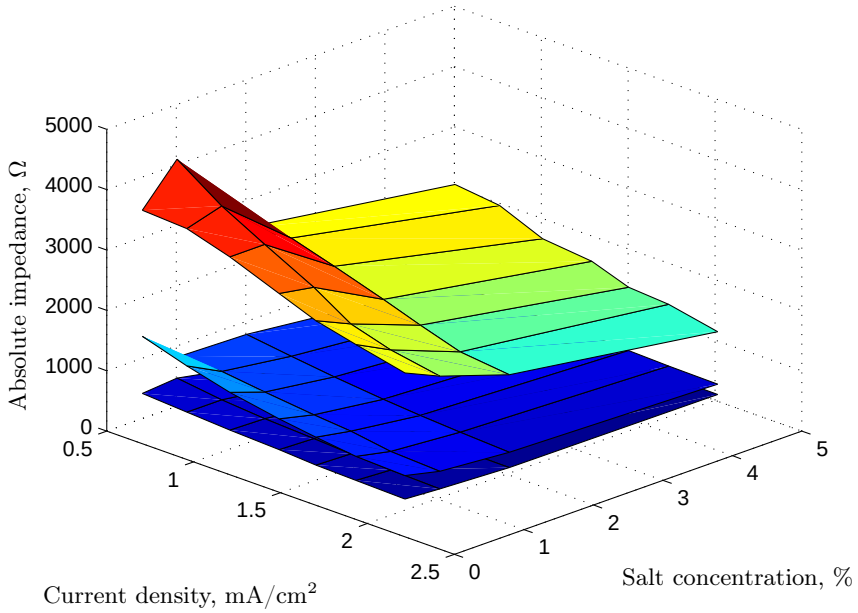

Figure A.7: Calculated data for brass probe.

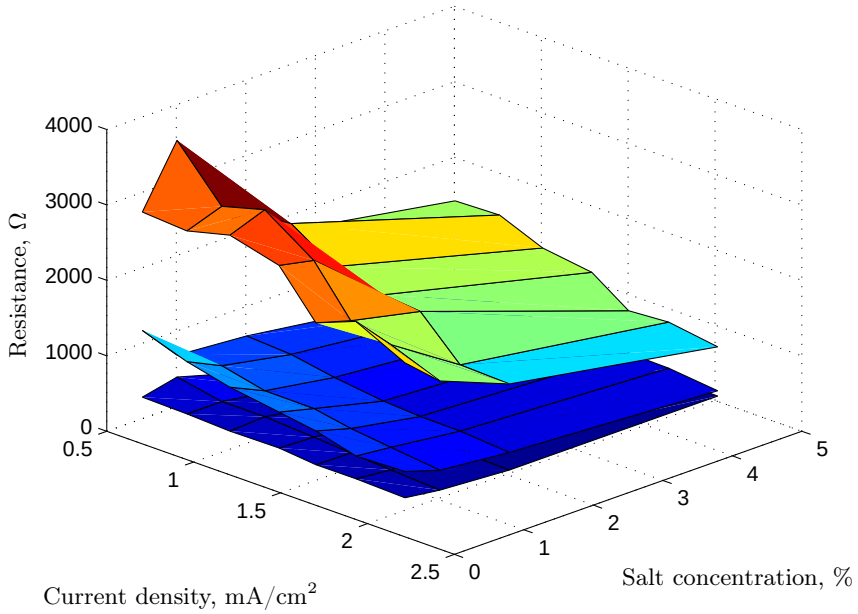

Figure A.8: Calculated data for brass probe.

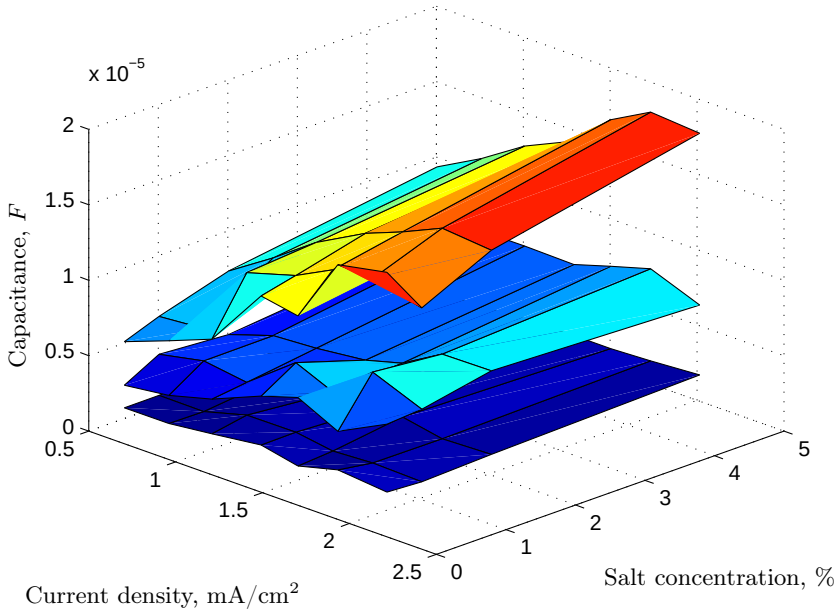

Figure A.9: Calculated data for brass probe.

X-Z plots

These plots will give more detailed views of the impedance vs. current density plots, as measured for different salinity concentrations and only for one depth (2 cm). These plots are extras only since all the information should be present in the three-dimensional plots.

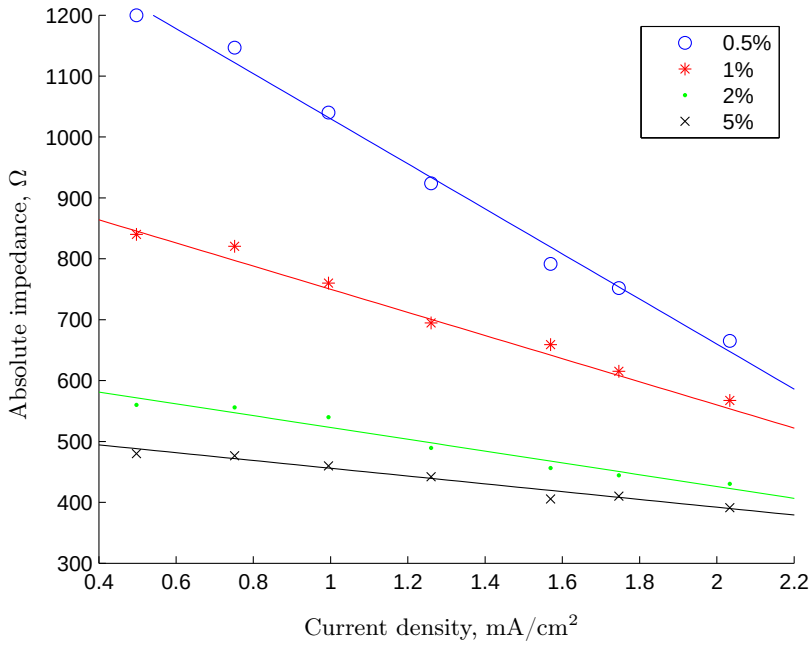

Figure A.10: Stainless steel probe data per saline concentration.

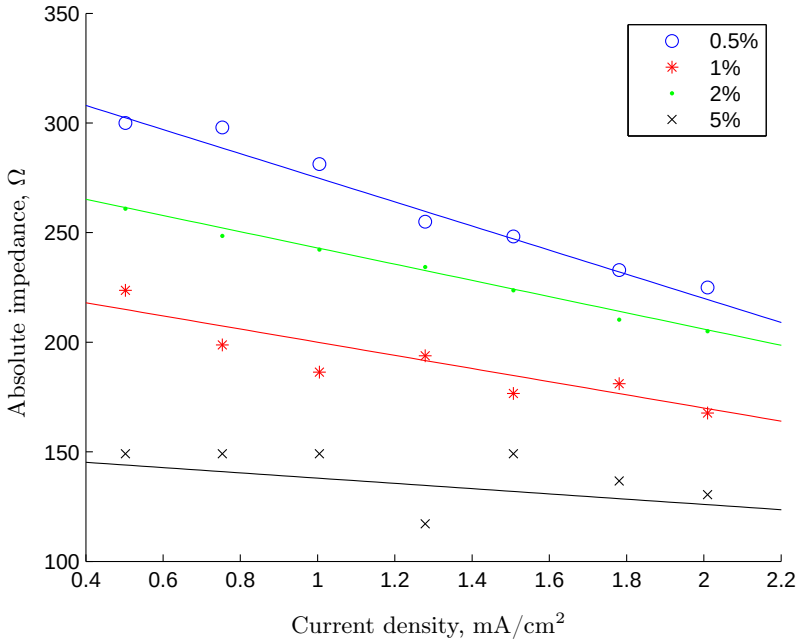

Figure A.11: Copper probe data per saline concentration.

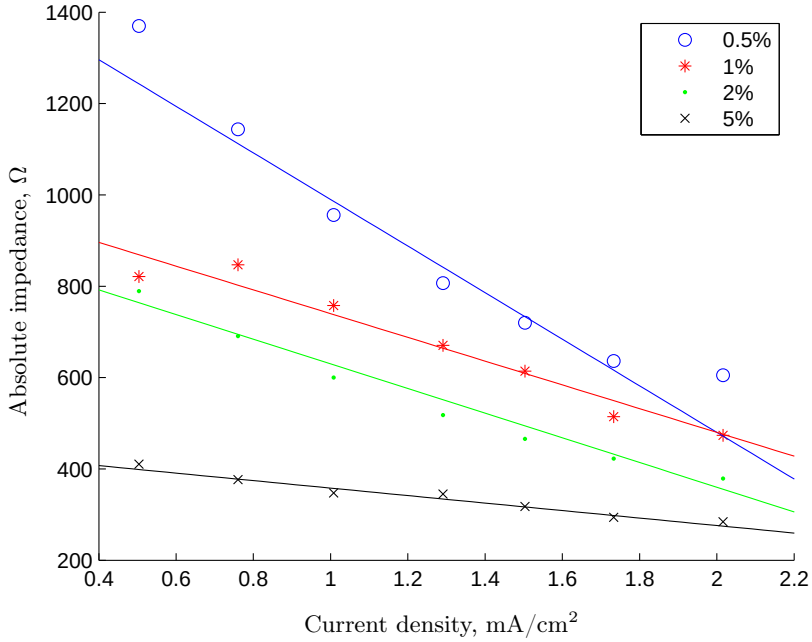

Figure A.12: Brass probe data per saline concentration.

Initial milk measurement test

The figure will show the measured result for a stainless steel probe at a depth of 5 cm in milk. The current density was set to 1 mA/cm^2 as measured through a series resistor of 820 Ω.

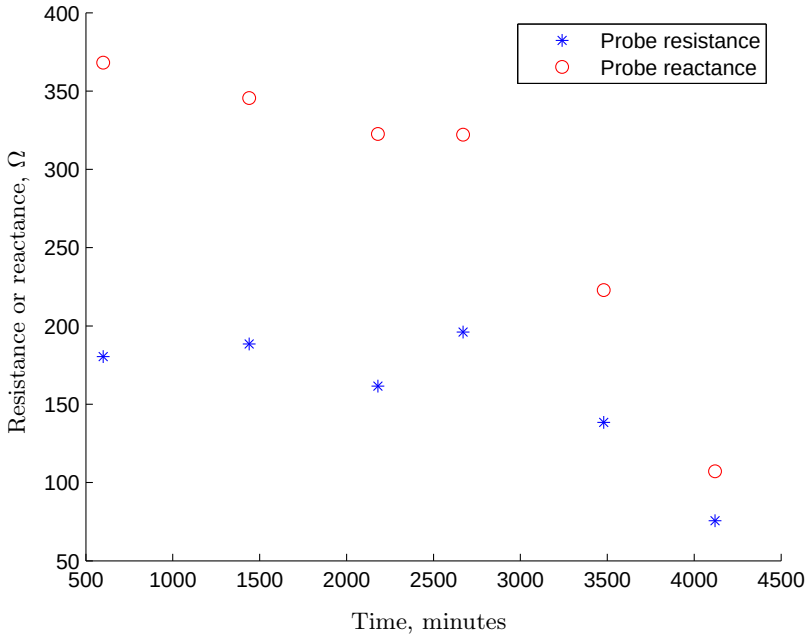

Figure A.13: Stainless steel probe measurements in milk.

Appendix B

Automatic measurement device schematic and photo

Figure B.1 will give the complete schematic of the automatic measurement device, as drawn with EAGLE 4.13. Figure B.2 is a photo of the final measurement device.

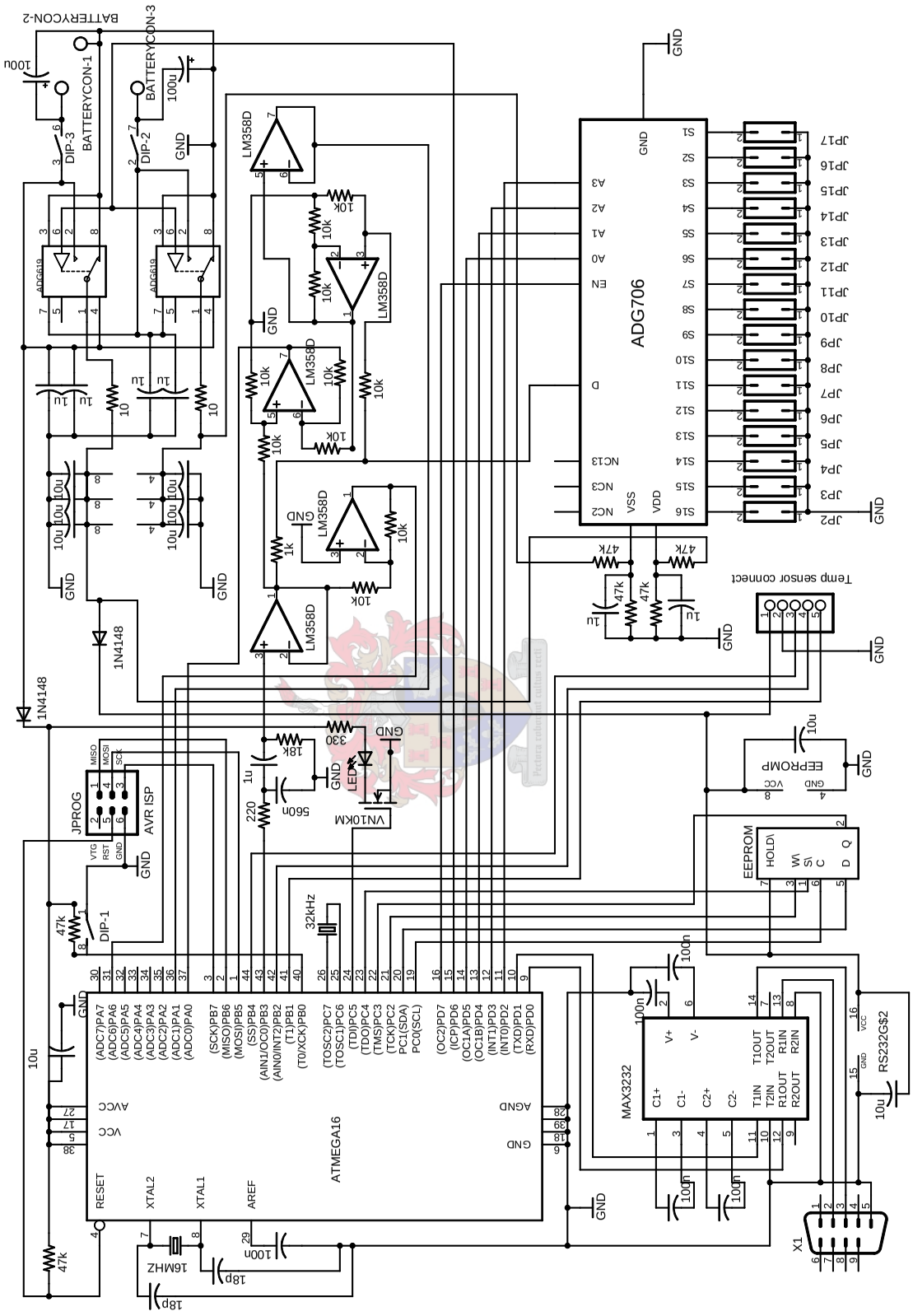

Figure B.1: Complete device schematic.

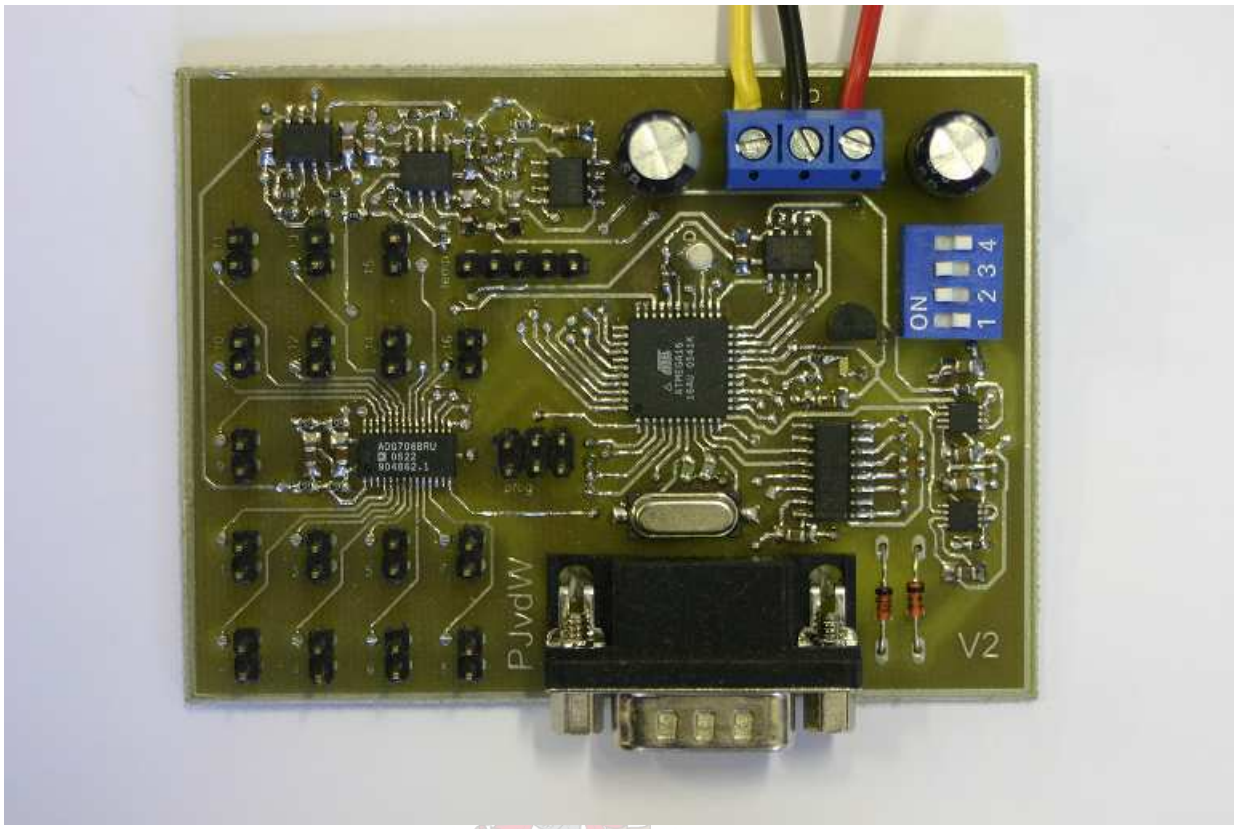

Figure B.2: Automatic measurement device photo.

Appendix C

Sine wave simulations

The sine wave simulations given in this appendix was created and simulated with Matlab and Simulink. The sine wave simulation analysis involved three steps: Create the PWM generated wave as it would be formed by the microprocessor, then simulate the different filter outputs, then investigate the results.

Figure C.1 will give an example of a PWM wave generated by the Matlab code.

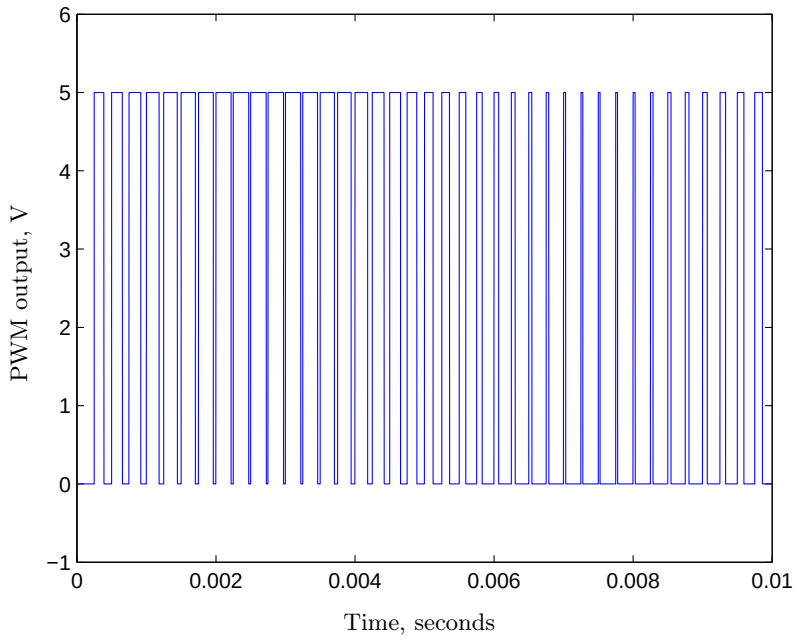

Figure C.1: PWM output for a 100 Hz sine wave.

Next, the Matlab code that created the PWM is given by the following algorithm:

Algorithm 1 Matlab PWM generation

```
clear all;
close all;
%sin_val = 157; % real PWM speed (16 MHz clock)
sin_val = 10; % example PWM speed (1 MHz clock)
t = 0;
j = 0;
DAC_vector = 0;
final = [];
for i = 0:sin_val
sine(i+1) = 102.*sin(((pi./2)./sin_val).*i)+127;, % 102 = 2V
end;
while (j < sin_val.*4) %resembles 4 quadrants of time, or 360 degrees
while (t < 256)
if (t >= DAC_vector)
out(t+1) = 0;
else
out(t+1) = 255;
end
t = t+1;
end;
final = [final,out];
j = j + 1;
if (j <= sin_val)
DAC_vector = sine(j+1);
elseif ((j >= (sin_val +1))&&(j <= (2.*sin_val)))
DAC_vector = sine((2.*sin_val) - j + 1);
elseif ((j >= ((2.*sin_val) + 1))&&(j <= (3.*sin_val)))
DAC_vector = 255 -sine(j - (2*sin_val)+1);
elseif ((j >= ((3.*sin_val) + 1))&&(j <= (4.*sin_val)))
DAC_vector = 255 - sine((4*sin_val) -j + 1);
end
t = 0;
end;
final = (final./255).*5;
time = linspace(0, 0.01, length(final)); % 0.01 is a 100 Hz period length.
plot(time,final)
axis([0,0.01,-1,6]);
xlabel('a'); % replace 'a' and 'b' with the labels of choice in Lyx
ylabel('b');
```

The following details must be noted:

- The generated PWM wave was generated to create a 100 Hz sine wave. However, the one visible in Figure C.1 is a representation of the PWM wave that will be generated by a microprocessor with a clock frequency of 1 MHz, instead of the one that will be generated by the automatic measurement device's clock frequency of 16 MHz. The real PWM wave would therefore contain 16 PWM periods for one of the PWM periods visible in the graph, which is why it will not display well here.
- The Matlab code will generate the correct PWM for the clock frequency of choice, based on the variable sin_val. Sin_val is computed based on the theory described in Section 5.3.3. The true sine wave PWM is generated by the sin_val value of 157.

- The microprocessor's code will be interrupt based, not sequential. However, the Matlab code has taken this into account by allowing a continuous loop to take place and by simulating the timer's counting in real time. The timer's counting is represented by the while (t<256) loop and the sine-table is taken into account by the while (j < sin_val*4) loop.

The resulting PWM wave was then used as an input to a Simulink simulation of the filters built in the automatic measurement device. Figure C.2 will give the block diagram of the simulation:

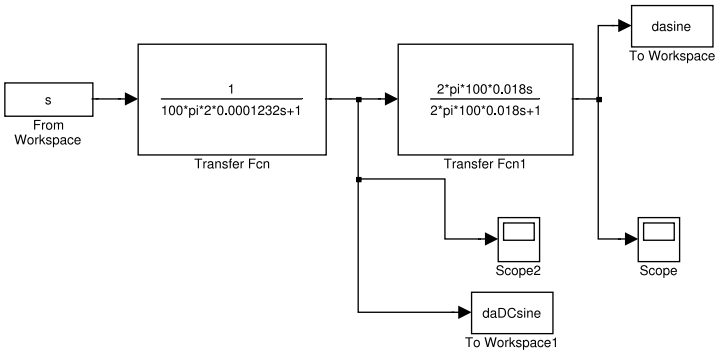

Figure C.2: Simulink block diagram of designed filters.

One very important part of the simulation was the block diagram setup. The block diagrams were based on the Laplace transforms of the voltage signals as obtained for the different circuit components of every filter. A transfer function was then obtained for every filter section and this function is represented by the different block diagrams.

The transfer function of the low pass filter, described by Figure C.3, was found as follows:

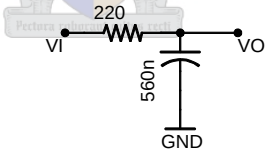

Figure C.3: Low pass filter.

The voltage VO is found by using simple voltage division and can be described by the following equation:

$$V_o = V_i \left(\frac{\frac{1}{jwC}}{R + \frac{1}{jwC}} \right) \tag{C.1}$$

Equation C.1 can be simplified into the following:

$$V_o = V_i \left(\frac{1}{jwRC + 1} \right) \tag{C.2}$$

By using the Laplace transform, the transfer function can be found from equation C.2, which looks as follows:

$$\frac{V_o}{V_i} = \left(\frac{1}{swRC + 1} \right) \tag{C.3}$$

If the resistor and capacitor values of the low pass filter is substituted into the variables, the first transfer function block is found. Next, the transfer function of the high pass filter, described by Figure C.4, was found as follows:

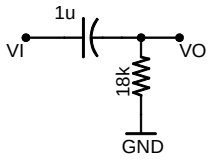

Figure C.4: High pass filter.

The voltage VO is once again found by using simple voltage division and can be described by the following equation:

$$V_o = V_i \left(\frac{R}{R + \frac{1}{jwC}} \right) \tag{C.4}$$

Equation C.4 can be simplified into the following:

$$V_o = V_i \left(\frac{jwRC}{jwRC + 1} \right) \tag{C.5}$$

And again, by using the Laplace transform, the transfer function can be found from equation C.5, which looks as follows:

$$\frac{V_o}{V_i} = \left(\frac{swRC}{swRC + 1} \right) \tag{C.6}$$

If the resistor and capacitor values of the high pass filter is substituted into the variables, the second transfer function block is found.

The simulation was then set to repeat the PWM input signal indefinitely, since one PWM period only described one 100 Hz sine wave period. The simulation time was then set to run long enough so that the output of the filters reached a steady state.

In order to understand the simulation results that will follow, it must be kept in mind that the simulation did not use the time specified by the PWM signal, but instead assigned its own data points based on the sampling rate specified by the input block, defined in Figure C.2 as 's'. In order to correctly sample the PWM wave, a sampling rate of 0.2 MHz, or 5 μs was chosen. If the sampling rate was too fast, the simulation time would be too long and if the sampling rate was too slow, the PWM signal would be incorrectly simulated. Furthermore, the PWM wave generated by the Matlab code had 159744 output values, or 159744 points between 0 and 0.01 seconds. The simulation calculated the amount of points the output would have by dividing the selected simulation time with the sampling time, which, for the outputs that will be given later, amounted to $\frac{60}{5.10^{-6}} = 12.10^6$ points. Therefore, in the time selected, the number of sine waves that will be displayed should be $\frac{12.10^6}{159744} = 75,12$. Now, we know that the sine waves generated were a 100 Hz. Therefore, the total amount of time that would have passed for the 12.10^6 points is $75,12.0.01 = 0.75$ seconds. Therefore, to compute the amount of time that passes for one simulation point, we simply divide the total time by the total points, which gives $\frac{0.75}{12.10^6} = 62.5$ ns. This value can now be used to determine the time that has passed for any of the simulation's output graphs by simply multiplying the number of points by the time passed per point.

The simulated outputs are given in Figures C.5 and C.6.

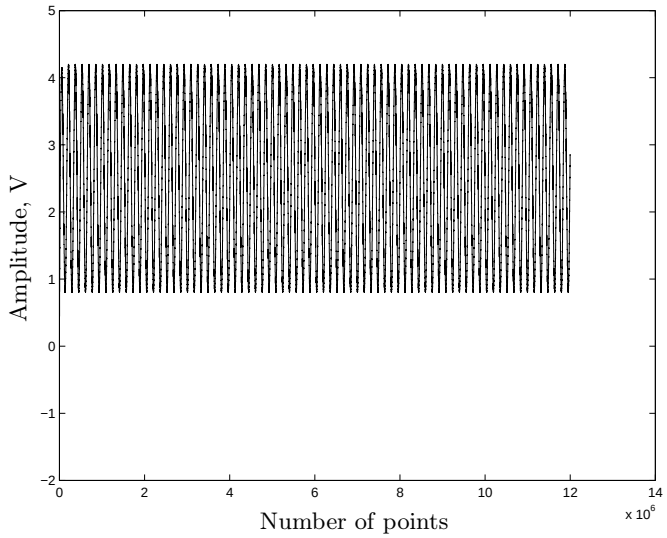

Figure C.5: Low pass filter outputs from startup to steady state.

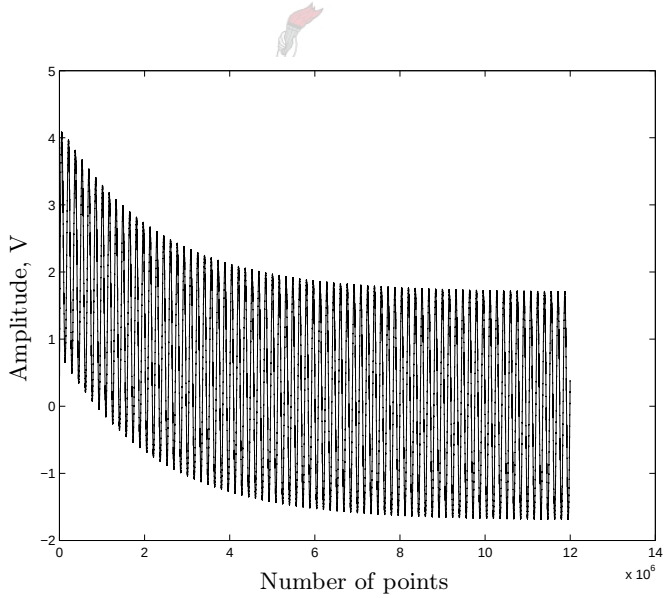

Figure C.6: High pass filter output from startup to steady state.

The simulation indicates that there is a transient response lasting about 0.75 seconds. In addition, the output values represent the result of a filtered PWM wave that was generated from a sine table that wanted a 2 V peak amplitude.

Finally, a close up view of the sine wave's peaks are given by Figure C.7.

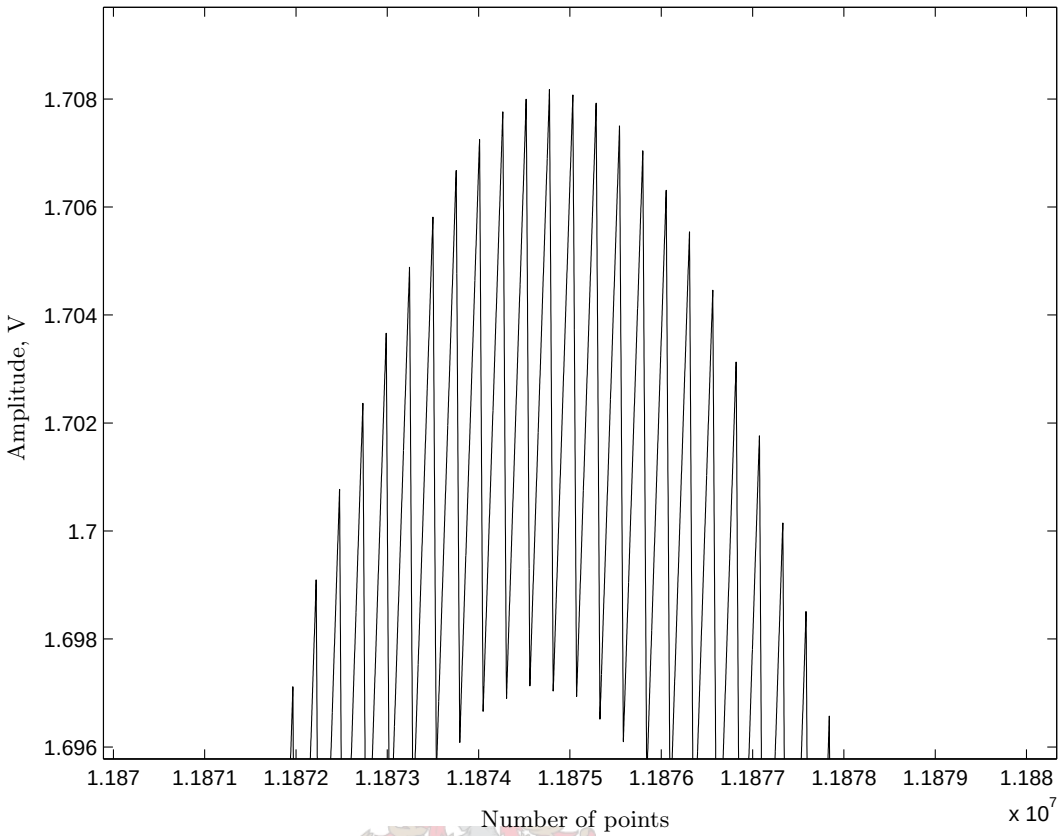

Figure C.7: Close up of sine peak.

The triangular output shown by the simulation was also observed in the filter's output of the automatic measurement device. It was this triangular variation that had to be taken into account during A/D sampling.

Appendix D

Programming code

The program code can be found on the inclosed CD, named *ProbeDev2.c*

Appendix E

Datasheets

The datasheets used during the design of the automatic measurement device will be named here. All of the datasheets that will be seen here were found on the internet, so a website location will be given as well.

Table E.1: Location and names of datasheets used in this thesis.

Chip, package and description	Datasheet	Location
ATMEGA16, TQFP44, microcontroller	ATMEL ATMEGA16/ ATMEGA16L	http://www.datasheetcatalog.com/ datasheets_pdf/ A/T/M/E/ATMEGA16.shtml
MAX232, SO16 (narrow), RS232 driver chip	MAXIM MAX220- MAX249	http://www.datasheetcatalog.com/ datasheets_pdf/M/A/X/2/MAX232.shtml
ADG619, MSOP8, CMOS switch	Analog Devices ADG619/ADG620	http://www.datasheetcatalog.com/ datasheets_pdf/A/D/G/6/ADG619.shtml
25AA256, SO08, EERPOM	Microchip 25AA256/ 25LC256	http://www.datasheetcatalog.com/ datasheets_pdf/2/5/A/A/25AA256.shtml
VN10K, TO92, MOSFET	Supertex Inc. VN10K	http://www.datasheetcatalog.com/ datasheets_pdf/V/N/1/0/VN10K.shtml
ADG706, TSSOP28, 16 channel CMOS analog multiplexer	Analog Devices ADG706/ADG707	http://www.datasheetcatalog.com/ datasheets_pdf/A/D/G/7/ADG706.shtml
LM358, SO08, operational amplifier	National Semiconductor LM158/ LM258/ LM358/ LM2904	http://www.datasheetcatalog.com/ datasheets_pdf/L/M/3/5/LM358.shtml
QTLP601C, 0603, yellow LED	Fairchild Semiconductor surface mount LED lamp	http://www.datasheetcatalog.com/ datasheets_pdf/ Q/T/L/P/QTLP601C-4.shtml
LM74, SO08, Temperature sensor	National Semiconductor LM74	http://www.datasheetcatalog.com/ datasheets_pdf/L/M/7/4/LM74.shtml
1N4148, D035, diode	Hitachi Semiconductor 1N4148	http://www.datasheetcatalog.com/ datasheets_pdf/1/N/4/1/1N4148.shtml

Appendix F

Experimental results

The experimental results will give all the measured probe impedance values per bacterial type. Every milk fermentation graph will also contain the salt "control" measurement. The different measurement devices, together with their connection ports, will be given as 16-pin, no(x) or 3-pin, no(x) where x is between 1 to 12 for the 16-pin device and from 1 to 3 for the 3-pin device. The average of the characterisation measurements done for the newly manufactured probes, as tested in a 1.6% salt solution, will also be given. Finally, the temperature measurements and pH measurements will be given.

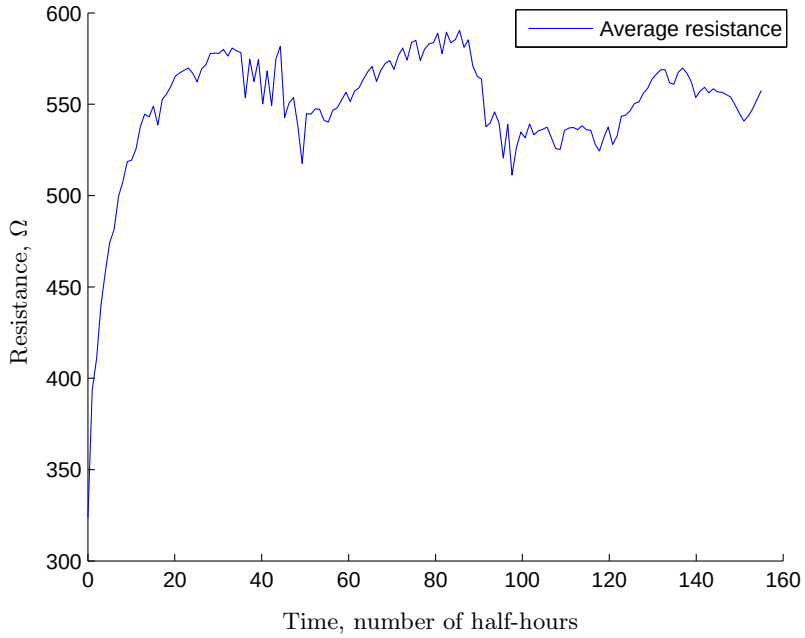

Figure F.1: Average probe resistance measurements in a 1.6% salt solution over a three day period.

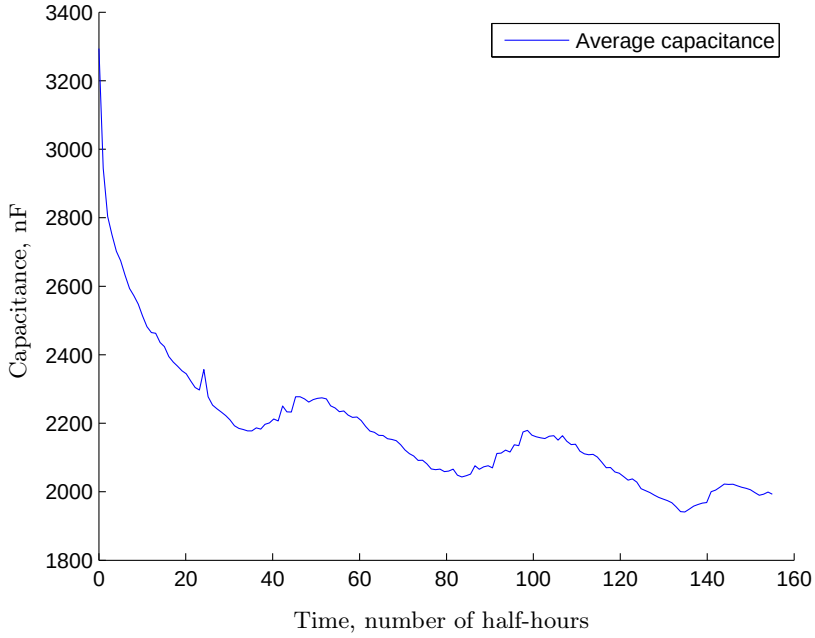

Figure F.2: Average probe capacitance measurements in a 1.6% salt solution over a three day period.

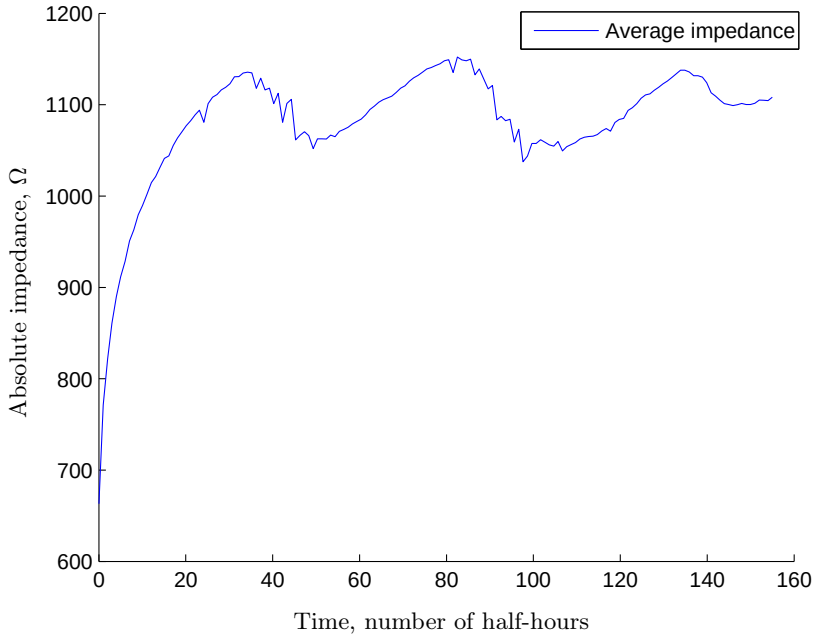

Figure F.3: Average probe absolute impedance measurements in a 1.6% salt solution over a three day period.

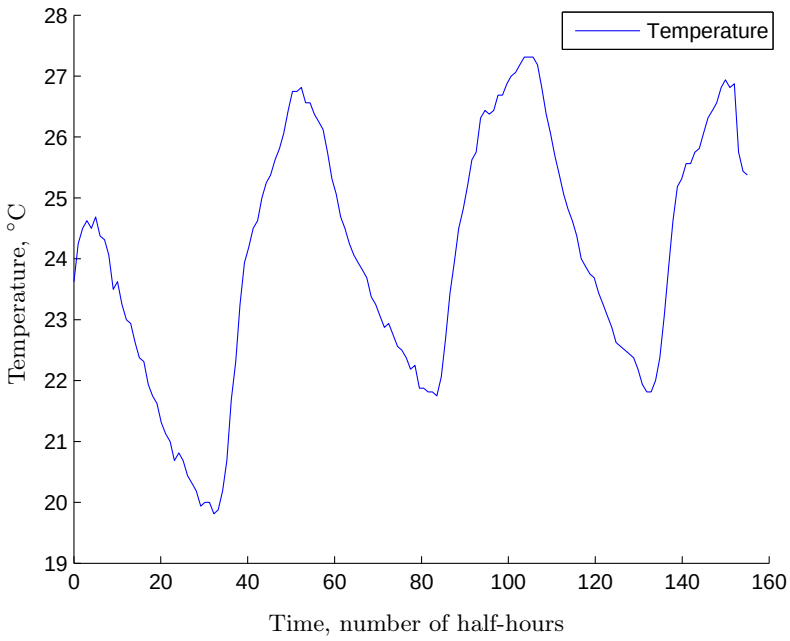

Figure F.4: Temperature measurements during probe characterisation tests. Tests were done in a normal room and temperature represents ambient temperature.

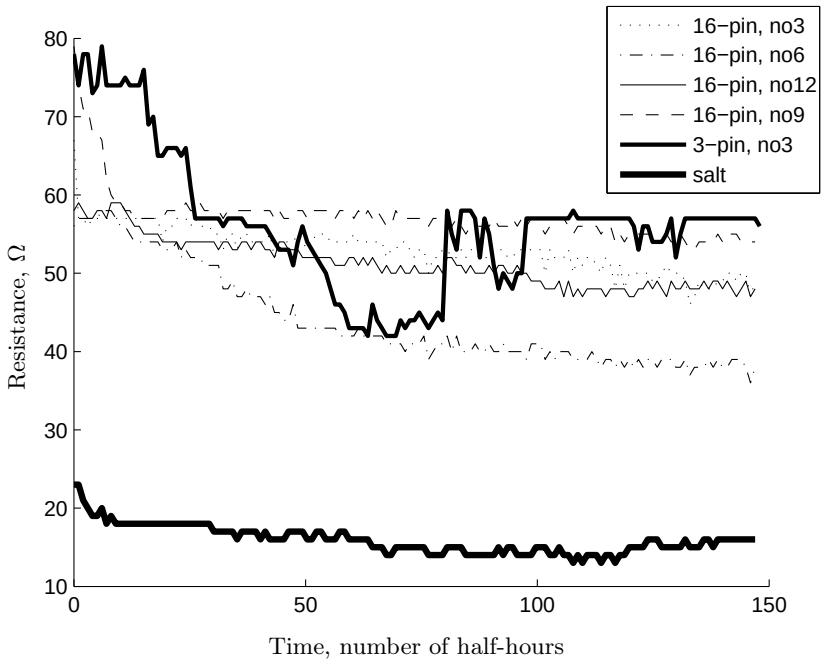

Figure F.5: Probe resistance change as measured in salt and in milk contaminated with HKLHS.

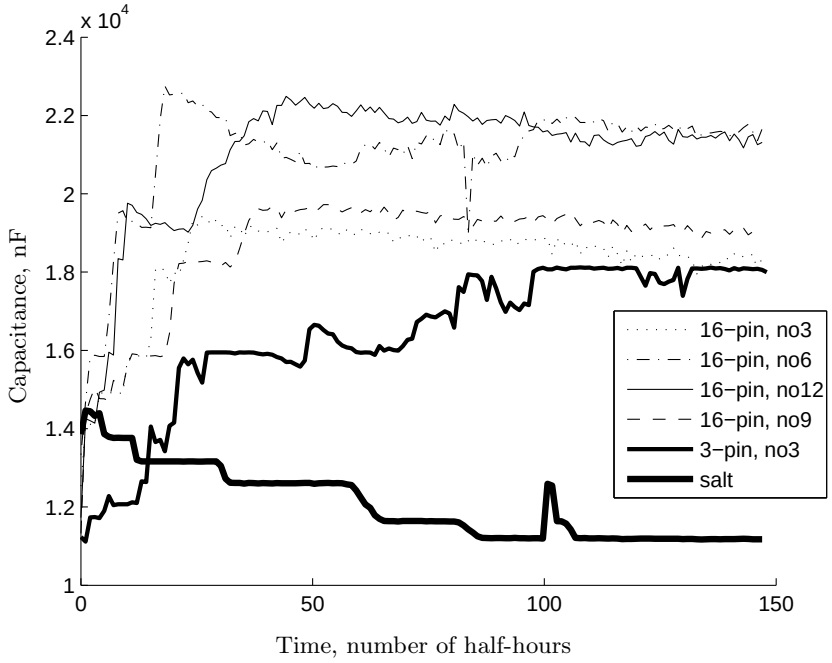

Figure F.6: Probe capacitance change as measured in salt and in milk contaminated with HKLHS.

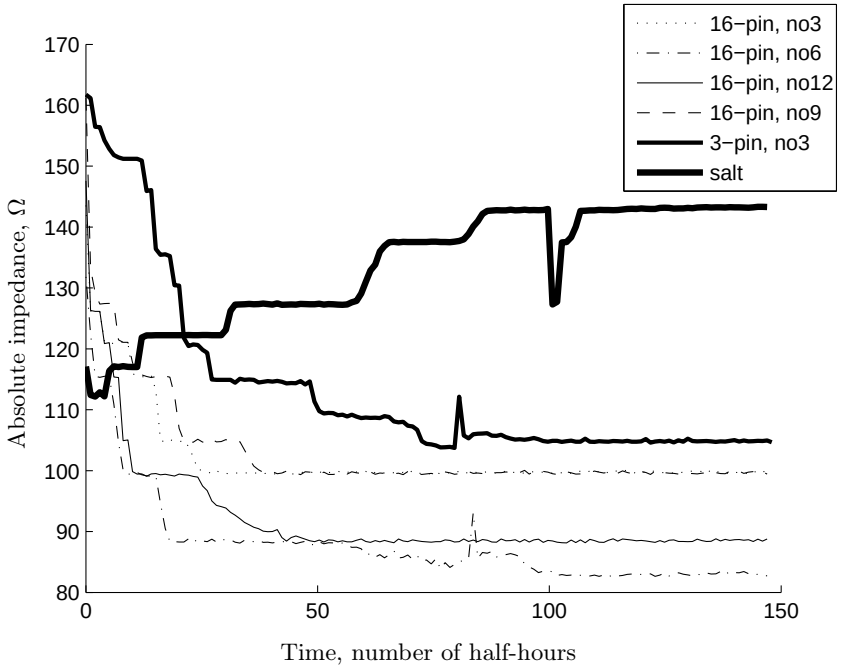

Figure F.7: Probe absolute impedance change as measured in salt and in milk contaminated with HKLHS.

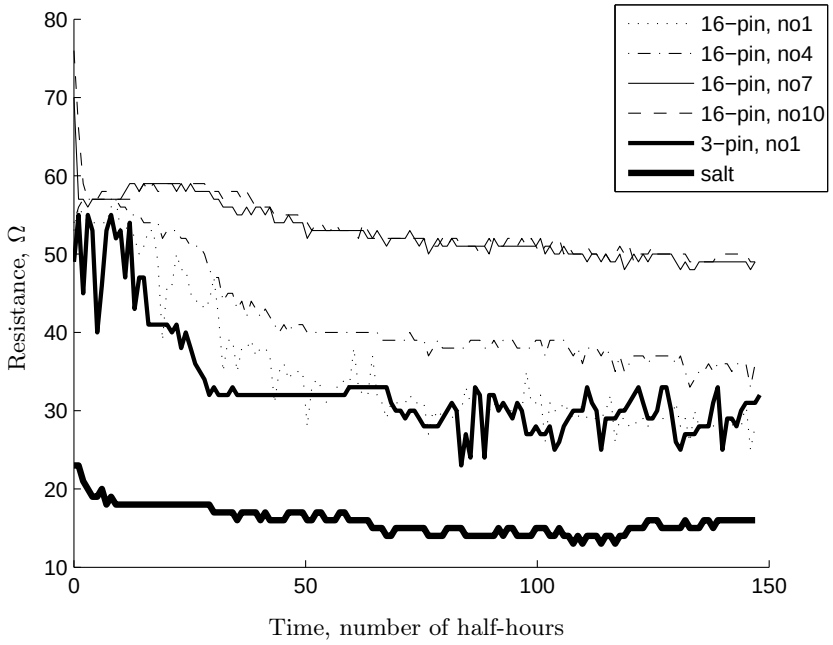

Figure F.8: Probe resistance change as measured in salt and in milk contaminated with Sakei.

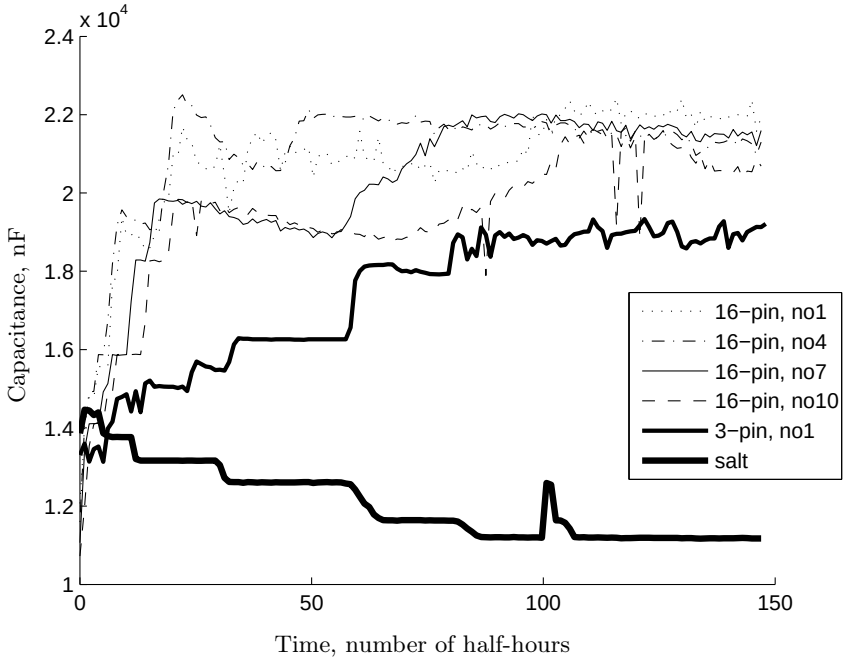

Figure F.9: Probe capacitance change as measured in salt and in milk contaminated with Sakei.

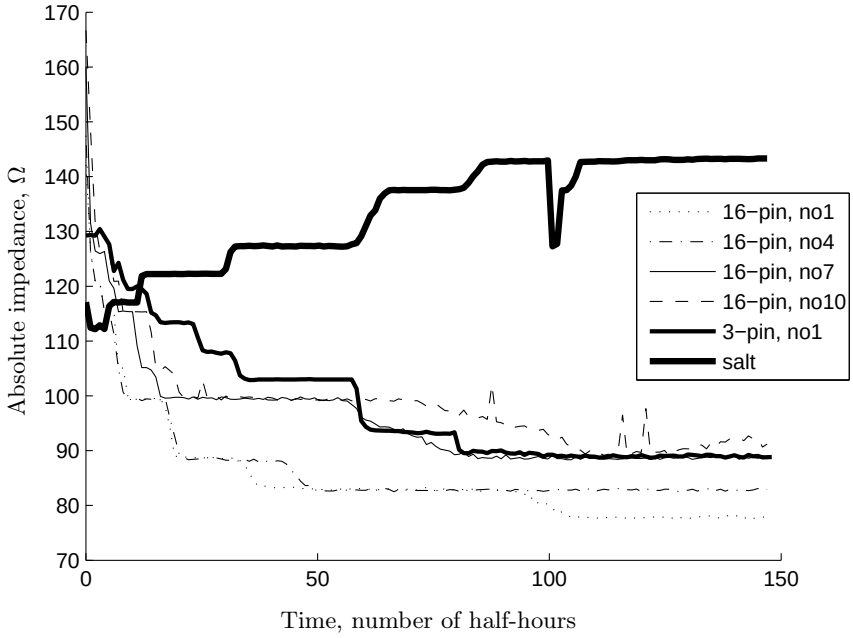

Figure F.10: Probe absolute impedance change as measured in salt and in milk contaminated with Sakei.

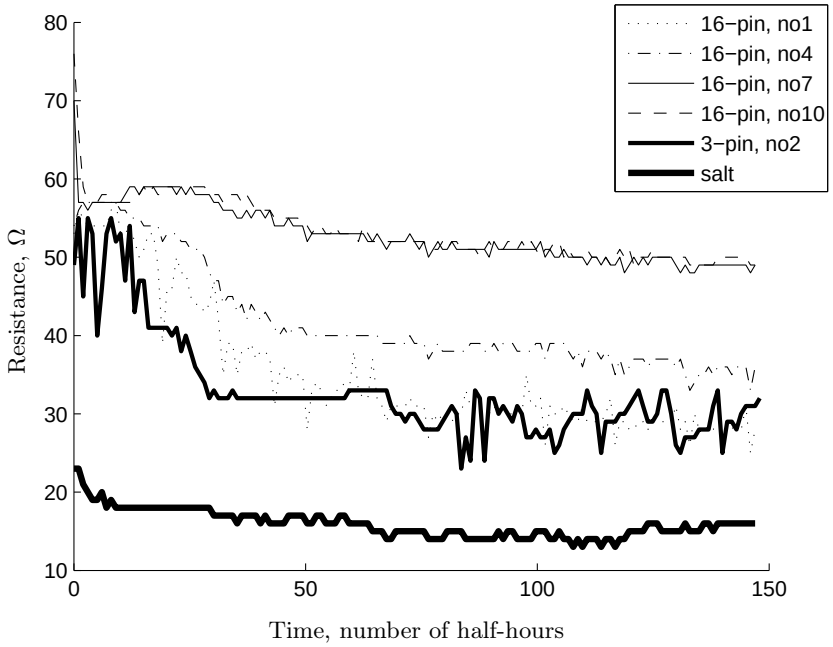

Figure F.11: Probe resistance change as measured in salt and in milk contaminated with 423.

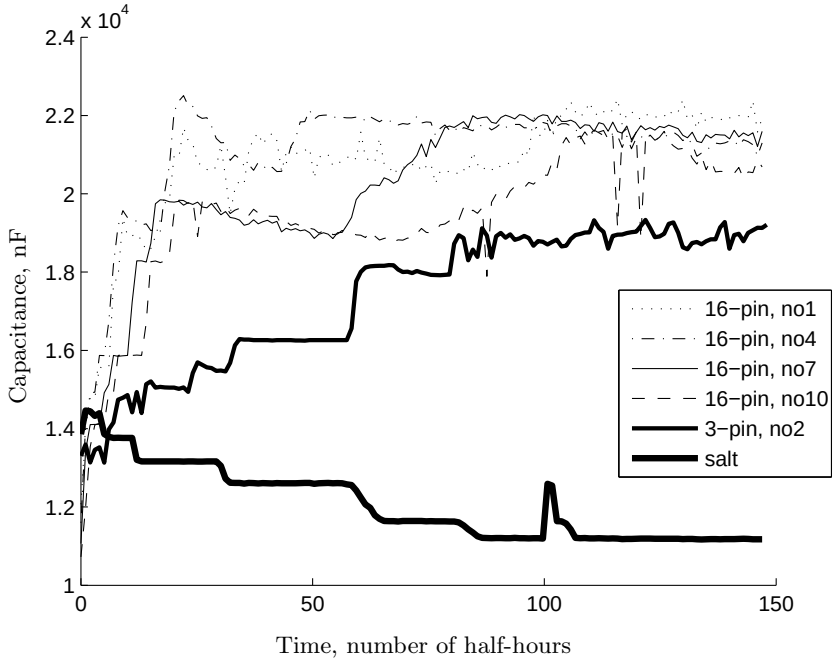

Figure F.12: Probe capacitance change as measured in salt and in milk contaminated with Sakei.

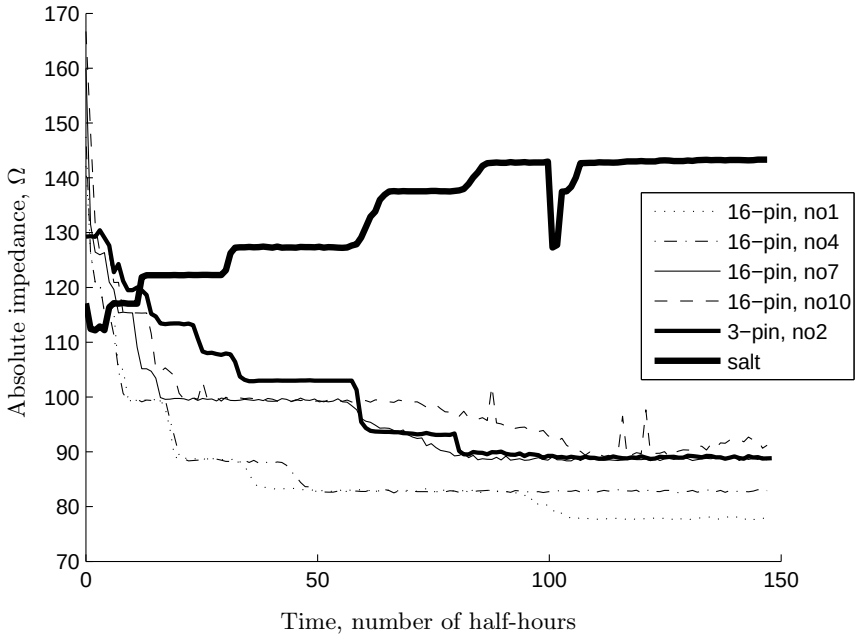

Figure F.13: Probe absolute impedance change as measured in salt and in milk contaminated with Sakei.

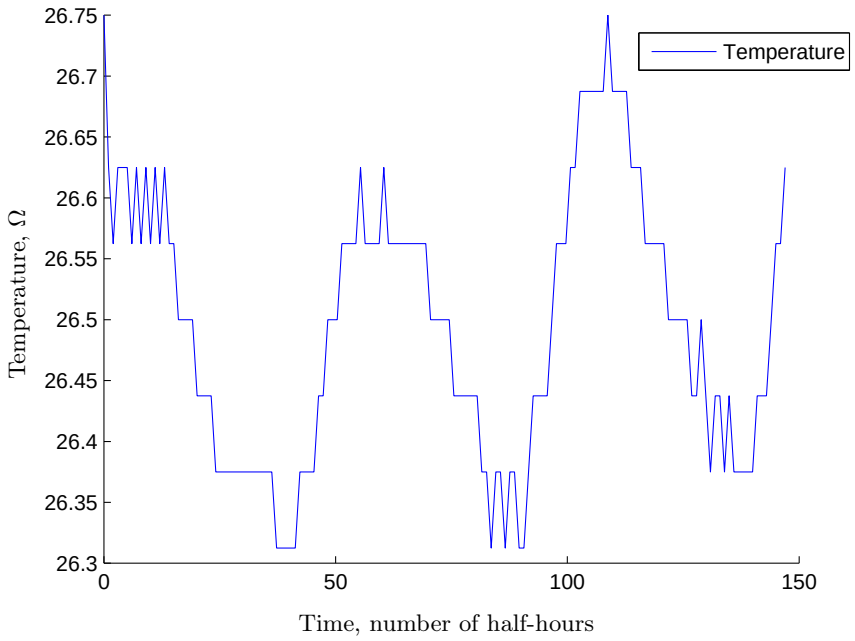

Figure F.14: Temperature measurements for entire milk run.

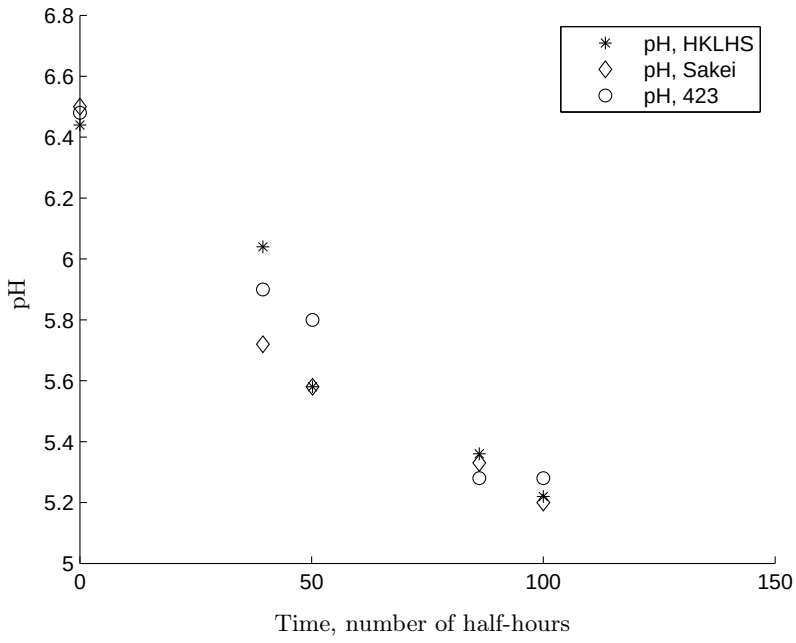

Figure F.15: pH measurements in milk contaminated with HKLHS, Sakei and 423.